Florida International University
FIU Digital Commons

FIU Electronic Theses and Dissertations | University Graduate School

11-22-2002

Determination of whole-body specific absorption rate (SAR) and characterization of ferris wheel radio frequency (RF) exposure system using calorimetric techniques

Subbarao V. Chebrolu
Florida International University

DOI: 10.25148/etd.FI14060155
Follow this and additional works at: https://digitalcommons.fiu.edu/etd

 Part of the Electrical and Computer Engineering Commons

Recommended Citation
Chebrolu, Subbarao V., "Determination of whole-body specific absorption rate (SAR) and characterization of ferris wheel radio frequency (RF) exposure system using calorimetric techniques" (2002). *FIU Electronic Theses and Dissertations*. 2123.
https://digitalcommons.fiu.edu/etd/2123

This work is brought to you for free and open access by the University Graduate School at FIU Digital Commons. It has been accepted for inclusion in FIU Electronic Theses and Dissertations by an authorized administrator of FIU Digital Commons. For more information, please contact dcc@fiu.edu.

FLORIDA INTERNATIONAL UNIVERSITY

Miami, Florida

DETERMINATION OF WHOLE-BODY SPECIFIC ABSORPTION RATE (SAR) AND CHARACTERIZATION OF FERRIS WHEEL RADIO FREQUENCY (RF) EXPOSURE SYSTEM USING CALORIMETRIC TECHNIQUES

A thesis submitted in partial fulfillment of the

requirements for the degree of

MASTER OF SCIENCE

in

ELECTRICAL ENGINEERING

by

Subbarao V. Chebrolu

2002

To: Dean Vish Prasad
College of Engineering

This thesis, written by Subbarao V. Chebrolu, and entitled Determination of Whole-Body Specific Absorption Rate (SAR) and Characterization of Ferris Wheel Radio Frequency (RF) Exposure System using Calorimetric Techniques, having been approved in respect to style and intellectual content, is referred to you for judgment.

We have read this thesis and recommend that it be approved

Subbarao V. Wunnava

Malcom Heimer

Chung-Kwang Chou

Antonio Faraone

Tadeusz M.Babij, Major Professor

Date of Defense: November 22 , 2002

The thesis of Subbarao V. Chebrolu is approved.

Dean Vish Prasad
College of Engineering

Dean Douglas Wartzok
University Graduate School

Florida International University, 2002

DEDICATION

To my parents and sister, for their support and encouragement.

ACKNOWLEDGMENTS

Several people have helped me to conduct and complete the research presented here. First and foremost, I would like to thank Dr. C.K.Chou and Dr. Antonio Faraone for their patience, understanding and moral support. I was fortunate in having the opportunity to discuss ideas with both of them, whose deep perception and constructive criticism helped to focus and refine myself. Their suggestions and constant encouragement gave me a boost of confidence and stimulation.

I am also grateful to Dr. Renato Cicchetti and Dr. Giorgi Bit-Babik for their support in deriving the mathematical model for the twin-well calorimeter and simulations on Ferris Wheel respectively. This thesis would have not been possible without the help and support from Wilson Luengas, Maurice Ballen, John McDougall, George Han, Andy Greesner and Mike Kanda for their technical contribution at the Motorola Florida Research Labs during this research.

I wish to thank Motorola for sponsoring my study, providing the laboratory and equipment for doing this research. I also want to thank the Electrical and Computer Engineering Department of FIU for the tuition waiver and teaching assistantship given to me.

My special thanks to my major professor and advisor Dr. T.M. Babij for his continued guidance and support during the preparation of this thesis and for Dr. Babij's opting me to work for Motorola's project was truly invaluable. I would also like to thank Dr. Subbarao Wunnava and Dr. Malcom Heimer who also served in my graduate committee for their valuable cooperation and priceless time throughout my Master's program at the Department of Electrical and Computer Engineering.

ABSTRACT OF THE THESIS

DETERMINATION OF WHOLE-BODY SPECIFIC ABSORPTION RATE (SAR) AND CHARACTERIZATION OF FERRIS WHEEL RADIO FREQUENCY (RF) EXPOSURE SYSTEM USING CALORIMETRIC TECHINQUES

by

Subbarao V. Chebrolu

Florida International University, 2002

Miami, Florida

Professor Tadeusz M. Babij, Major Professor

The "Ferris Wheel" RF Exposure System was designed by Motorola Inc. to study the long-term biological effects due to RF exposure [3]. The main goal of this research project was to characterize the "Ferris Wheel" to know how efficient and symmetrical was the exposure system in distributing the RF power among its loads. The characterization of the system was done in terms of power efficiency, SAR, Whole-Body SAR and Localized SAR.

Exposure to RF sources is quantified in terms of SAR which defines the rate of electromagnetic deposition per unit mass. Determination of Whole-Body averaged SAR requires to have the actual amount of energy absorbed where as the temperature increase in the tissue material yields the Localized SAR. Calorimetric Techniques were used to characterize the "Ferris Wheel" exposure system in terms of Whole-Body SAR and efficiency. Microwave Studio and XFDTD simulation programs based on *Finite Difference Time Domain* method were also used to determine the Whole-Body SAR and

E-field distribution in the "Ferris Wheel." The E-field distribution inside the FW was measured by using E-field probes and result was compared to that of simulated.

TABLE OF CONTENTS

LIST OF TABLES

TABLE PAGE

LIST OF FIGURES

FIGURE PAGE

CHAPTER I

INTRODUCTION

Over the past several decades a large number of scientific studies have been published worldwide on biological effects from exposures to extremely low frequency (ELF) fields and radio frequency (RF) fields such as emitted by radars and telecommunication transmitters. Some of these studies have reported a number of hazards from electromagnetic fields (EMF) exposures, but these are generally at very high exposure levels. International exposure guidelines have been developed to protect against them.

There are several important considerations when evaluating possible health effects of RF fields. One is the frequency of the radiation. By virtue of their frequencies, the photon energies associated with RF are insufficient to cause ionization in matter such as body tissue. Because of this, RF fields are called non-ionising, which unlike X-rays and gamma radiations can cause ionisation leading to the breakup of the molecular structure of matter.

Mobile telephones, often called cell phones, are now an integral part of modern telecommunications. The technology of the mobile phone system necessitates the installation of a large number of antennas or base-stations in order to accommodate the large number of users, and to provide the necessary coverage. Many of these antennas and base-stations are installed on top of high-rise buildings. Because of the large number of users, there is now considerable public concern about possible health hazards from EMF exposures from mobile phones or their base stations.

Mobile phone handsets and base stations present quite different exposure situations. Mobile phone handsets are low-powered RF transmitters, emitting maximum powers in the range of 0.13 to 0.6 watts. The RF field strength (and hence RF exposure to a user) falls off rapidly with distance from the handset. Therefore, the RF exposure to a user of a mobile phone located tens of centimeters from the head using a "hands free" appliance is far lower than to a user who places the headset against the head. RF exposures to nearby people from these devices are very low.

Base stations transmit power levels typically from a few watts to less than 100 watts, depending on the size of the region or "cell" that they are designed to service. The antennas emit RF beams that are typically very narrow in the vertical direction but broad in the horizontal direction. Because of the narrow vertical spread of the beam, the RF field intensity at the ground directly below the antenna is low. The RF field intensity increases slightly as one moves away from the base station and then decreases for greater distances from the antenna. Paging and other communications antennas used by fire, police and emergency services, operate at similar power levels as cellular base stations, and often at a similar frequency. Television and radio broadcast antennae commonly transmit much higher RF levels than mobile base stations.

RF fields penetrate exposed tissues to depths that depend on the frequency, usually up to a centimeter at the frequencies used by mobile phones. RF energy is absorbed in the body and produces heat, but the body's normal thermo-regulatory processes carry this heat away. Health effects due to RF exposure have shown to be related to heating. RF energy which interacts with body tissues at levels used by mobile

phones are too low to cause any significant heating. No consistent studies have shown adverse health effects at exposure levels below international guideline limits.

Current scientific evidence indicates that exposure to RF fields, such as those emitted by mobile phones and their base stations, is unlikely to induce or promote cancers. Several studies of animals exposed to RF fields similar to those emitted by mobile phones found no evidence that RF causes or promotes cancer. Epidemiological studies found no convincing evidence of increase in risk of cancer or any other disease with use of mobile phones.

A study was conducted at Royal Adelaide Hospital lead by Dr. Michael Repacholi exposing lymphoma prone mice to digital Global Systems Mobile (GSM) 900 Megahertz fields over a 9 to 18 month period [1]. The mice were divided into two groups of 100 each and placed in the cages, housed in identical conditions in two different chambers and subject to the same amount and type of handling. The match extended even to having a sham antenna hanging over the control group.

One of the two groups was subject to GSM pulsed signal at a power-density roughly equal to a cell-phone transmitting for two half-hour periods each day [1]. The only difference between the "shams" (controls) and the exposed mice, was that one group had an antenna which was radiating cell phone-type RF signals (at handset powers) for two hours a day, while for the other group, power was never switched to the antenna.

The study found that the exposed mice had more than two fold increase in lymphoma as compared to the controls. This study provoked concern worldwide, because it was the first reputable research to point to a positive link between mobiles and cancer.

Dr. Repacholi et al study was criticized since the RF exposure dose used is poorly defined and only one RF exposure dose level was used, so that the nature of the dose-response was unknown. The mice used were *Pim1* mice, so there was no way to determine whether the effect was unique to the animals that had been genetically engineered to make them lymphoma prone. Hence, the study is being considered more like a pilot study than a comprehensive bioassay

Because of its findings, the Australian government funded a follow up study to establish whether or not the same results could be produced once again with natural and lymphoma prone mice at different dosage levels. A different type of exposure system was required so that RF exposure doses could be more tightly defined and in a more controlled environment in order to give a precise dose of exposure. The RF exposure System used in this study was the "Ferris Wheel (FW)"exposure system [3] designed by Motorola Florida Research Labs, which provides a Whole-Body exposure for mice. A detailed explanation regarding construction and design of this system is discussed in Chapter II.

The result of this new study lead Dr. Tammy Utteridge using 600 normal and 600 lymphoma-prone mice were exposed to 898 MHz GSM-modulated RF energy for 1 hour per day for 24 months. Four different exposure levels of 0.25, 1.0, 2.0 and 4.0 W/kg were tested. The results show no significant increase in lymphoma and no significant dose-response trend [2].

The main goal of this research is to have a detailed dosimetric characterization of the "Ferris Wheel" RF exposure system designed for mice to know how efficient and symmetrical is the exposure system in distributing the RF power into the mice. The

dosimetric parameter used for the dosimetric characterization of the system is Specific Absorption Rate (SAR) that is widely used in the research will be discussed in Chapter III.

There are a number of Techniques used for the SAR measurements. Chapter IV discusses the various techniques used for the measurement of the Whole- Body SAR and Localized SAR with examples using the Ferris Wheel as an exposure system.

In Chapter V the electric field distributions inside the FW cavity using cylindrical FDTD code developed at Motorola are simulated and compared to that of the measured electric fields using E-field probes. Effects in the field distributions due to some intentional geometrical asymmetries are analyzed using simulation software Microwave Studio.

Chapter VI deals with the Whole-Body SAR characterization of FW using Calorimetric technique. Mathematical modeling and simulations in MATLAB for the Twin-Well calorimeter used for measurement of Whole-Body SAR is described as well. Detailed description of calorimetric test procedure used for different types of loads is also provided.

Chapter VII lists the results for the calorimetric tests performed for different types of loads.

CHAPTER II

THE "FERRIS WHEEL" AS AN EXPOSURE SYSTEM

As discussed in Chapter I, biological effects due to the RF exposure can be studied by carrying out long-term exposure to animals. The exposure environment used in Dr. Repacholi et al for the mice was not well controlled i.e., all the mice didn't had the same nominal levels and Whole-Body exposure to the RF fields as they were allowed to move freely inside their cages [1].

The RF system called "Ferris Wheel" developed at the Motorola Florida Research Labs allows a Whole-Body exposure to mice and provides symmetrical distribution of RF fields to the mice located around the transmitting antenna [3]. The earlier Whole-Body animal exposure to (locally) plane waves has been accomplished in the past by means of circular or rectangular wave-guides, radial wave-guides, and rectangular horns. In these structures, the matching of the antenna to the RF source is fairly insensitive of the loading, e.g., animal orientation with respect to the incident field [4-6]. Electromagnetic cavities have been employed with tuning, as they are very sensitive to load changes. By forcing the animals into restrainers will allow a Whole-Body exposure of the animals, as well as an efficient use of the available RF power. One of the basic advantages of this exposure system is that, being a closed electromagnetic structure; straightforward power balance can be employed to assess the average Whole-Body SAR of the mice [3].

2.1 Design and Construction of the "Ferris Wheel" Exposure System

The Ferris Wheel exposure system shown in Fig.1 is made up of a radial electromagnetic cavity formed by two parallel circular plates mounted on a polycarbonate frame. The two circular plates are single-side copper-clad laminate printed circuit boards (PCBs), and are mechanically supported by a 10 cm hollow Teflon ring long and about 10 cm in radius and 1.8 cm thick. The circular plates are joined around the perimeter by an array of shorting posts to form the radial cavity. Forty mice are placed at 9 cm apart at 44 cm from the center, co-polarized with respect to the incident TEM wave. The cavity is fed at the center by an internal tunable transition from the coaxial feed line [3]. The Ferris Wheel is loaded with forty mice periodically distributed around the perimeter.

Fig.1. Ferris Wheel Exposure System [3].

A tunable transition from a 50-ohm coaxial feed line excites a cylindrical TEM wave that impinges on 40 symmetrically arranged mice, which are equidistant from the exciter. The mice, restrained in plastic tubes inserted through circular holes in the plates, as shown in Fig.2, are held co-polarized with the incident electric field (E-polarization) to maximize the absorption of RF energy [3].

The symmetric arrangement provides uniform exposure to the mice, while the Whole-Body TEM illumination induces fairly uniform RF absorption within each mouse. Depending on the position of a mouse in the Ferris Wheel, the wave impinges from different directions.

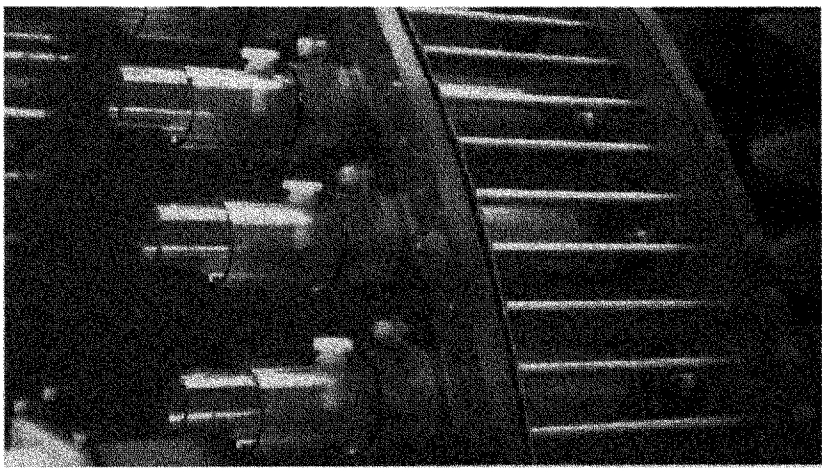

Fig.2. Mouse restraining mechanism [3].

Fig.2 shows the mouse holder that slides and locks to a plastic sleeve attached to the cavity frame. A pusher is held to the restrainer by means of a thumbscrew to keep the mouse exposed inside the "Ferris Wheel"[3].

An array of 120 shorting posts is preferred to a solid electric wall since it lets light into the cavity, which is needed for the mice. The posts are 10 cm long and 6.35 mm in diameter. They are symmetrically distributed around the perimeter of the cavity at 48 cm from the center, co-polarized with the electric field of the impinging TEM wave, and less than one-tenth of a wavelength apart to ensure low RF leakage. Return-loss measurements of the unloaded cavity shown that appreciable radiation would not result, which was confirmed by radiation measurements of the loaded cavity [3].

2.2. Field equations for the Ferris Wheel system

Since the Ferris Wheel exposure system is radial wave-guide has a cylindrical structure as shown in Fig.3. The electromagnetic fields inside in the cylindrical reference frame are derived in the following way [7].

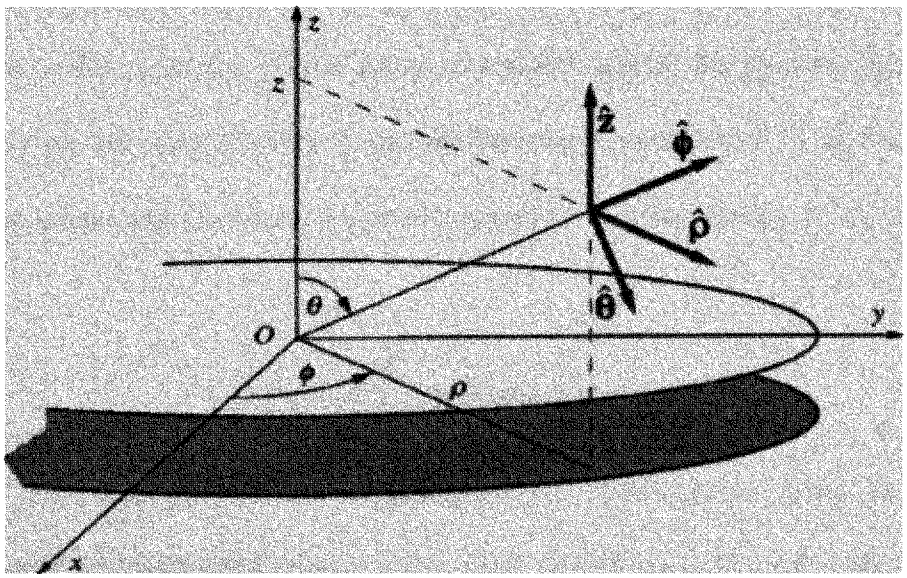

Fig.3. Reference cylindrical coordinates for Ferris Wheel Exposure system [7].

Assuming no vertical variation i.e. $\partial / \partial z = 0$ and perfect metal conductors, it yields

$$E_t = \hat{\rho} E_\rho + \hat{\varphi} E_\varphi = 0 \tag{2.1}$$

and

$$\nabla . E = 0 \tag{2.2}$$

in the field domain.

Assuming the impressed current is uniformly distributed on a vertical cylinder of radius a

$$J = \hat{z} \frac{I_o}{2a\pi} \delta(\rho - a), \qquad 0 \le z \le h \tag{2.3}$$

where h is the thickness of the cylindrical cavity.

The Maxwell's equations yield

$$\nabla_t^2 E_z + k^2 E_z = j\omega\mu \frac{I_o}{2a\pi} \delta(\rho - a) \qquad 0 \le z \le h \tag{2.4}$$

with $k^2 = -j\omega\mu(\sigma + j\omega\varepsilon)$

where σ is the dielectric conductivity.

Due to the symmetry of the structure and the source, the electromagnetic fields depend only on the radial variable ρ and the boundary condition of E_z on the source is obtained by integrating the above Maxwell's equation over the surface $\rho' \le \rho$ as $\rho \to a$, resulting

$$\lim_{\rho \to a} 2\pi\rho \frac{\partial E_z}{\partial \rho} = j\omega\mu I_0 \tag{2.5}$$

As the incident field is a free-space-like TEM plane wave, as long as circumferential or longitudinal higher order mode excitation is not very significant, the field components in the cylindrical reference frame can be expressed as follows,

Applying the above condition to equation (2.4) results in

$$E_z(\rho) = A_r H_0^{(1)}(k\rho) + A_f H_0^{(2)}(k\rho) \tag{2.6}$$

where $H_0^{(1)} and\ H_0^{(2)}$ are the zeroth order Hankel functions that describe the inward and outward cylindrical waves respectively [7].

The magnetic field is simply derived from the relation

$$\boldsymbol{H} = -\nabla \times \boldsymbol{E}/j\omega\mu \tag{2.7}$$

and is expressed as

$$H_\phi(\rho) = \frac{1}{j\omega\mu}\frac{\partial E_z}{\partial \rho} = \frac{1}{-j\eta}\left[A_r H_1^{(1)}(k\rho) + A_f H_1^{(2)}(k\rho)\right] \tag{2.8}$$

where $\eta = \sqrt{j\omega\mu/(\sigma + j\omega\varepsilon)}$ is the wave impedance and k is the wave number of the medium.

Even at a short distance, the cylindrical wave impedance approaches the plane-wave impedance, therefore an exposure in the radial waveguide is very similar to free space, provided the cross section of the exposed body is much smaller than its distance from the center so that the impinging wave front can be considered locally flat and uniform.

2.3 Tunable Coax-to-Radial Cavity Transition

Tuning ability of the cavity exciter is desired to ensure proper matching to the RF source over a relatively wide range of possible loading conditions. A tunable transition from the coaxial feed line to the radial cavity was designed with the objective of

maximizing the modal conversion to the fundamental cavity mode by keeping the exciter's current as uniform as possible.

As depicted in Fig.4, the transition is formed by a top-loaded monopole antenna, which is capacitively coupled with a passive counterpoise. In this way, the accumulation of electric charges is concentrated in the small region comprising the capacitive loads so that the current along the monopole as well as the counterpoise is kept fairly uniform.

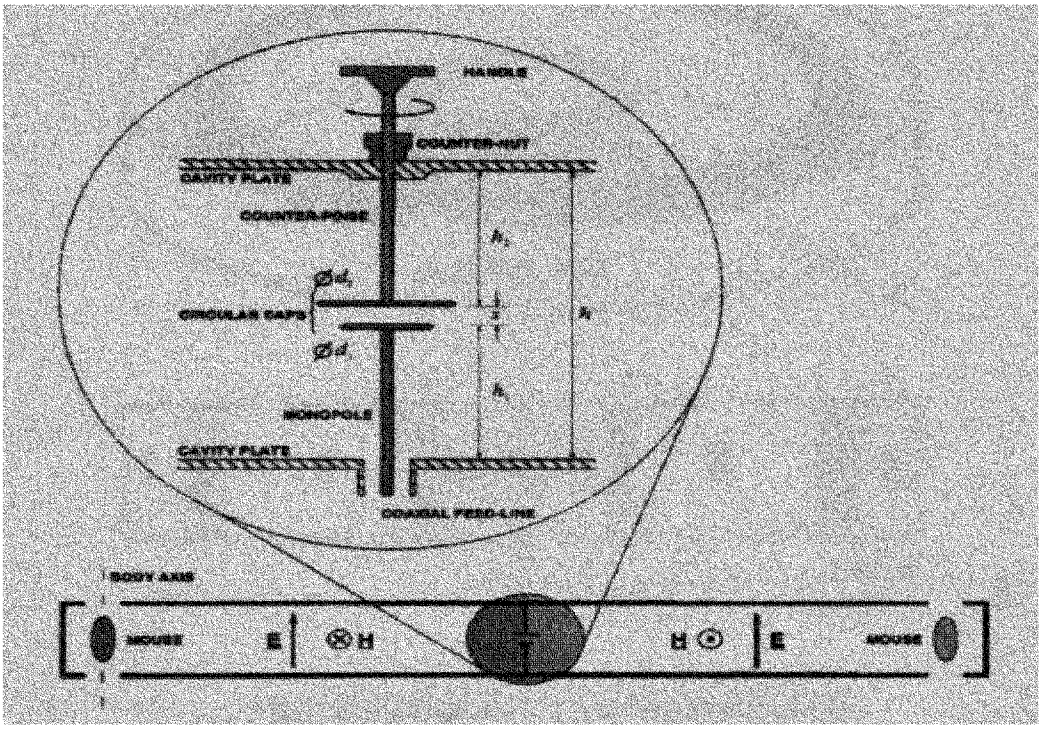

Fig.4. Schematic of Tunable Transition from the coaxial feed [3].

Tuning of the loaded cavity is performed through adjusting the capacitive coupling by moving the counterpoise closer or farther from the monopole, which is easily accomplished by threads on its arm. A plastic counter-nut ensures good electrical contact

of the counterpoise with the cavity plate. The actual implementation of the tuning element is shown in Fig.4 [3].

The Fig.5 shows the electric wall formed shorting posts and the loads. In the figure δ is the distance between the position of the center of the carrousel and the electric short post and, λ_o is the wavelength of the incident wave.

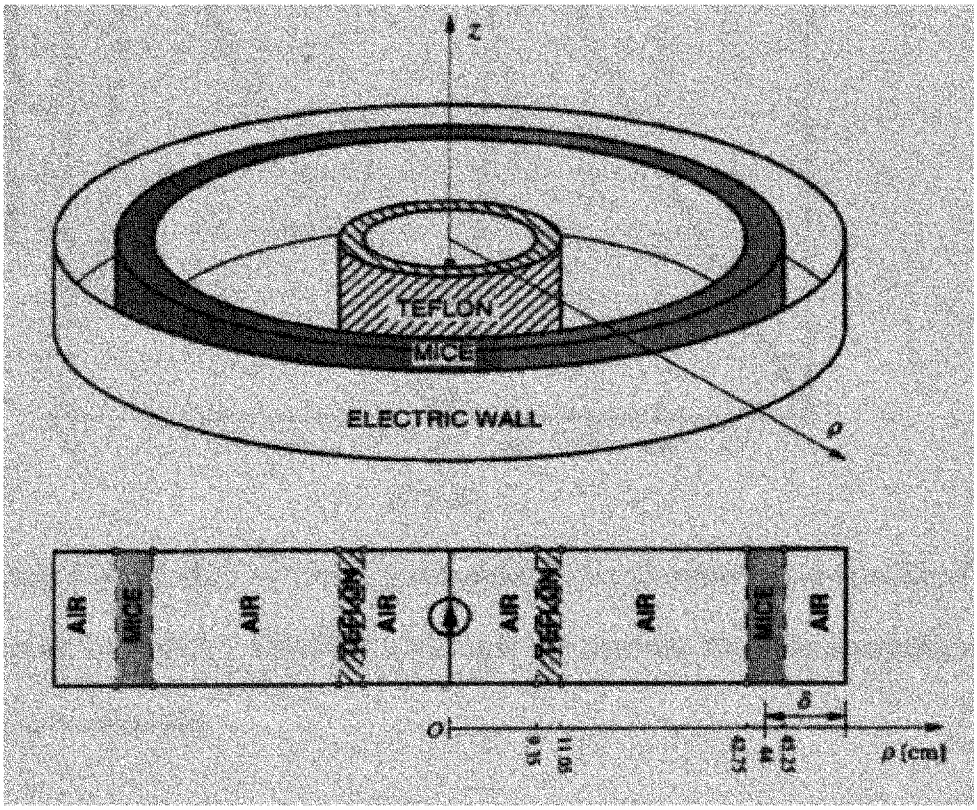

Fig.5. Horizontal view of the Ferries Wheel [3].

The distance δ is determined by using a prototype cavity where the shorting poles are placed at different distances from 48 to 50 cm from the center. On the base of return loss the optimal distance is determined to be at 48 cm from the center. At this distance the

ratio of δ/λ_0=0.12 is where the peak of the efficiency curve exists as shown in the Fig.6. Any slight variations may result in the fall of step region and the efficiency drops sharply.

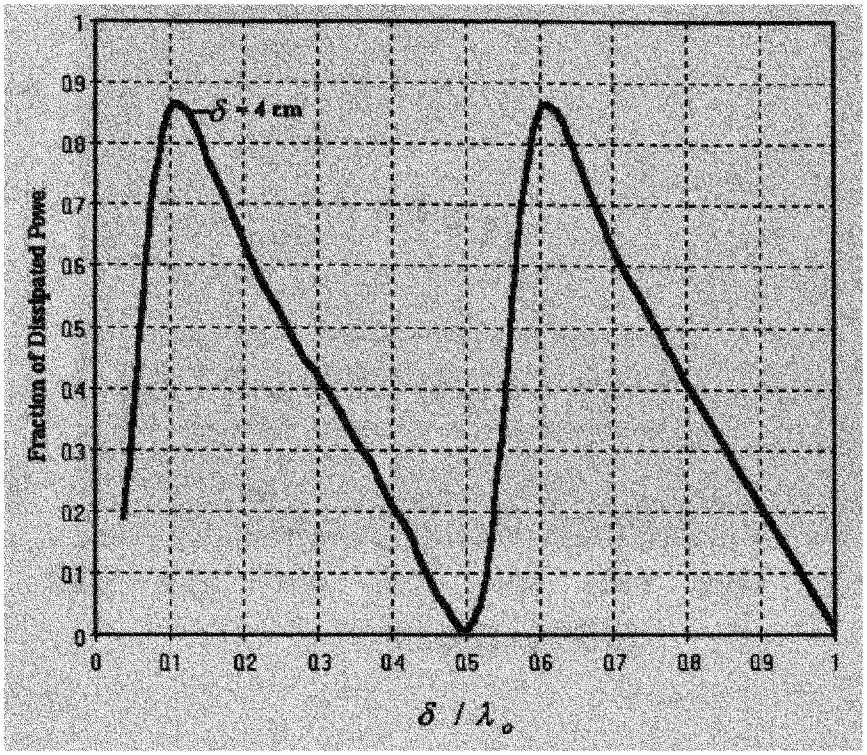

Fig.6. Fraction of the incident RF power that is dissipated in the mice versus distance of the shorting wall, according to the radial-transmission-line model. The optimal distance is shown to be at $\delta \approx 4$ cm [3].

The wide band tuning capability of the exciter is shown in the Fig.7. This figure shows good matching to the source at 900 MHz with relatively low percent of power is reflected back into the cavity. At 915 MHz the separation between the caps of the passive counter poise to the cap of the monopole antenna is around 8 mm and the return loss is around 9 dB.

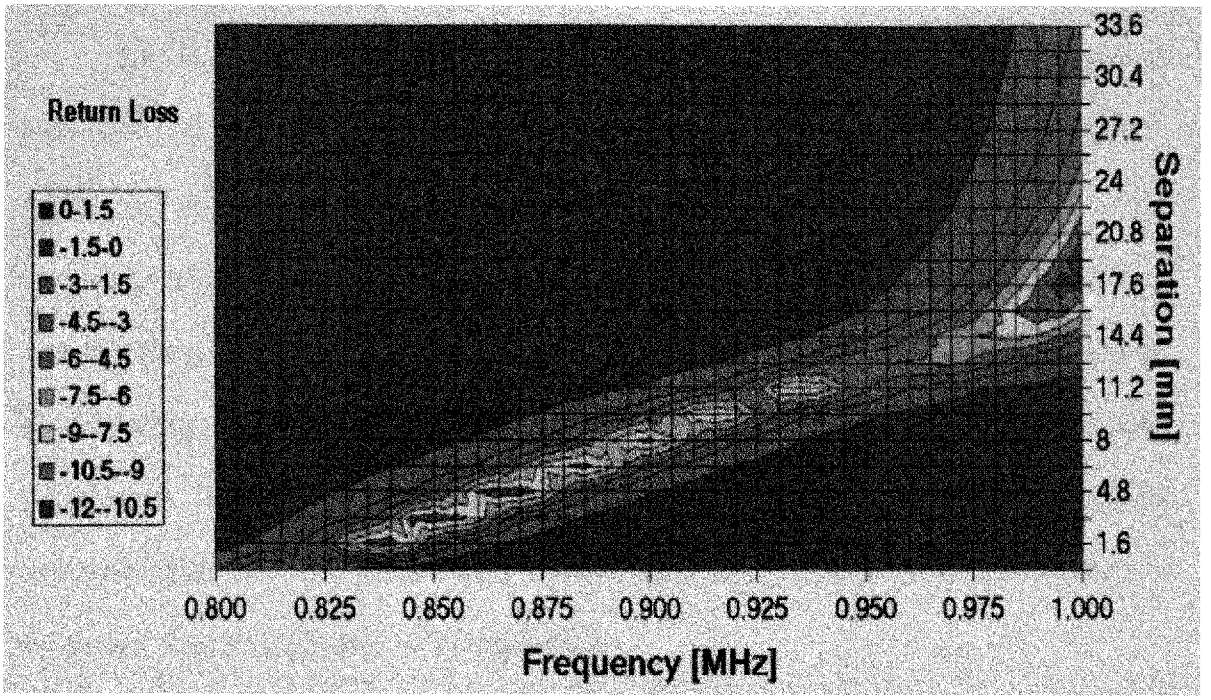

Fig. 7. Return loss of the "Ferris Wheel," achieved by using the tunable exciter to optimize the impedance match to the 50- feed line [3].

CHAPTER III

RF DOSIMETRY

RF interactions with biological materials are complex functions of numerous parameters [8]. These interactions produce highly non-uniform distributions of EM fields within the object, which are related to the dielectric properties and the density of the tissue regardless the external exposure field uniformity. Dosimetry studies are done to quantify these electromagnetic interactions. Radio waves in free space are characterized by frequency, intensity of electric (E) and magnetic (H) fields, their direction, and polarization. The internal fields and currents are related to the incident external and magnetic fields in a very complicated manner. The results obtained from animals cannot be always directly applicable to human beings.

The RF interactions as well as the resultant deposition of microwave power in the body are measured in terms of Specific Absorption Rate (SAR). The mass normalized rate of energy absorption or dose rate was introduced to microwave research in the late 1960s formerly known as "absorbed power density". This parameter was officially designated Specific Absorption Rate (SAR) by the National Council on Radiation Protection and Measurements [11].

Definition

Specific Absorption Rate (SAR): the time derivative of the incremental energy *(dW)* absorbed by an incremental mass *(dm)* contained in a volume element *(dV)* of given mass density (ρ)[11].

SAR is measured in Watts per kilogram (W/kg) of body mass, which represents the RF absorption rate in body tissue [8]. SAR is the parameter used by government regulatory agencies to determine compliance with non-ionizing radiation hazard standards.

The power absorption usually takes place in a confined body region, as in the case of the head exposed to a cellular phone, even if the (SAR_{WB}) is well below the basic limit, the local SAR can assume rather high values. In the frequency range of 100 kHz to 6-10 GHz, SAR is the relevant dosimetric quantity. SAR is a quantity that describes the amount of absorbed energy for a specific material at a certain frequency. For the purpose of radiation protection, dosimetric quantities are needed to estimate the absorbed energy and its distribution inside the body. Regulatory agencies have established Specific Absorption Rate guidelines, standards and test procedures to define SAR levels that can be safely absorbed by the body.

The value of 4 W/kg Whole-Body SAR is accepted worldwide as the threshold for the induction of biological harmful effects [9]. Up to now, the most recognized RF exposure standards adopt the SAR, averaged over the Whole-Body (SAR_{WB}), as the basic parameter to establish the safety of an exposure [10]. According to the ANSI/IEEE (*American National Standard Institute/Institute of Electrical and Electronics Engineers*) standard the maximum SAR averaged over 1 g should not exceed 1.6 W/kg and that the Whole-Body mass averaged SAR should not exceed 0.08W/kg for uncontrolled environments.

3.1 Equations Relating Specific Absorption Rate (SAR)

The Specific Absorption Rate limits have been defined in different ways but all of them are related to the same basic principle of transferring energy from electromagnetic fields to an absorbing object. The quantity can also be derived from either the temperature gain or from an electric field.

SAR defined in terms of energy as the time derivative of the incremental energy absorbed by (dissipated in) an incremental mass contained in a volume of a given density

SAR is simply defined as the mass averaged rate of energy absorption in tissue

$$SAR = \frac{d}{dt}\left(\frac{dW}{dm}\right) = \frac{d}{dt}\left(\frac{dW}{\rho dV}\right) \tag{3.1}$$

and is related to the internal E-Field by

$$SAR = \frac{\sigma}{\rho}E^2 \tag{3.2}$$

where σ is the conductivity of the tissue in S/m,

ρ is the mass density in kg/m^3,

and E is the rms electric field strength in V/m.

Thus, SAR is a measure of the electric field, and indirectly the magnetic field and current density at the point of interest [11].

Also SAR is a measure of the local heating rate *dT/dt*, which in terms of relation is

$$\frac{dT}{dt} = \frac{SAR}{c} \quad °C/s \tag{3.3}$$

where *c* is the specific heat capacity of the tissue in J/kg/°C.

ΔT is the temperature change in °C,

Δt is exposure time in seconds

This assumes "ideal" thermodynamic circumstances, i.e., no heat loss by thermal diffusion, heat radiation, or thermoregulation (blood flow, sweating, etc.). The SAR distributions are quite complicated even when resulting from plane-wave exposure. Depending upon the size and orientation of the animal and the frequency, it is possible that one or more SAR peaks ("hot spots") could occur.

3.2 Localized and Whole-Body SAR

There are two types of SAR measurements:

1. Localized SAR
2. Whole-Body SAR

Localized SAR is a measure of the rate of energy absorbed by (dissipated in) an incremental mass contained in a volume element of dielectric materials such as biological tissue [12].

$$Localized \quad SAR = \frac{d}{dt}\left(\frac{dW}{dm}\right) = \frac{d}{dt}\left(\frac{dW}{\rho dV}\right) \tag{3.4}$$

It is called the Localized SAR because it changes from point to point according to the dielectric properties of the absorbing object and the distribution of dissipated RF energy.

Average SAR is defined as the rate of change of total energy stored in the volume integral of the absorbing object divided by the total mass of the body [10]. This Average SAR is also commonly known as Whole-Body SAR

$$Average \ SAR = \int_v PdV / M \tag{3.5}$$

Both Whole-Body and Localized SAR's are expressed in terms of watts per kilogram (W/kg) or milliwatts per gram (mW/g).

3.3 Factors that Determine the Value of SAR

The following factors and conditions have an influence in heat absorption of a biological object, which determine the value of SAR [8].

Dielectric Properties

The magnitude and special distribution of EM fields within the biological tissues depend on the dielectric properties of the tissue (dielectric constant and conductivity).

Tissue Structure

The highest local SAR is usually at or near the surfaces of an externally exposed object. In general absorbing tissue material is a complex biological system consisting of multiple layers of tissue. When exposed to the field propagates thorough these layers of tissue, a portion of energy is reflected from each boundary, and a portion is transmitted into the next layer. The amount of transmission and reflection at each boundary depends on the difference in dielectric properties of the tissues at that layer.

Tissue Orientation and Field Polarization

It has been shown both theoretically [13] and experimentally [14] that the SAR in a exposed object is maximal when the long axis of the body is parallel to the direction of a uniform external electric field. For some cases the average SAR in a human body is about 20 times higher than that occurring when the electric field is perpendicular to the long axis of the model.

Field Frequency

Dielectric properties, the field strength and spatial distribution of internal fields also vary with frequency.

Source Configuration

The most important conditions of the exposure field is whether it is a *far field* or *near field* The far field extends from a certain minimum distance from the source to infinity. In this region the field has predominantly plane–wave character i.e., E fields and H fields are spatially uniform and mutually perpendicular. The far field typically begins at a distance of $(2D^2/\lambda)$ from the radiating source, where D is the longest dimension of the radiating structure.

Exposure Environment

The quantity of energy absorbed by a body in the RF field depends on environmental factors like free space, on ground plane, near metal reflectors, metallic conductive structures like waveguides. Metal implants can cause intense modifications in SAR distribution in the exposed object.

Time-Intensity Factors

Exposure duration and external field strength are very important parameters that determine the total amount of energy absorbed.

Specific heat capacity (c)

The amount of heat absorbed by a tissue material depends on the specific heat capacity of the tissue.

Methods for Determination of SAR

The SAR measurement is very important in terms of dosimetry. Different procedures were used to measure SAR in terms of heat absorbed and temperature raise and E-fields according to the equations in section 2.2. The methods employed for dosimetry studies are as follows [12]:

1) Calorimetric technique to quantify the average or Whole-Body SAR in the whole object.
2) Power balance methods to quantify Whole-Body SAR.
3) Measurement of Localized SAR using Thermometric or Temperature probes.
4) SAR distribution patterns in biological object by Thermography.
5) Implanting E-field probes to measure the Local SAR.
6) Simulations in an electromagnetic simulation codes like Microwave Studio and XFDTD.

CHAPTER IV

SAR MEASUREMENT TECHNIQUES

This Chapter discusses some other methods that help in determining the Whole-Body SAR and Localized SAR. Whole-Body SAR can also be measured by the help of differential power technique which is a very simple straight forward measurements of forward and reflected power into the system also known as the power balance method for SAR measurements.

SAR distribution patterns and the Localized SAR in biological object can be analyzed by the SAR thermography and thermometric techniques. Both these procedures are employed to determine the SAR distribution in the sagittal plane of the mice. It also helps in making the absolute SAR in some organs of interest like the brain, belly etc.

In a thermography procedure the SAR distribution patterns are analyzed using an infrared camera that scans the temperature reading on flat surface. Thermometric measurements are made on the biological tissue to observe the temperature variation inside the load by using temperature probes. A Luxtron fiber optical temperature probe, which is transparent to the electromagnetic field, is placed between the two halves to sense the temperature. For both procedures the mouse is encapsulated in a Styrofoam holder where it is frozen after that and cut along the sagittal plane. E-field probes are also used to measure SAR values from point-to-point in a simulated phantom.

4.1 Differential-Power Technique

The Whole-Body SAR in the loads of the Ferris Wheel can be obtained by dividing the power dissipated in the loads by their mass. A directional coupler and two power meters to read forward and reflected powers into the port of the Ferris Wheel exposure system. This method is based on the power balance of the system and thus, it is important to obtain these power readings precisely.

The power balance equation is,

$$P_{loads} = (P_{inc} - P_{ref}) - (P_{\Omega} - P_{rad}) \tag{4.1}$$

states that the power dissipated in the mice can be found by measuring the incident P_{inc} and reflected P_{ref} power at the cavity port, and estimating the ohmic losses in metal and dielectric losses in plastics P_{Ω} and the radiated power P_{rad}. The first two contributions are measurable throughout the exposure using a bi-directional coupler. The ohmic and dielectric losses have been estimated measuring the return loss and the power radiated by the unloaded cavity at 900 MHz in an anechoic chamber and the missing power accounted for is about 1% of the incident power [3].

Assuming that the loss of energy due to ohmic effects and radiation do not vary significantly over relatively wide changes of the loading conditions [3]. Therefore, the amount of power dissipated in the loads can be determined just by monitoring bi-directional power flow, so that the collective Whole-Body average SAR is

$$SAR_{Dummy} = \frac{P_{Dummy}}{m_{Dummy}} = \frac{P_{inc} - P_{ref} - (\alpha_{\Omega} + \alpha_{rad})P_{inc}}{m_{Dummy}} \tag{4.2}$$

where, $\alpha_{\Omega} \approx 0.01$, $\alpha_{rad} \approx 0.01$ and m_{Dummy} is the total mass of the 40 loads.

The dummy load was a 30 cm^3 plastic bottle filled with tissue-simulated liquid (water: sugar: salt: hydroxethylcellulose ~53.5:44.25:1.15:1 weight wise) of 37 grams, which is equivalent to 30g mice, are used as loads [3].

The determination of the Whole-Body SAR using this technique is quite accurate but mainly relies on power measurements. The assumption here is that the dissipated RF power is equally spread among the dummy loads, which may not be the case due to some asymmetry in positioning of these dummy loads. The accuracy of these measurements can be improved by collecting the forward and reverse power meter reading with the help of Lab View data acquisition software. Controlling temperature of the couplers and power meter heads also improves the stability of the measurements. A number of experiments were done using the simulated tissue bottles as loads at different positions on the FW. The average normalized SAR obtained is 0.66 W/kg/W.

But since we are using a dummy load which is equivalent to mice in terms of dielectric properties but not in terms of average density. Assuming the dummy load as real mice, the Whole-Body SAR in the mice by taking into account the difference in density is

$$SAR_{WB-Mice} = SAR_{Dummy} \frac{\rho_{Dummy}}{\rho_{Mice}} \tag{4.3}$$

where ρ_{Dummy} and ρ_{Mice} are the average density of dummy load and mice respectively [3]. The ratio of the densities between dummy load to that of mice is about 1.25. Therefore, the average normalized SAR obtained is 0.8 W/kg/W.

4.2 Thermography

The SAR distributions in the biological objects are complex. A scanning infrared thermographic camera can be used to provide detailed SAR distribution or temperature distribution in tissue equivalent phantom models or animals exposed to the high RF radiation fields in a short time. Suitable material to separate sections of the phantom or cadaver must be used, and readout after termination of exposure must be rapid. If the output of the thermographic camera is put into a computer, average SAR can be easily computed using special software codes [15].

A model of an animal or other object is made of tissue equivalent materials and cut along planes whose two-dimensional SAR (temperature) distribution is to be determined. To avoid water loss from the material, the open surfaces are covered with a very thin (0.05 mm or less) polyethylene film [15]. A frozen animal is cast a Styrofoam block, bisected, covered with polyethylene film and equilibrated to the room temperature. During exposure, the bisected halves are joined. The model or cadaver is then exposed under specific test conditions for a pre-determined limited time to a high-intensity field. The parts quickly are separated and the internal surface of one of the halves is immediately scanned with an infrared thermal camera. To obtain the temperature or SAR information undistorted by thermal conduction, the exposure time and the delay between taking thermal scan must be minimized. The delay and the recording time must be no longer than 10 seconds [8]. Large temperature gradients should be avoided, as they will result in thermal conduction; gradients of 5 to 10 degrees C are normal.

This technique has proven valuable in assessing SAR distribution for laboratory animals and models of man and was first introduced by A.W. Guy and has gained worldwide acceptance [8]. The procedure involves using a thin sheet of plastic to facilitate separating the halves of the phantom; thus the procedure was limited to top and bottom slots in the Ferris Wheel to have a exposure to linearly polarized field (E-field parallel to the interface) in order to avoid interrupting induced currents that would normally flow perpendicular to the median plane of separation.

Thermographic Imaging Procedures:

1. For thermographic procedure it is needed to prepare the mice for taking the thermo graphic pictures using a thermal camera. This process is called `Foaming & Cutting`. The Styrofoam mixture is prepared using equal quantities of A & B solutions. The thawed mouse is properly aligned with reference axis in a cylindrical mould with open top and closed bottom. The mixture is poured into the mould so that the foaming takes place. The obtained mouse with the foam is allowed to solidify and then refrigerated so that it can be cut easily using an electrical saw [16].
2. Now it is ready to test the mice by wrapping each half of the mouse with silk screen/plastic wrap. Place both halves of the mouse (the two slides) on their flat surfaces and are allowed to thaw to room temperature. Now they are ready for taking thermal pictures. One of the halves is placed on the apparatus made up of styrofoam, which allows the flat surface of the mice half facing parallel to the thermal camera.

3. Take a picture by connecting the thermographic camera's processing unit to a PC loaded with Lab View data acquisition software created for collecting data from this camera through the General Purpose Interface Board (GPIB) card slot. Start up the Lab View software and run the data acquisition software. Turn the data acquisition on and capture an image. This first image data file that will be used in post-processing.
4. During the exposure, the bisected halves are joined and are placed in top or bottom slots of the Ferris Wheel exposure system. The exposure inside the Ferris Wheel is done at high RF power (300 W) for determined amount of time (30 seconds) and one of the halves (used before) is place back onto apparatus immediately. The data acquisition is started immediately as above outlined to take the picture of the exposed mouse. This will be the second image. Fig.8 shows an illustrative example of mice and the gradients of temperature are shown as different colors.
5. Since the image files are in terms of temperature measurements of each pixel of the image files, the differential of the above two taken picture files or picture should result in the temperature gradients in the mouse. A special software written in FORTRAN code helps in making the differential can run program to process the before and after shots into one picture that shows the differential. Fig.9 shows the resultant differential picture and different color lines show the temperature increase in the tissue of the mice.

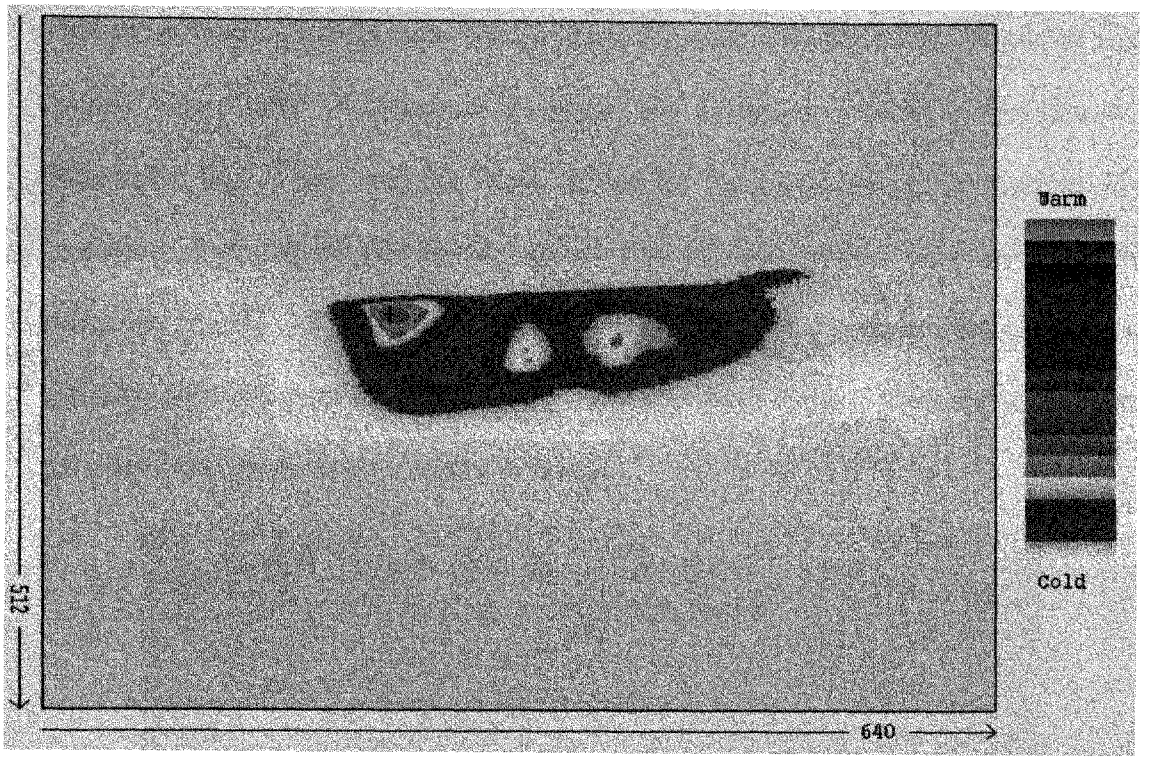

Fig.8. Thermal image showing the temperature distribution after exposure [16].

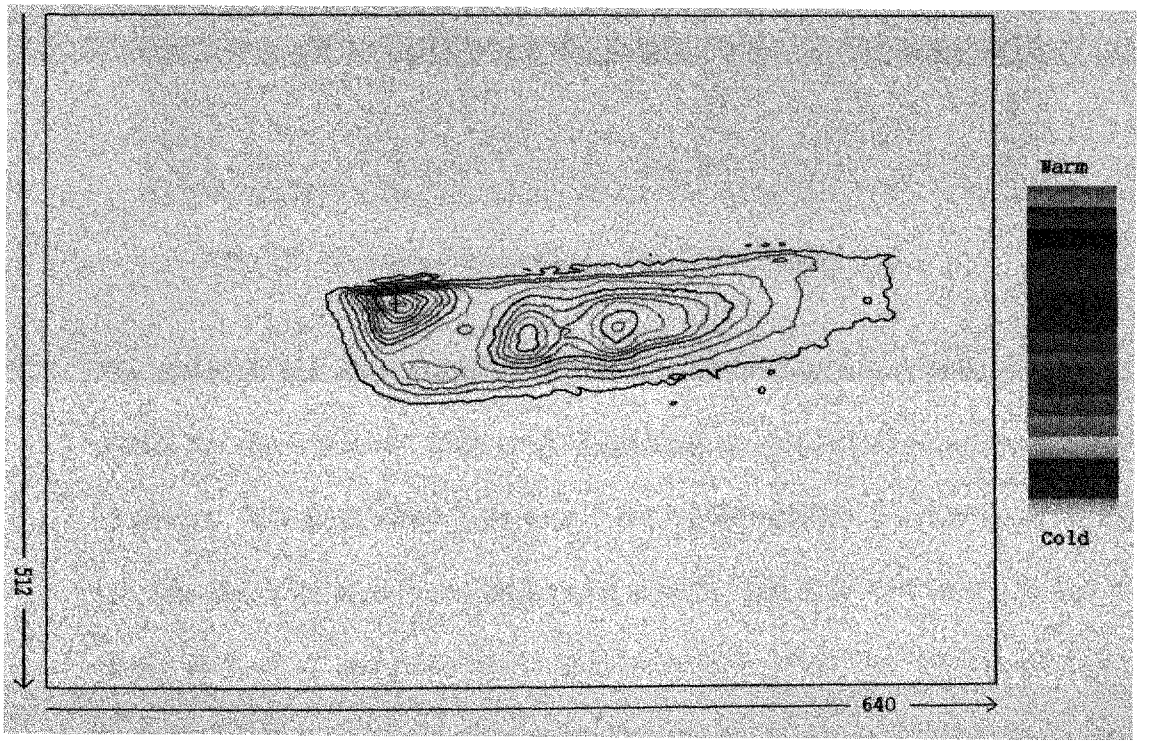

Fig.9. Differential image showing the heat counters and hot spots inside mouse [16].

This software can process many sets of image files into corresponding differential files (ofiles). The "ofile" designation is simply the designation used to describe the differential file. These will be used in further data processing. A colored line represents each degree of variation across the collected images. The increments of color line can also be set to half or quarter degree. Fig.10 shows the heat counters of the mice obtained from the differential picture overlapped on the original picture taken for one of the halves using a digital camera.

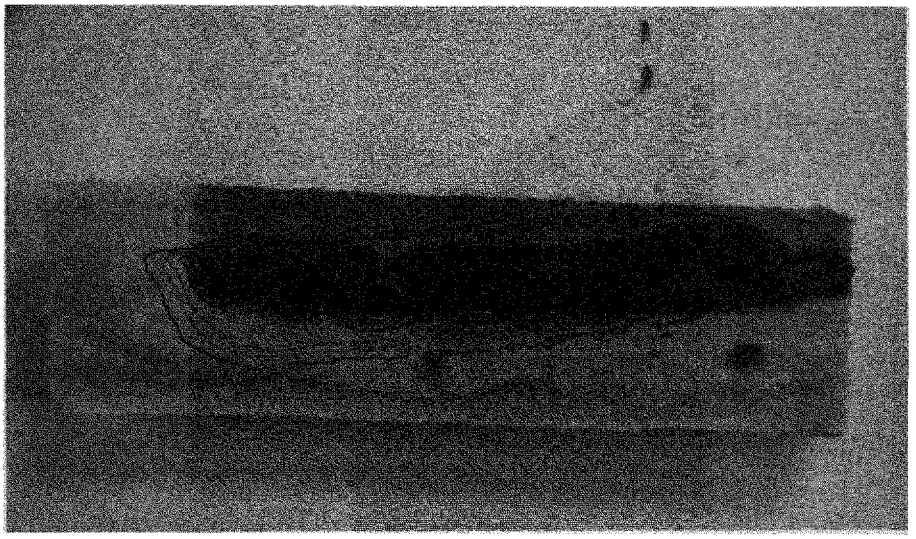

Fig.10. Mouse picture with the Thermal contours [16].

6. The software not only makes a differential picture but also a SAR distribution profile for the exposure. This is the final stage of the software program is also known as "The Big Picture", because it has six different plots as shown in the Fig 11. The first plot shows the differential picture with four reference axes points named as A, B, C and D on the differential thermal scan. The software according to the temperature raises in the picture allocates the locations of these axes on the scale.

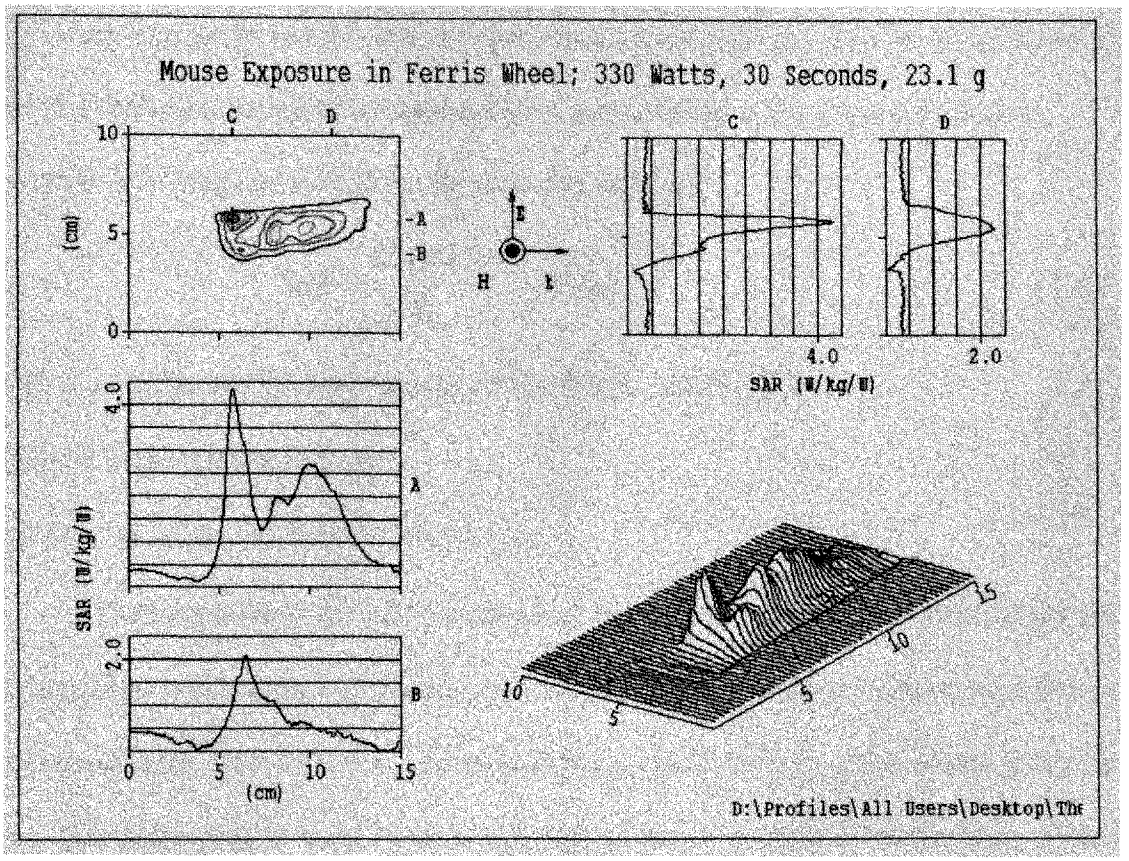

Fig.11. SAR Distribution Profile [16].

The four small graphs show the one-dimensional SAR distribution pattern about their respective axis. The last graph is a two-dimensional SAR distribution pattern obtained by a simple combination of two of these four graphs. The cross hair in the picture shows the highest hot spot location in the mouse. SAR values obtained from the thermographic procedure are normalized to the input power. The peak Normalized SAR at head for the above example is 4.0 W/kg/W.

4.3 Thermometry

As long as the tissue temperature increases linearly during short-term exposure to high-RF radiation, SAR can be obtained from thermal or temperature measurements using the following equation [8] as discussed in section 2.2

$$SAR = \frac{C_H \Delta T}{\Delta t} \qquad (W/kg) \tag{4.4}$$

where C_H is the specific heat capacity of the tissues (kcal/kg °C)

ΔT in °C is the temperature rise

and Δt is the exposure duration in seconds

The temperature rise can be measured at a particular point of interest, taking into account heat conduction for the time period Δt. Thus, by employing above equation we can calculate the SAR that would be assessed by a non-perturbing probe at that point. The term non-perturbing is used here as opposed to the conventional temperature probes, which not only might interact with the electromagnetic field but also measure the mean temperature of a discrete volume, introducing further errors in the experimental assessment of SAR [15].

SAR measurements with Temperature Probes

The difficulty of measuring temperature in electromagnetic fields with many conventional thermometers stems form three types of interaction between the thermometer and the field. They are electromagnetic interference (EMI); direct heating of temperature sensor, and perturbation of the field by the thermometer. Placing the leads of the sensor perpendicular can minimize the interference and induction pick-up to the E-field. Magnetic induction pick-up is reduced when the leads are slightly twisted [12]. Out

of several types of non-perturbating temperature probes have been developed Vitek probe [BSD Company, Salt Lake City, Utah] and Luxtron probes [Luxtron Corporation, Santa Clara, California] are used.

4.3.1. Thermal SAR Measurements on Dummy Loads

The experimental setup comprises of the "Ferris Wheel" loaded with dummy equivalents, with one of the dummies encapsulated in a styrofoam shell as shown in Fig.12.

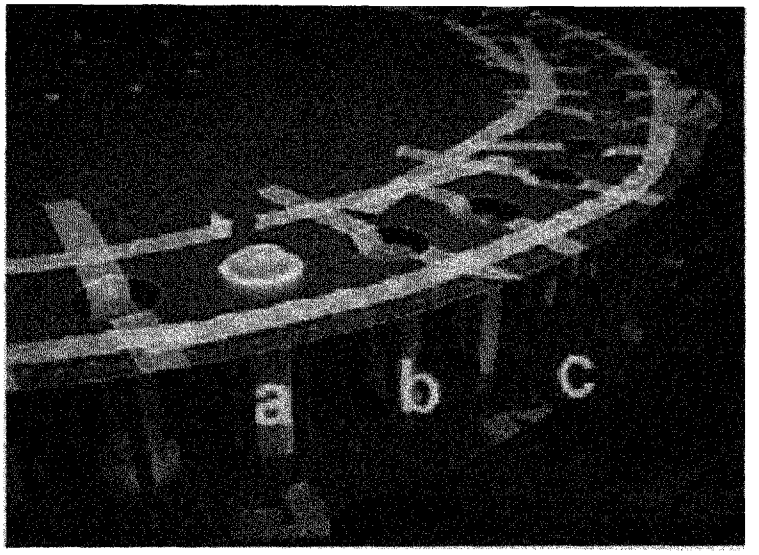

Fig.12. Experimental setup for thermal SAR measurements using Vitek thermistor probe [3].

A Vitek-101 thermistor probe is inserted through a small hole into the solution of the dummy bottle containing the tissue equivalent solution. A short high-power RF exposure of 30 W for 2 min induces a temperature rise in the dummy. The dummy is vigorously shaken after exposure to equalize the temperature throughout so that the average temperature increase reading can be recorded regardless of the actual position of

the thermistor inside the dummy [3]. Assuming the heat loss exchange to the external environment is negligible due to of the styrofoam enclosure, the difference between the final and initial average temperature in the dummy is proportional to the dissipated RF power, therefore,

$$SAR_{Dummy} = \frac{C_{Dummy} \cdot \Delta T}{\Delta t} \qquad (W/kg) \qquad (4.5)$$

where C_{Dummy} is the specific heat of the particular tissue-equivalent solution used and is equal to 2.8 J/g/K that was employed, and Δt is the exposure duration.

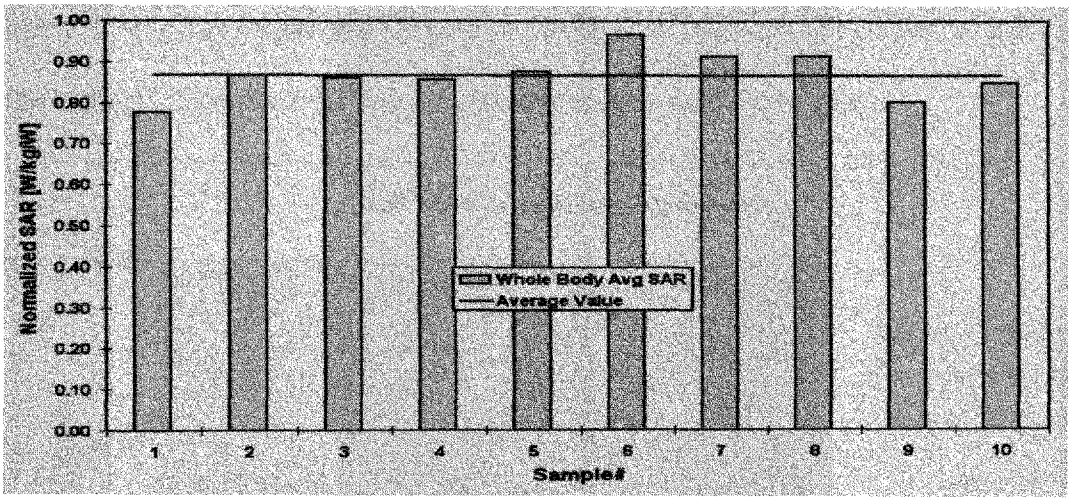

Fig.13. Normalized thermal SAR measurements of dummy Loads using Vitek probe [3].

Fig.12 shows the details of the experimental setup, while Fig.13 reports the results of ten thermal measurements performed on dummy equivalents, given in terms of the fraction of the incident power.

The Normalized thermal SAR is the Fraction of the incident RF power that is dissipated or absorbed in the dummy load. The obtained Normalized thermal SAR measurements are performed on 30-g dummy equivalents. Averaged Normalized SAR is about 0.85 W/kg/W.

4.3.2. Thermal SAR Measurements on Mice

As discussed in the previous section, the mice used thermography is also used for making thermal measurements during the exposure time. Three temperature probes (Vitek/Luxtron) were placed at position of interest like the brain, neck and belly where the local hot spot locations are usually found using thermography. The thermography process helps in recognizing the hotspot locations so that the probes are placed at that point approximately. The Localized SAR in these regions is calculated from the rate of temperature rise during the exposure as per the above equation (4.4). Fig.14 shows the linear raise of the temperature raise at the position of interests. The equation and slope for the highest temperature raise at the position of interest were computed.

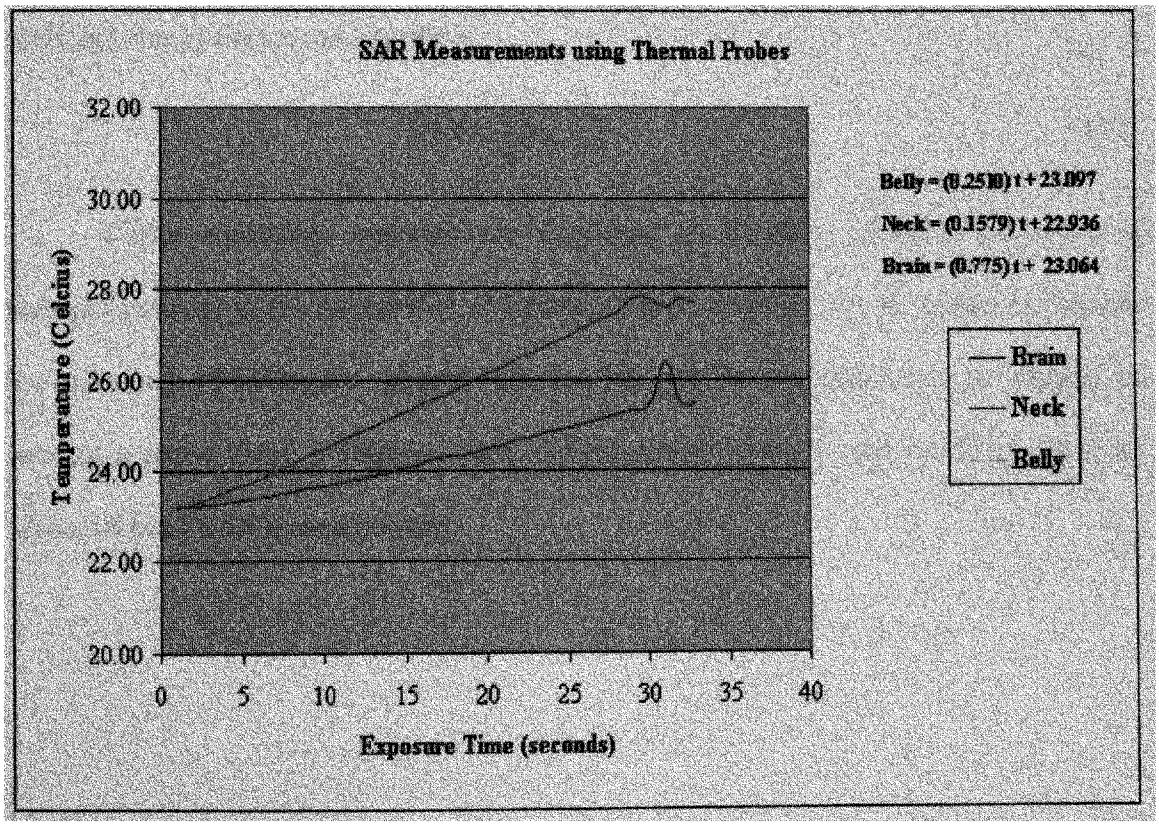

Fig.14. Linear raise in temperature at the positions of interest [16].

The Normalized SAR is obtained as follows

$$N - SAR = (C_{Mice} \cdot Slope) / P_{Net} \tag{4.6}$$

where C_{Mice} is the specific heat of mice and is equal to 3.2 J/kg/°C,

Slope is the ratio of ΔT raise in temperature and t is the time of exposure.

P_{Net} is the net power applied during the exposure period.

In this particular case the temperature raise is high in belly with a slope of 0.2510. Normalized SAR value at this point of interest is 2.41 (W/kg/W) [16].

4.4 E-field probe

An E-field can be measured at a point or points with in the tissue equivalent "phantom" model or a biological system by an E-field probe [8]. The equation relating SAR and rms E-field measurement is

$$SAR = \frac{\sigma}{\rho} \left| E_{rms}^{\ 2} \right| \tag{4.7}$$

Tissue equivalent materials are developed to simulate dielectric properties of biological tissues at the frequencies of interest. These materials can be shaped to simulate the geometry of biological objects. The E-field with in the object can be mapped by moving a probe along a selective path. E-field probes provide most sensible and direct means of local SAR measurements.

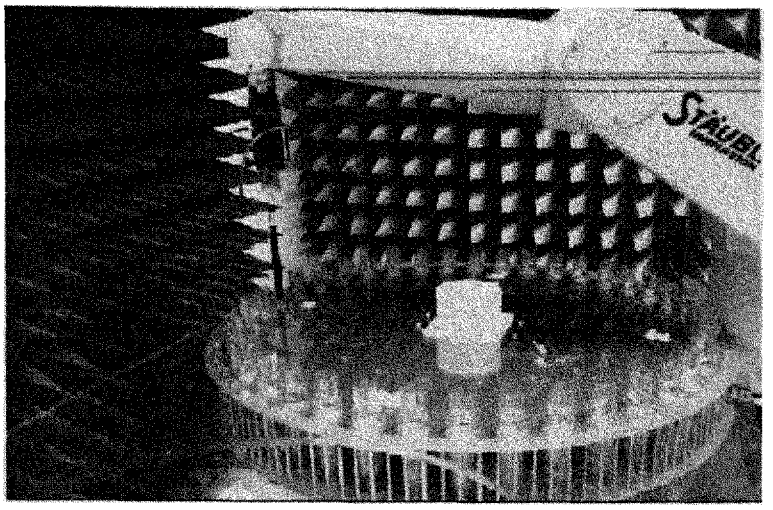

Fig.15. Experimental setup for E-field measurements inside the restrainer.

The E-field probes usually use three small orthogonal dipole antennas to provide isotropic measurements to determine the SAR using E-field probes accurately the probes must be calibrated. The E-field measurements through the middle of the dummy load at four different positions i.e., Top, Bottom, Left and Right of the "Ferris Wheel" are measured by using E-field probes with small 1-mm tip diameter. The arrangement for the measurements using the DASY Robot is shown in Fig.15.

The E-field distribution along the Z-axis through the middle of the dummy is found to be symmetrical at all the positions of interest. It is found that the distributions at open end is small and increases to the peak in the middle of the cavity as shown in Fig.16. The deviation in the peak SAR obtained between Top and Bottom positions is 1.25 dB and to that of the Left and Right is about –0.5dB.

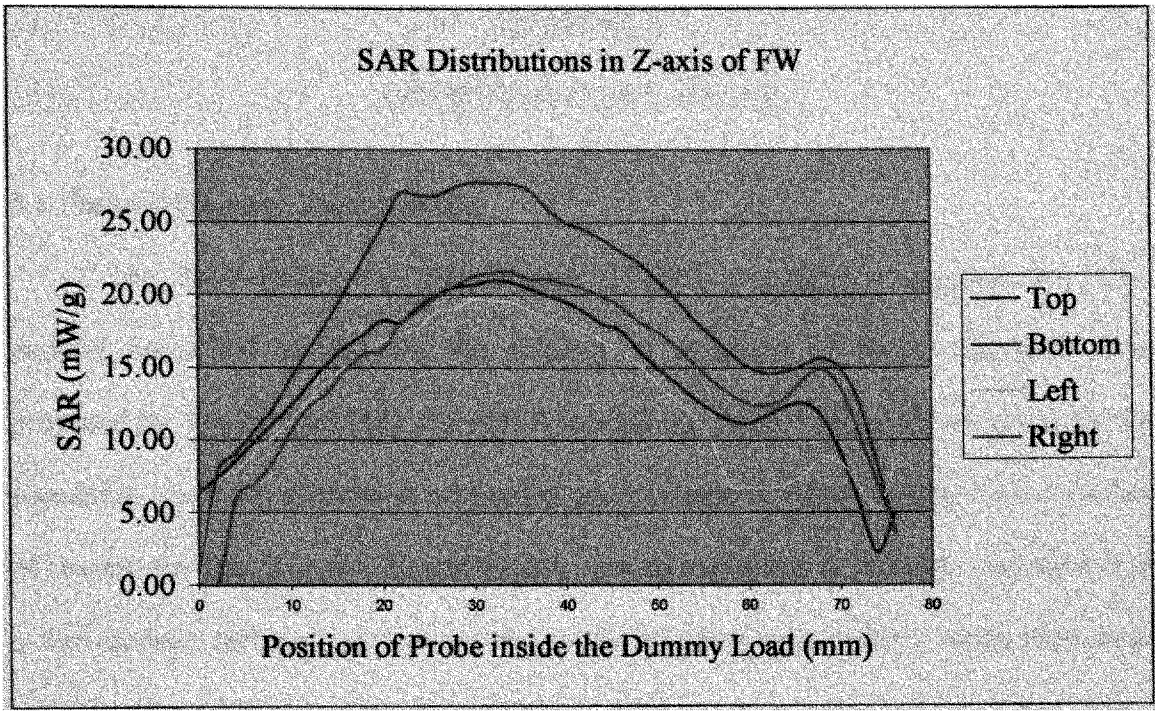

Fig.16. E-field distribution through the dummy along z-axis in the FW reference plane.

CHAPTER V

COMPUTER SIMULATIONS

5.1 Finite-Difference Time Domain

The Finite-Difference Time-Domain (FDTD) technique is arguably the most popular numerical method for the solution of problems in electromagnetics. First proposed by Yee in 1966 [17], the FDTD method has existed for nearly 30 years, and its popularity continues to grow as computing cost continue to decrease. There are a number of reasons for this; it is easy to understand, easy to implement in software, and since it is a time-domain technique, it can cover a wide frequency range with a single simulation run.

The Yee cell is the basis of the FDTD numerical method and usually is a three dimensional cube in which the permittivity, permeability and conductivity of the material surrounded by the perimeter of the cube is defined. For the Ferris Wheel exposure system the Yee unit cell is defined in terms of cylindrical coordinates [17]. Any electromagnetic field (E and H vectors) that impinges on one face of the unit will be scattered or absorbed within the cell depending upon the characteristics of the cell, the remainder of the field will be propagated to other faces. When two or more cells are neighbors, the propagated field on the face of one cell becomes the impinging field of the next cell ie., becomes the boundary conditions for next cell.

Maxwell's (differential form) equations are simply modified to central-difference equations, discretized, and implemented in software. The electric field is solved at a given

instant in time, then the magnetic field are solved at the next instant in time, and the process is repeated over and over again [17].

A simple description on the operation of this method is discussed. When Maxwell's differential form equations are examined, it can be seen that the time derivative of the E field is dependent on the Curl of the H field. This can be simplified to state that the change in the E field (the time derivative) is dependent on the change in the H field across space (the Curl). This results in the basic FDTD equation that the new value of the E field is dependent on the old value of the E field (hence the difference in time) and the difference in the old value of the H field on either side of the E field point in space.

Naturally, this is a simplified description with the constants omitted. The H field is found in the same manner. The new value of the H field is dependent on the old value of the H field (hence difference in time), and also dependent on the difference in the E field on either side of the H field point. This description holds true for 1D, 2D and 3D, FDTD techniques.

However, when multiple dimensions are considered, the difference in space must be considered in all appropriate dimensions. In order to use the FDTD, a computational domain must be established. The computational domain is simply the 'space' where the simulation will be performed. The E and H fields will be determined at every point within the computational domain. The material of each cell within the computational domain must be specified. Typically, the material will be either free-space (air), metal (perfect electrical conductors), or dielectrics; any material can be used, as long as the permeability, permittivity, and conductivity can be specified.

Once the computational domain and the grid material are established, a source is specified. The source can be an impinging plane wave, a current on a wire, or an electric field between metal plates (basically a voltage between the two plates), depending on the type of situation to be modeled. Since the E and H fields are determined directly, the output of the simulation is usually the E or H field at a point or a series of point within the computational domain.

Since the Ferris Wheel system has a cylindrical geometry, as shown in Fig.3 the FDTD code is developed in cylindrical coordinates. The below figure shows the FDTD cell used in cylindrical co-ordinates.

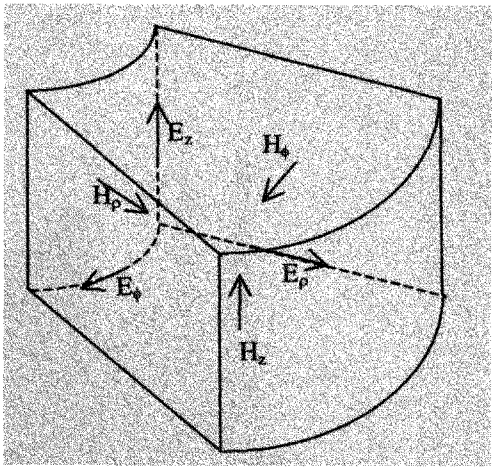

Fig.17. FDTD Cylindrical unit cell [7].

Inside the empty cavity, the TEM field components can be expressed in the cylindrical reference as from the above equations; we notice that when the mice are placed inside the cavity, they can be considered exposed to an incident TEM-like wave. The mice are placed with their body axis at 44 cm from the "Ferris Wheel" center, so their axis is co-polarized with the incident electric field. Such a position enhances the efficiency of the cavity [7].

As the mice tissue is complex, heterogeneous and has a non-uniform body they change the incident field characteristics and alter its uniformity. Equations (2.6) and (2.8) cannot be employed to assess SAR uniformity inside the animal. On the other hand, SAR measurements everywhere inside the animal are extremely difficult, if not impossible. For this reason an FDTD simulation code is necessary developed to perform the analysis. The analysis is performed at 900 MHz with dummy loads into the cavity.

5.1.1 Simulation for Radial E-field for Ferris Wheel at 900 MHz

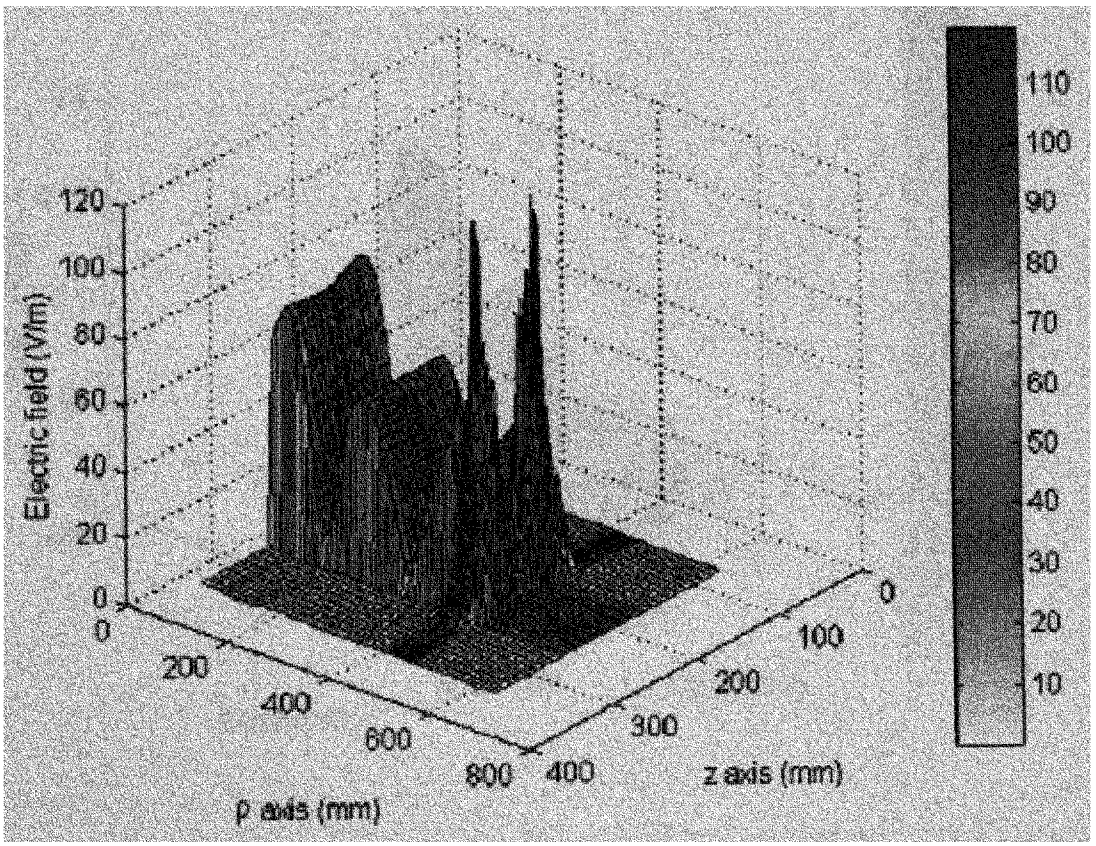

Fig.18. Distribution of the total electric field inside the cavity for the ρ-z cut through the middle of the dummies at 900 MHz [7].

Fig.18 shows the E-field distributions inside the loaded cavity along the ρ-Z cut through the middle of the dummy. The figure also shows the standing wave formed inside the loaded cavity due to the shorting posts. The field amplitude decreases as it penetrates the dummy but increases gain at the other side of the dummy because of wave reflection at the shorting posts. The input power is about 50 mV in this simulation.

5.1.2 Simulation for SAR Distribution Inside the Dummy Load at 900 MHz

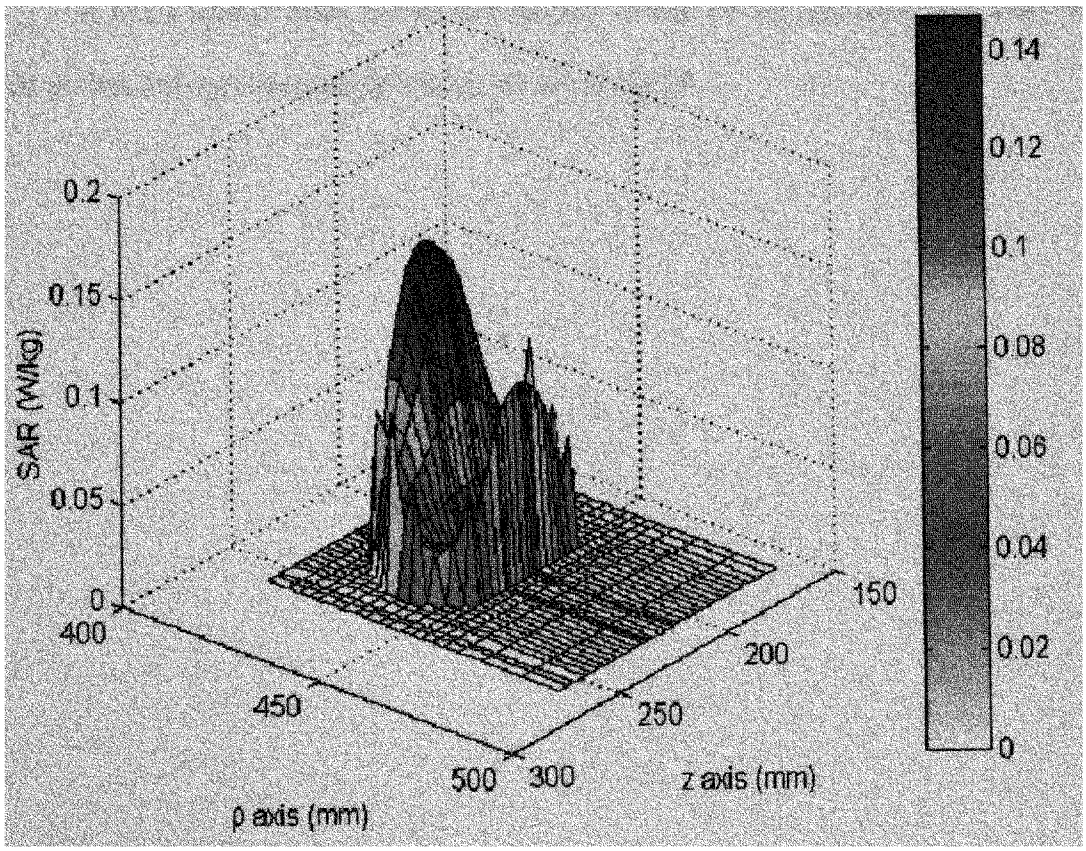

Fig.19. SAR distribution inside the dummy for the ρ-z cut through the middle of the dummies at 900 MHz [7].

Fig.19 shows the simulation for the SAR distribution inside the dummy load at 900 MHz. It can seen that SAR at the open ends is smaller and increases to the maximum at the center. This increase in the SAR distribution at the center is due to the shorting posts placed at 40 mm from the center of the restrainer. The center of the dummy load is at 440 mm and the shorting posts are placed at 480 mm from the exciter of the Ferris Wheel respectively. The maximum peak SAR inside the dummy is 0.145 W/kg and the Whole-Body average SAR is 0.041 W/kg.

It has a similar SAR distribution pattern to that of the measured with help of E-field probes through the dummy load as shown in Fig.16.

5.2 Experimental validation for XFDTD Simulations

In order to validate the FDTD code, experimental measurements are done by loading "Ferris Wheel" with forty dummy bottles with dielectric parameters of the dummies bottles are ε_r=52 and σ=1 S/m [17]. A miniature field probe is inserted between the shorting posts and measuring the radial E-field distribution. The miniature probe features three small dipole sensors with rectifying diode detectors placed along three orthogonal directions in the so-called I-beam arrangement as shown in the Fig.20 below [18].

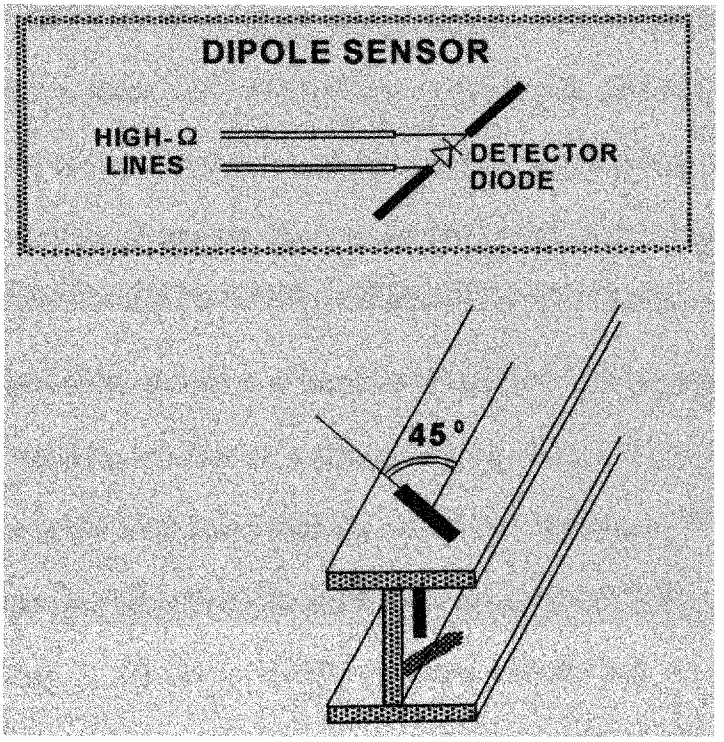

Fig.20. Sketch of the miniature electric field probe, realized in the I-beam configuration, used for the measurements inside the "Ferris Wheel" at 900 MHz [7].

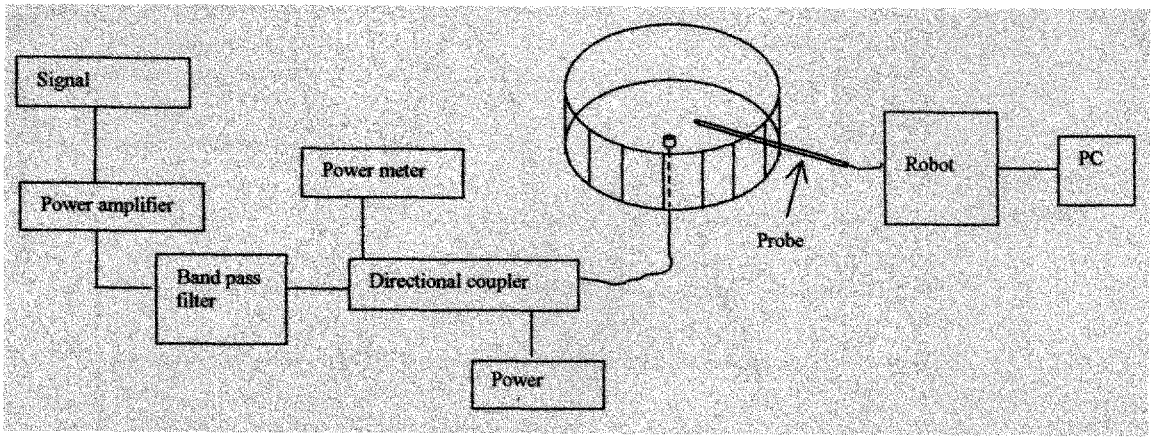

Fig.21. Measurement set-up for the radial distribution of the E- field at 900 MHz. [7]

The miniature probe was connected to an automated data acquisition system by IDX, Inc. Forward and reflected power were measured at the "Ferris Wheel" feed-point by means of a bi-directional coupler. The experimental set-up is sketched in Fig.21.

5. 2.1. Comparison of Measured and Simulated Radial E-field at 900 MHz

For best matching conditions, a comparison between the measured and calculated radial distribution of the total field inside the cavity were performed. The results reported in Fig.22, which are normalized to the same net input power (0.3 W), show a very good agreement. Looking at the radial VSWR, they also indicate that the structure stores a good amount of reactive energy, as confirmed by its relatively narrow impedance bandwidth.

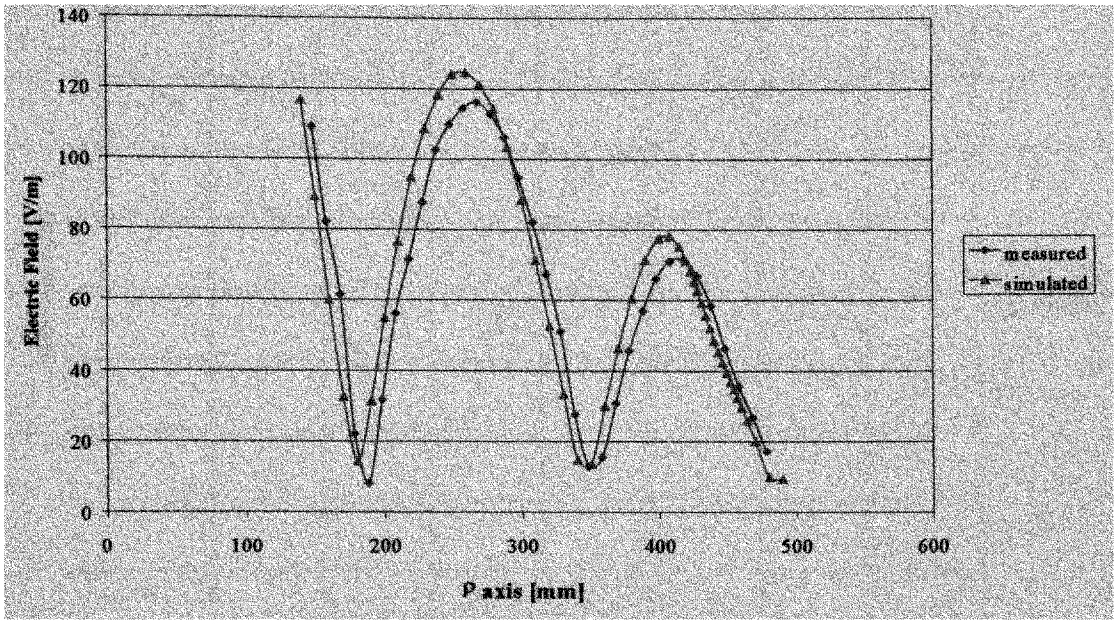

Fig.22. Comparison between the simulated and measured total electric field radial distribution at 900 MHz [7].

5.2.2. Comparison between Measured and Simulated Return Loss

The Simulations computed for cavity's return loss at 900 MHz to a 50-ohm source, for different positions of the tuning counterpoise show good correlation with the measured return loss. In Fig. 23, a comparison between measured and simulated return loss versus counterpoise position shows good agreement [7]. The offset is just 1 *mm*, which is probably due to uncertainty of distance measurement and neglecting of the two small caps thickness.

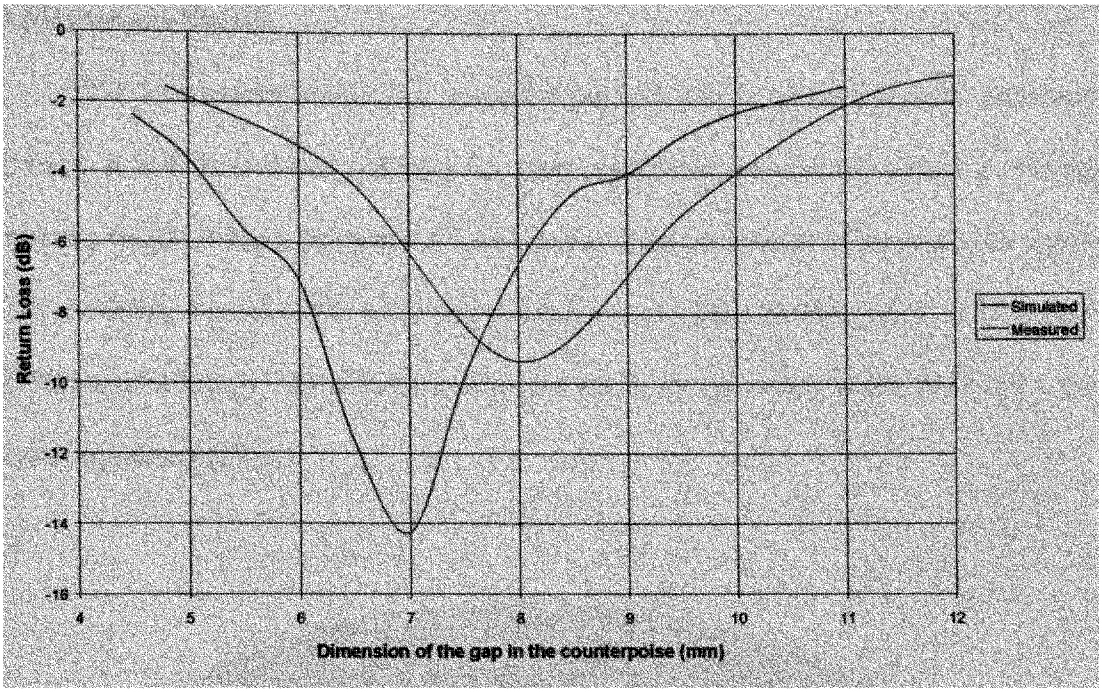

Fig.23. Comparison between the measured return loss of the cavity and the simulated one versus counterpoise distance at 900 MHz [7].

The prediction accuracy of the return loss value is satisfactory, since the net input power difference amounts to less than 15% at the best match. Such a small discrepancy could be due to the ideal materials considered in the simulation and to uncertainties of the dummies dielectric parameter. Another source of uncertainty could be associated with the description of the region where the coaxial feed-line enters the cavity.

5.3 Microwave Studio

CST Microwave Studio is a powerful and easy to use electromagnetic simulation software. It is fully featured software for electromagnetic analysis and design in the high frequency range. It has a powerful solid modeling front-end which is based on the famous ACIS modeling kernel. CST Microwave Studio uses Finite-Difference in Time Domain (FDTD) methodology based on fine adaptive mesh for geometry using Maxwell's time varying equations [19].

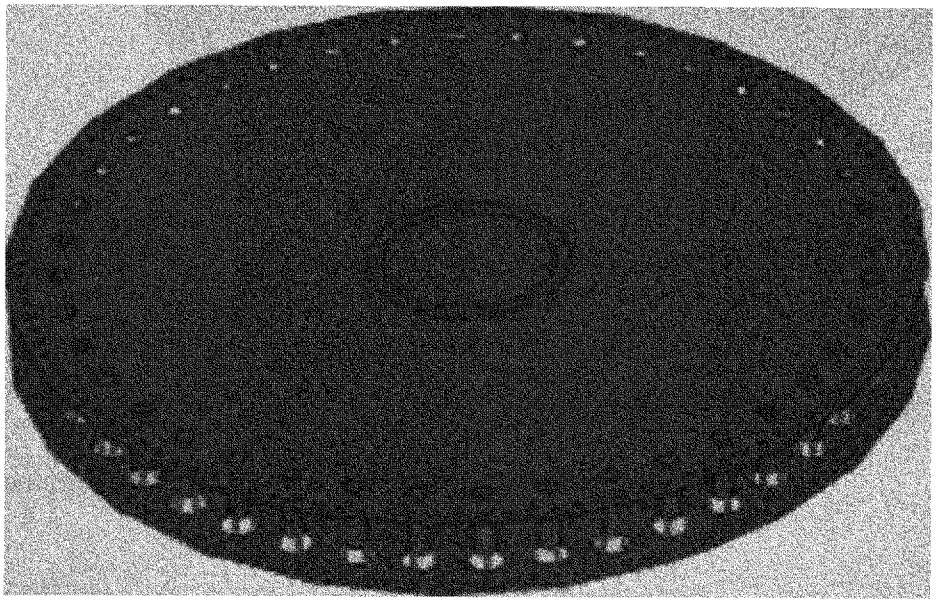

Fig.24. Model of FW in Microwave Studio [19].

Fig.24 shows the computational model of Ferris Wheel created in Microwave Studio loaded with forty identical cylinders that simulate the electrical load by the mice. A number of numerical simulations of the FW system are performed to identify the

condition upon which the geometrical asymmetries might have produced severe unbalance in the RF energy distribution.

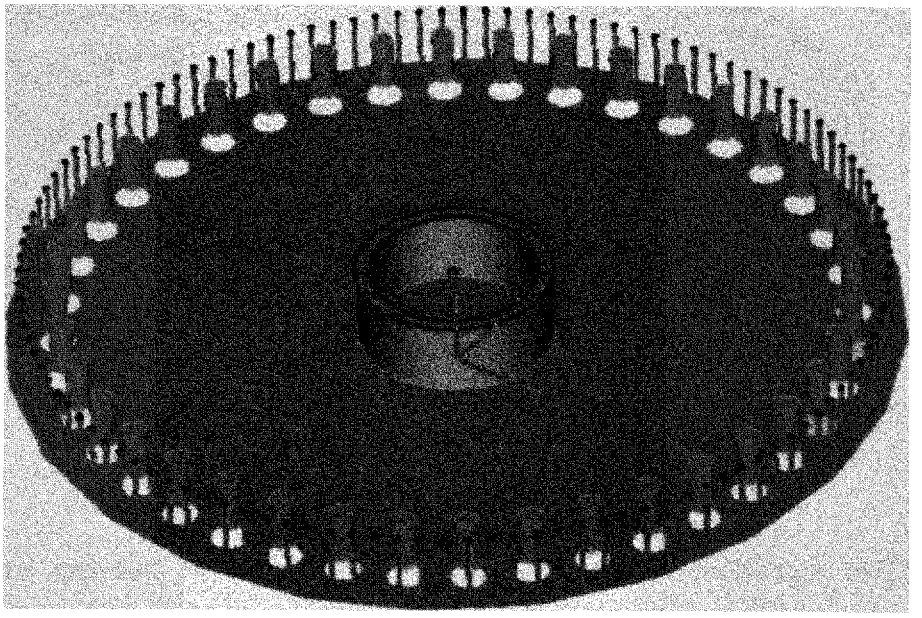

Fig.25. Internal details of the Ferris Wheel [19].

Fig. 25 shows the internal details about the Monopole antenna (field exciter), Teflon ring, holes for inserting the mice and the shorting poles.

Asymmetries in the Ferris Wheel.

The Ferris Wheel exposure system is simulated for the following geometrical asymmetries:

1. Different mouse weight: In the mouse model the length of the mouse phantoms is kept constant and varied along the diameter [19].

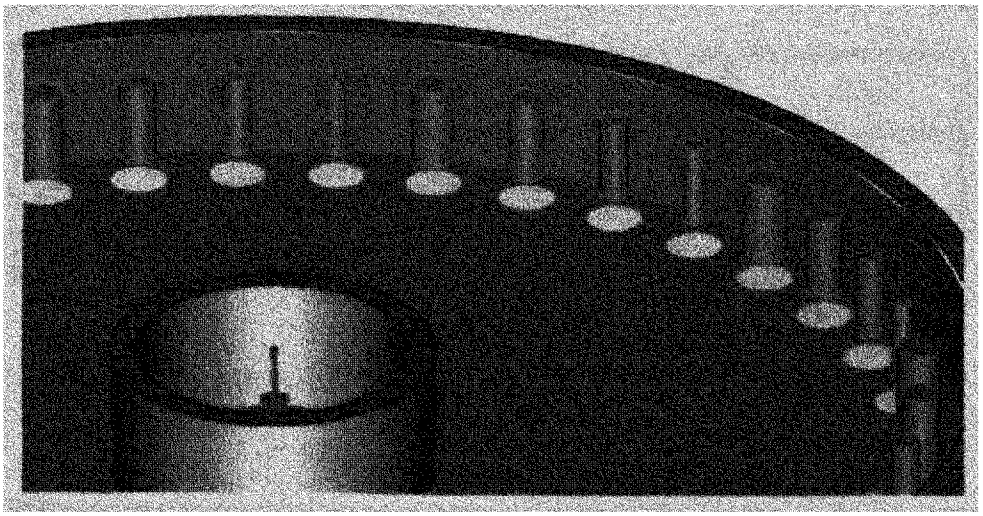

Fig.26. Ferris Wheel loaded with four different loads [19].

Two cases were analyzed, one with two weights and other with four different weights as shown in the Table 1.

Table 1. Asymmetric weight loading is repeated several times to fill the FW [19].

CASE #1 (Two weights)			CASE #2 (Four weights)		
H [mm]	D [mm]	Mass [mm]	H [mm]	D [mm]	Mass [mm]
60	10	18.8	60	7.5	10.6
60	15	42.4	60	10	18.8
60	10	18.8	60	12.5	29.5
60	15	42.4	60	15	42.4

Case#1: The following table shows the results for two different mice for 1 W net input power. The larger mouse exhibits larger peak 1-g to Whole-Body SAR ratio.

Table 2.Case#1 Results [19].

Mass [g]	SAR WB	SAR 1-g	1-g/WB
18.8	0.65	1.29	1.98
42.4	0.86	2.17	2.51

Case#2: Table: 3 Shows the results for four different mice for 1 W net input power.

Table 3:Case#2 Results [19].

Mass [g]	SAR WB	SAR 1-g	1-g/WB
10.6	0.88	1.28	1.45
18.8	0.71	1.40	1.98
29.5	.84	2.02	2.40
42.4	1.13	2.82	2.51

The most important results of the simulations are that the ratios of the 1-g and Whole-Body averages are insensitive to the asymmetries introduced in the FW [19]. The SAR distribution with in the mice is negligibly affected by rather significant, thus indicating small mutual coupling between the mice.

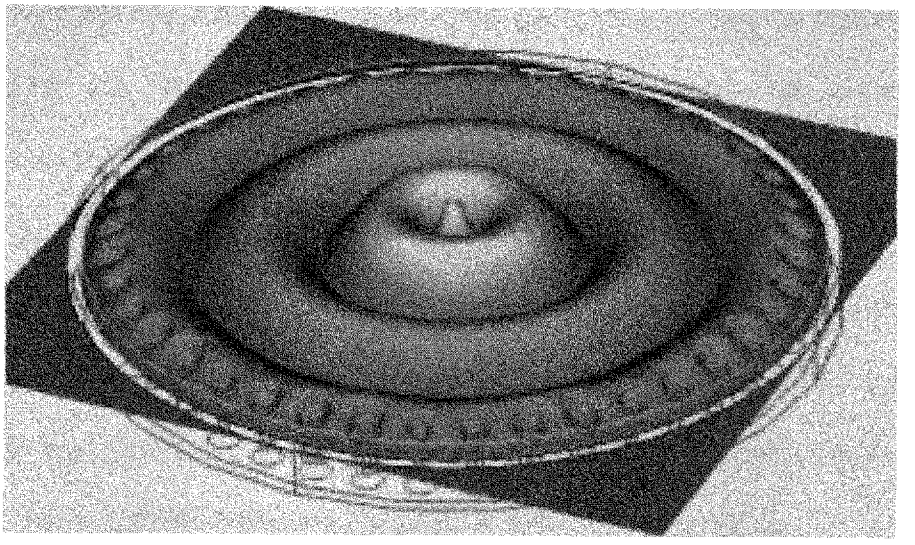

Fig.27. Electric field distribution for FW using four different weight mice [19].

In practice, the nearby mice minimally affect the mechanism of energy absorption. The total electric field plot over the bisecting cut plane shown in Fig.27. The electric distribution preserves an excellent azimuthally symmetry.

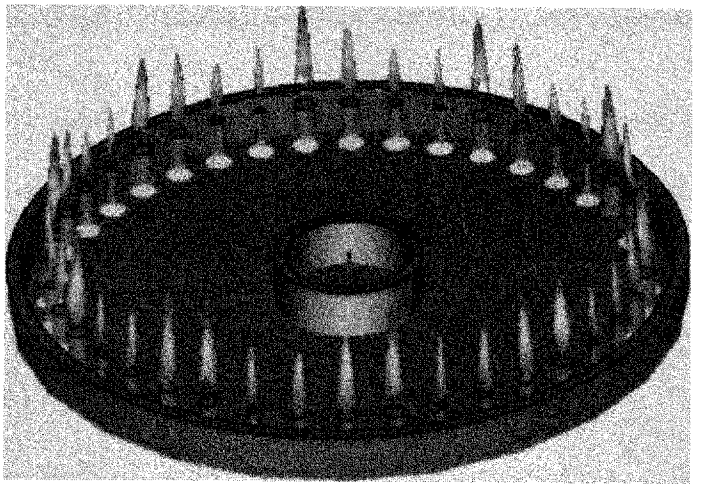

Fig.28. SAR distribution over a cut-plane bisecting the FW loaded with four different weights [19].

2. Offset of the collective mouse barycentre: This asymmetry consists in shifting the center of mass of mice, which ideally coincides with the geometrical center of the FW. All mice are assumed (H=60 mm, D =12.5, Mass =29.5) for three cases of offset of 2.5,10,10 mm respectively.

The below table shows the asymmetry resulting from an offset of the center of mass of the mice with respect to the geometrical center of the FW can potentially introduce a very high degree of non-uniformity in the Whole-Body and peak 1-g SAR.

Table 4.Whole-Body and 1-g SAR for different Offsets [19].

Offset [mm]	SAR WB	SAR 1-g	1-g/WB
0.0	1.0	1.0	2.38
2.5	2.6	2.4	2.39+/-10%
5.0	4.2	3.7	2.37+/-11%
10.0	24.9	20.4	2.36+/-20%

In the Fig.29.a shows the marked asymmetry in the total electric field distribution is caused by the 10 mm offset, which is responsible for the dramatic non-uniformity in the SAR distribution across the mice.

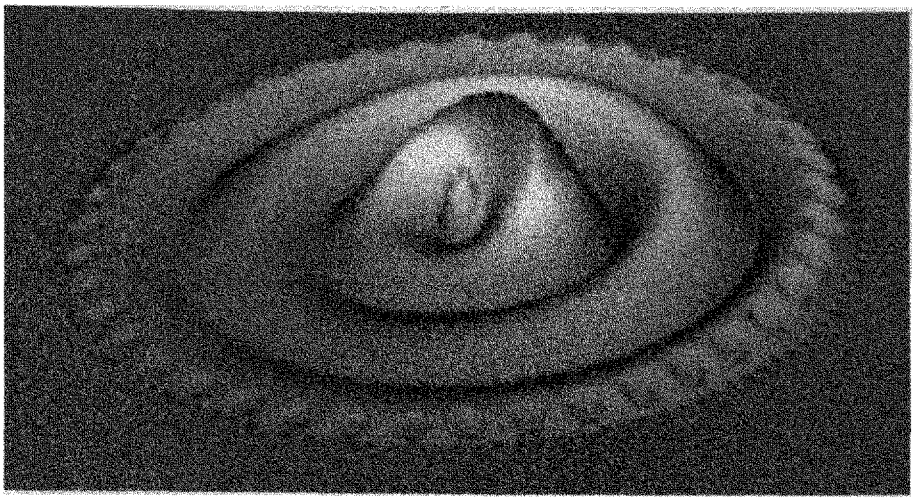

Fig.29.a

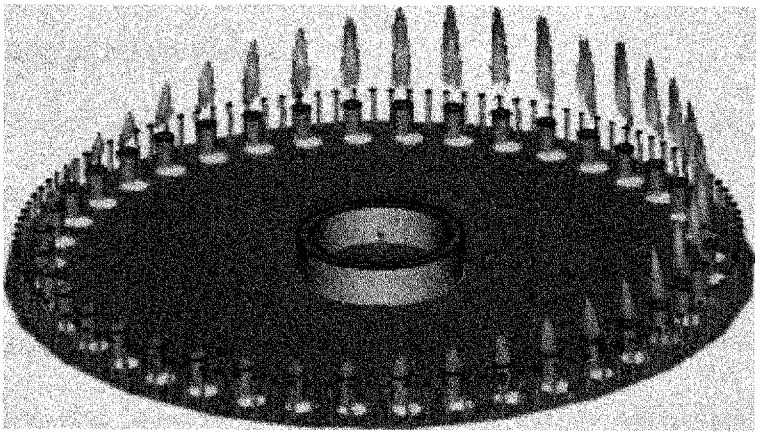

Fig.29.b

Fig.29. Total electric field simulation (a) and SAR distribution (b) in a FW loaded with 29.5 g mice arranged witha10mm offset between the collective mass and the geometrical center of FW [19].

In general it is found that the SAR is lower for the samples closer to the lateral wall, which is intuitive since the electric field associated to the dominant mode vanishes.

CHAPTER VI

DETERMINATION OF WHOLE-BODY SAR AND CHARACTERIZATION OF FERRIS WHEEL USING CALORIMETRIC PROCESS

As already discussed in the previous Chapters it is necessary to characterize the behavior of the Ferris Wheel in terms of symmetry and efficiency. In order to confirmation the reliability of the exposure system the results obtained in terms of SAR and efficiency should be of good repeatability. For SAR measurements the actual power absorbed by the load must be measured very precisely. This chapter discusses the calorimetric process, which helps in precise determination of Whole-Body SAR.

6.1 Characterizing of Ferris Wheel

The most ideal condition to start the initial characterization on the "Ferris Wheel" exposure system is to have symmetrical loading structure, which can be achieved by using dummy bottles filled with simulated tissue material as loads, discussed in Chapter IV. The net energy radiated from the radiating element will be assumed to be equally distributed among the symmetrical loads, as they are of approximately equal and equidistant from the center. As already discussed the simulated tissue material doesn't have the any complexity in terms of shape and dielectric properties. Since the Ferris Wheel has forty slots and it is impractical to test every position for the amount of power absorbed by each load, four different position of interest are chosen as shown in Fig.30.

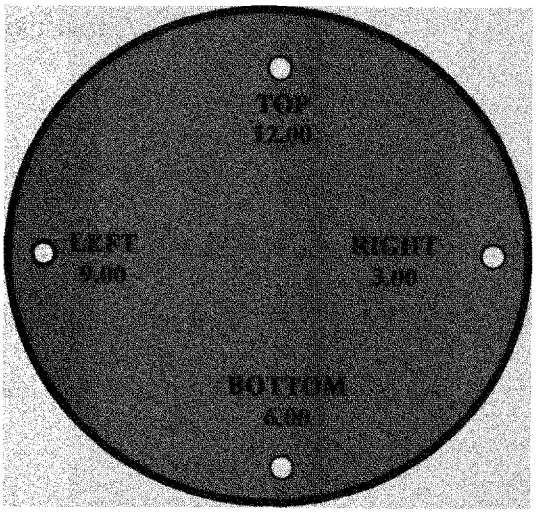

Fig .30. Four different positions of interest on the wheel

Several exposures were done using simulated tissue at the four different locations (TOP, BOTTOM, LEFT, RIGHT) on the Ferris Wheel to measure the amount of energy absorbed by the dummy bottles for each of one these locations. These four locations TOP, BOTTOM, LEFT, RIGHT are also known as 12.00 clock, 6.00 clock, 9.00 clock and 3.00 clock respectively. For the specific Left Position, an intentional delay time was introduced in between end of exposure and putting the mice into the calorimeter, This delays were 5, 10 and 15 seconds which will be explained in next sections.

Since the Ferris Wheel is designed for the exposure of mice and to replicate the Australian experiment in terms of loading, the actual characterization should be done with experiments containing realistic type of loads i.e., mice into the "Ferris Wheel".

In order to replicate the Australian study in terms of the loading, it was chosen to use mice of three different weights to simulate the life cycle of a mouse. The weights used to simulate the life cycle of a mouse are 25 g, 32 g and 36g respectively. The

experimental procedure using the mice is almost the same as that of the dummy bottles containing the simulated tissue.

6.2 Experimental setup for the Ferris Wheel exposure system

The following schematic shows the RF setup for the Ferris Wheel exposure system, comprising of the signal generator at 915 MHz, Bi-directional coupler and power meters to measure the forward and reflected powers.

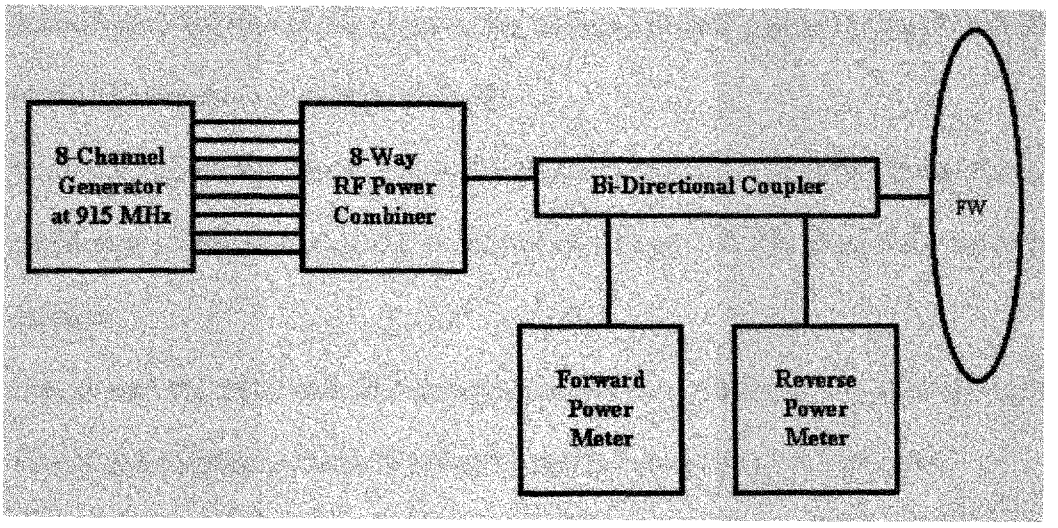

Fig.31. Schematic of RF setup for "Ferris Wheel" Exposure System

Before an exposure is performed the "loaded" exposure system should be tuned in order to maximize the energy transferred to the loads. The following tuning procedure should be followed whenever new loads are used, which change the loading conditions

1. Calibrate the network analyzer to take account the losses of the cable and connectors used. The standard S11 calibration procedure should be performed for

short, open and load conditions. Make sure the frequency range is adjusted from 850 MHz to 950 MHz.

2. Disconnect the cable from the directional coupler and connect the network analyzer to the feeding point in the "Ferris Wheel" through the cable used for calibration. Check for the single dip on network analyzer screen. Enable the marker to be shown in the screen and set it up at 915 MHz.
3. Inside the part of the Teflon ring outside the cavity a long shaft (counter-poise) is seen. Loose the plastic screw to release the shaft. Let it rotate to right or left according to the dip displacement in the analyzer screen. Adjust the shaft until the marker points the lowest part of the dip.
4. Carefully tighten the plastic nut to disable any rotation of the shaft. The reflection coefficient reading in the analyzer should be around −11 dB when mice are used as loads.
5. Disconnect the cable from the network analyzer and reconnect the cable from the directional coupler. Make sure to have a tight connection at the feed point.
6. It's advisable to check the internal components of the connector from time to time to evaluate their integrity.
7. After the above steps were done, the load position (Top, Left, Right, and Bottom) should be chosen.

6.3 Twin-Well Calorimeter for Whole-Body SAR Measurements

A calorimeter helps us in determining the RF dosage in the absorbing objects. Whole-Body SAR of a biological object can be determined by using a "Twin-Well" Calorimeter. It consists of two identical cylinders large enough to contain the objects. Each cylinder is surrounded by a thermopile, an array of thermocouples connected in series (voltage additive). The thermopiles of the two cylinders are connected in opposite polarities so that the voltages are subtracted. Therefore when both cylinders are at the same temperature, the resulting voltage from the thermopiles is zero.

The amount of heat energy absorbed during an exposure in an object is determined by using two similar bodies, but at different temperatures $T_1(t)$ and $T_2(t)$, in the wells of the calorimeter. It was given the name "differential Twin-Well" calorimeter because it measures the difference in heat between the bodies that are placed in two copper wells.

During Ferris Wheel exposure tests using loads, twin-well calorimeter allows to make differential heat measurements between loads used as exposed and sham of similar weight. Due to the difference in temperature or heat content between exposed and sham, the heat flows from higher temperature well to the lower temperature. The process of heat transfer is very slow as a low conductive material separates the wells and surrounds the envelope.

6.3.1 Mathematical Modeling for the "Twin-Well" Differential Calorimeter

Twin-Well is employed to determine the RF dose variation verses load position in the carousel. It helps in determining the Whole-Body SAR in dummy bottles or mice cadavers. Highly precise measurements are made of the quantity of microwave energy absorbed by models or bodies of exposed animals. A reference or non-exposed

target is placed in one well, an exposed target in the other well; the difference in thermal loading is then detected by sensitive thermocouples. The difference in heat exchanged between the wells having a reference constant temperature T_0 (usually Room temperature at 23°C) is determined by monitoring the output voltage from the calorimeter, which is proportional to the temperature difference between the wells. The amount of energy absorbed by the sample tissues in terms of temperature changes is used for determination of SAR value.

Under this hypothesis the amount of the heat flowing by the first body in the time interval $(t, t+dt)$ can be approximated as follows [20]

$$dq_1 = \{R_{10}[T_1(t) - T_0] + R_{12}[T_1(t) - T_2(t)]\}dt \tag{6.1}$$

with

$$dq_1 = -m_1 c_1 \, dT_1 \tag{6.2}$$

where m_1 is the mass of the body, while c_1 is its specific heat. Equating (6.1) and (6.2) it results

$$-m_1 c_1 \frac{\partial}{\partial t} T_1(t) = \{R_{10}[T_1(t) - T_0] + R_{12}[T_1(t) - T_2(t)]\} \tag{6.3}$$

Proceeding in the same way for the second body we obtain

$$-m_2 c_2 \frac{\partial}{\partial t} T_2(t) = \{R_{20}[T_2(t) - T_0] + R_{21}[T_2(t) - T_1(t)]\} \tag{6.4}$$

The differential equations governing the twin-well calorimeter are then

$$\begin{cases} m_1 c_1 \dfrac{\partial}{\partial t} T_1(t) = -\{R_{10}[T_1(t) - T_0] + R_{12}[T_1(t) - T_2(t)]\} \\ m_2 c_2 \dfrac{\partial}{\partial t} T_2(t) = -\{R_{20}[T_2(t) - T_0] + R_{21}[T_2(t) - T_1(t)]\} \end{cases} \tag{6.5}$$

To obtain the solution of the above differential equations we employ the Laplace transform obtaining

$$\begin{cases} m_1 c_1 [s T_1(s) - T_{10}] = -\left\{R_{10}\left[T_1(s) - \dfrac{T_0}{s}\right] + R_{12}[T_1(s) - T_2(s)]\right\} \\ m_2 c_2 [s T_2(s) - T_{20}] = -\left\{R_{20}\left[T_2(s) - \dfrac{T_0}{s}\right] + R_{21}[T_2(s) - T_1(s)]\right\} \end{cases} \tag{6.6}$$

After some simple mathematical manipulations the following system of linear equations are derived

$$\begin{cases} [m_1 c_1 s + R_{10} + R_{12}] T_1(s) - R_{12} T_2(s) = m_1 c_1 T_{10} + R_{10} \dfrac{T_0}{s} \\ [m_2 c_2 s + R_{20} + R_{21}] T_2(s) - R_{21} T_1(s) = m_2 c_2 T_{20} + R_{20} \dfrac{T_0}{s} \end{cases} \tag{6.7}$$

or in a more compact form

$$\begin{bmatrix} m_1 c_1 s + R_{10} + R_{12} & -R_{12} \\ -R_{21} & m_2 c_2 s + R_{20} + R_{21} \end{bmatrix} \cdot \begin{bmatrix} T_1(s) \\ T_2(s) \end{bmatrix} = \begin{bmatrix} m_1 c_1 T_{10} + R_{10} \dfrac{T_0}{s} \\ m_2 c_2 T_{20} + R_{20} \dfrac{T_0}{s} \end{bmatrix} \tag{6.8}$$

The Laplace transforms of the terms $T_1(t)$ and $T_2(t)$ are then determined by solving the above system of linear equations. Solving (6.8), we obtain

$$T_1(s) = \frac{\begin{bmatrix} m_1 c_1 T_{10} + R_{10} \dfrac{T_0}{s} & -R_{12} \\ m_2 c_2 T_{20} + R_{20} \dfrac{T_0}{s} & m_2 c_2 s + R_{20} + R_{21} \end{bmatrix}}{\begin{bmatrix} m_1 c_1 s + R_{10} + R_{12} & -R_{12} \\ -R_{21} & m_2 c_2 s + R_{20} + R_{21} \end{bmatrix}} \tag{6.9}$$

$$T_2(s)=\frac{\begin{bmatrix} m_1 c_1 s+R_{10}+R_{12} & m_1 c_1 T_{10}+R_{10}\dfrac{T_0}{s} \\ -R_{12} & m_2 c_2 T_{20}+R_{20}\dfrac{T_0}{s} \end{bmatrix}}{\begin{bmatrix} m_1 c_1 s+R_{10}+R_{12} & -R_{12} \\ -R_{21} & m_2 c_2 s+R_{20}+R_{21} \end{bmatrix}} \tag{6.10}$$

from which it results

$$T_1(s)=\frac{\left[m_1 c_1 T_{10}+R_{10}\dfrac{T_0}{s}\right]\left[m_2 c_2 s+R_{20}+R_{21}\right]+R_{12}\left[m_2 c_2 T_{20}+R_{20}\dfrac{T_0}{s}\right]}{\left[m_1 c_1 s+R_{10}+R_{12}\right]\left[m_2 c_2 s+R_{20}+R_{21}\right]-R_{12}R_{21}} \tag{6.11}$$

$$T_2(s)=\frac{\left[m_2 c_2 T_{10}+R_{20}\dfrac{T_0}{s}\right]\left[m_1 c_1 s+R_{10}+R_{21}\right]+R_{21}\left[m_1 c_1 T_{10}+R_{10}\dfrac{T_0}{s}\right]}{\left[m_1 c_1 s+R_{10}+R_{12}\right]\left[m_2 c_2 s+R_{20}+R_{21}\right]-R_{12}R_{21}} \tag{6.12}$$

or

$$T_1(s)=\frac{\left[s m_1 c_1 T_{10}+R_{10}T_0\right]\left[m_2 c_2 s+R_{20}+R_{21}\right]+R_{12}\left[s m_2 c_2 T_{20}+R_{20}T_0\right]}{s\left\{\left[m_1 c_1 s+R_{10}+R_{12}\right]\left[m_2 c_2 s+R_{20}+R_{21}\right]-R_{12}R_{21}\right\}} \tag{6.13}$$

$$T_2(s)=\frac{\left[s m_2 c_2 T_{10}+R_{20}T_0\right]\left[m_1 c_1 s+R_{10}+R_{21}\right]+R_{21}\left[s m_1 c_1 T_{10}+R_{10}T_0\right]}{s\left\{\left[m_1 c_1 s+R_{10}+R_{12}\right]\left[m_2 c_2 s+R_{20}+R_{21}\right]-R_{12}R_{21}\right\}} \tag{6.14}$$

If the calorimeter is symmetric and the two bodies have the same characteristics the above equations can be rewritten as

$$T_1(s)=\frac{\left[s m c T_{10}+R_{10}T_0\right]\left[m c s+R_{10}+R_{12}\right]+R_{12}\left[s m c T_{20}+R_{10}T_0\right]}{s\left\{\left[m c s+R_{10}+R_{12}\right]^2-R_{12}^2\right\}} \tag{6.15}$$

$$T_2(s)=\frac{\left[s m c T_{10}+R_{10}T_0\right]\left[m c s+R_{10}+R_{12}\right]+R_{12}\left[s m c T_{10}+R_{10}T_0\right]}{s\left\{\left[m c s+R_{10}+R_{12}\right]^2-R_{12}^2\right\}} \tag{6.16}$$

The denominator of (6.15)-(6.16) can be expanded in the following form

$$[mcs+R_{10}+R_{12}]^2-R_{12}^2=(mcs+R_{10})^2+2R_{12}(m_1c_1s+R_{10})+R_{12}^2-R_{12}^2 \tag{6.17}$$

and rewritten as follows

$$[mcs+R_{10}+R_{12}]^2-R_{12}^2=(mcs+R_{10})[mcs+R_{10}+2R_{12}] \tag{6.18}$$

Using (6.18) we have

$$T_1(s)=\frac{[smcT_{10}+R_{10}T_0][mcs+R_{10}+R_{12}]+R_{12}[smcT_{20}+R_{10}T_0]}{s(mcs+R_{10})[mcs+R_{10}+2R_{12}]} \tag{6.19}$$

$$T_2(s)=\frac{[smcT_{10}+R_{10}T_0][mcs+R_{10}+R_{12}]+R_{12}[smcT_{10}+R_{10}T_0]}{s(mcs+R_{10})[mcs+R_{10}+2R_{12}]} \tag{6.20}$$

or $$T_1(s)=\frac{\left[sT_{10}+\frac{R_{10}T_0}{mc}\right]\left[s+\frac{R_{10}+R_{12}}{mc}\right]+R_{12}\left[sT_{20}+\frac{R_{10}T_0}{mc}\right]}{s\left(s+\frac{R_{10}}{mc}\right)\left[s+\frac{R_{10}+2R_{12}}{mc}\right]} \tag{6.21}$$

$$T_2(s)=\frac{\left[sT_{10}+\frac{R_{10}T_0}{mc}\right]\left[s+\frac{R_{10}+R_{12}}{mc}\right]+R_{12}\left[sT_{10}+\frac{R_{10}T_0}{mc}\right]}{s\left(s+\frac{R_{10}}{mc}\right)\left[s+\frac{R_{10}+2R_{12}}{mc}\right]} \tag{6.22}$$

From the equations (6.21)-(6.22) it appears that the thermal system formed by the two bodies is characterized by two time constants given by

$$\alpha=\frac{R_{10}}{mc} \tag{6.23}$$

$$\beta=\frac{R_{10}+2R_{12}}{mc} \tag{6.24}$$

The Laplace transforms $T_1(s)$ and $T_2(s)$ can then be rewritten in a form useful to derive their time domain counterpart. We have

$$T_1(s) = \frac{T_{1\infty}}{s} + \frac{T_{1\alpha}}{s+\alpha} + \frac{T_{1\beta}}{s+\beta} \tag{6.25}$$

$$T_2(s) = \frac{T_{2\infty}}{s} + \frac{T_{2\alpha}}{s+\alpha} + \frac{T_{2\beta}}{s+\beta} \tag{6.26}$$

The coefficients $T_{j\infty}$, $T_{j\alpha}$, and $T_{j\beta}$, with j=1,2, can be determined using the well-known formulas

$$T_{j\infty} = \underset{s \to 0}{Lim}\, sT_j(s) \tag{6.27}$$

$$T_{j\alpha} = \underset{s \to -\alpha}{Lim}\, (s+\alpha)T_j(s) \tag{6.28}$$

$$T_{j\beta} = \underset{s \to -\beta}{Lim}\, (s+\beta)T_j(s) \tag{6.29}$$

We obtain

$$T_{1\infty} = T_0 \tag{6.30}$$

$$T_{1\alpha} = \frac{1}{2}(T_{10} + T_{20} - 2T_0) \tag{6.31}$$

$$T_{1\beta} = \frac{1}{2}(T_{10} - T_{20}) \tag{6.32}$$

$$T_{2\infty} = T_0 \tag{6.33}$$

$$T_{2\alpha} = \frac{1}{2}(T_{10} + T_{20} - 2T_0) \tag{6.34}$$

$$T_{2\beta} = \frac{1}{2}(T_{20} - T_{10}) \tag{6.35}$$

Using the above equations it is straightforward to express $T_1(t)$ and $T_2(t)$ as follows

$$T_1(t) = T_0 + \frac{1}{2}(T_{10} + T_{20} - 2T_0)e^{-\frac{R_{10}}{mc}} + \frac{1}{2}(T_{10} - T_{20})e^{-\frac{R_{10}+2R_{12}}{mc}} \tag{6.36}$$

$$T_2(t) = T_0 + \frac{1}{2}(T_{10} + T_{20} - 2T_0)e^{-\frac{R_{10}}{mc}} - \frac{1}{2}(T_{10} - T_{20})e^{-\frac{R_{10}+2R_{12}}{mc}} \tag{6.37}$$

Consequently, the voltage appearing at the port of the thermocouple, which is proportional to the difference between $T_1(t)$ and $T_2(t)$, writes

$$v(t) = (T_{20} - T_{10})e^{-\frac{(R_{10}+2R_{12})t}{mc}} \tag{6.38}$$

Finally, integrating the voltage $v(t)$ we obtain a term proportional to the heat difference between the two bodies

$$v(t) = \int_0^\infty (T_{20} - T_{10})e^{-\frac{(R_{10}+2R_{12})t}{mc}} dt = \frac{mc(T_{20} - T_{10})}{R_{10} + 2R_{12}} \tag{6.39}$$

where R_{10} is the thermal resistances between the well to envelope maintained at constant temperature T_0,and R_{12} is the thermal resistances between the two wells of the calorimeter.

It should be noted that (6.39) applies only when the two bodies have the same characteristics (mass and specific heat).

6.3.2 Numerical Analysis for "Twin-Well" Calorimeter

MATLAB was used to numerically solve the heat flow between the wells of the Twin-Well calorimeter; a partial differential equation was used for the heat flow in the twin-well calorimeter. Since the Twin-Well is a complex but symmetrical system containing two identical well for loads, to simplify matters a one-dimensional section of the calorimeter system is chosen as shown in the Fig.32.

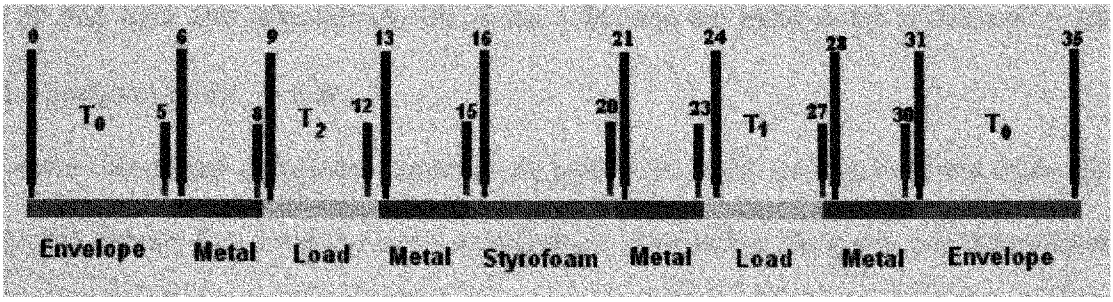

Fig.32.One-Dimensional Structure of Twin-Well Calorimeter used for Simulation.

In a one -dimensional medium between two points x_1 and x_2 with in a solid is, the conduction of heat is given by the equation

$$q_x = -k\left(\frac{T(x_2)-T(x_1)}{x_2-x_1}\right) \tag{6.40}$$

Where $T(x)$ is the local temperature and q_x is the thermal flux and has units W/m^2 .The quantity k is the material thermal conductivity with units $J/m\text{-}K$ [21]. The flux is proportional to the temperature difference and inversely proportional to the distance between the locations.

As the thermal flux or the heat flow is proportional to the thermal conductivity at a position and temperature at an instance. The one-dimensional heat flow inside the calorimeter can be treated in terms of temperature and conductivity.

The partial differential equation in terms of temperature is

$$\frac{\partial T}{\partial t} = k(x)\frac{\partial^2 T}{\partial x^2} \tag{6.41}$$

where $T(x, t)$ is the temperature at time t a distance x along one-dimensional section of the calorimeter.

The solution space is divided into uniform sections of width Δx as shown in the Fig.32 and time into intervals Δt. the index i denotes the mesh point position $x_i = i\Delta x$ and n designates time, $t = n\Delta t$.

To solve this partial differential equation we need both initial conditions of the form $T(x, 0) = f(x)$, where $f(x)$ gives the initial temperature distribution along the one dimensional line of the calorimeter as shown in the figure as the value of x varies from 0 to 35. At $t = 0$, and *boundary conditions* at the envelope of the system are $x_i = T_0$ for $5 \geq x_i \geq 1$ and $35 \geq x_i \geq 31$ and remains the same for all the time t.

The partial differential equation in terms of finite difference approximations to the derivatives, we get

$$\frac{T_i^{n+1} - T_i^n}{\Delta t} = k\frac{T_{i+1}^n - 2T_i^n + T_{i-1}^n}{\Delta x^2} \tag{6.42}$$

Thus if for a particular n, we know the values of T_i^n for all i, we can solve the equation above to find T_i^{n+1} for each i:

$$T_i^{n+1} = T_i^n + \frac{k\Delta t}{\Delta x^2}\left(T_{i+1}^n - 2T_i^n + T_{i-1}^n\right) = s\left(T_{i+1}^n + T_{i-1}^n\right) + (1-2s)T_i^n \tag{6.43}$$

where $s = k(x)\Delta t/(\Delta x)^2$ [21]. In other words, this equation tells us how to find the temperature distribution at time step $n+1$ given the temperature distribution at time step n.

The above equation can be interpreted, as the temperature at a given location at the next time step is a weighted average of its temperature and the temperatures of its neighbors at the current time step. In other words, in time Δt, a given section of length Δx transfers to each of its neighbors a portion s of its heat energy and keeps the remaining portion $1-2s$ of its heat energy.

The following M-file, which is named twin.m, iterates the procedure described above.

```
t = linspace(0,1200,6200);
x = linspace(0,35,35);
k(1,1:5)=0.2;
k(1,6:8)=1;
k(1,9:12)=.7;
k(1,13:15)=1;
k(1,16:20)=0.2;
k(1,21:23)=1;
k(1,24:27)=.7;
k(1,28:30)=1;
k(1,31:35)=0.2;
J = length(x);
N = length(t);
dx = mean(diff(x));
dt = mean(diff(t));
s = k*dt/dx^2;
T = zeros(N,J);
T(:,1:5) = 23;
T(1,6:8)=23;
T(1,9:12)=40;
T(1,13:15)=23;
T(1,16:20)=23;
T(1,21:23)=23;
T(1,24:27)=30;
T(1,28:30)=23;
T(:,31:35)=23;
for p= 2:N
   for n = 6:30
        T(p,n) = s(1,n)*(T(p-1,n+1) + T(p-1,n-1)) + (1 - 2*s(1,n))*T(p-1,n);
end
end
figure(1);
surf(T)
```

```
v1=T(:,7);
v2=T(:,29);
figure(2);
contour(T);
M=(v1-v2)/3;
figure(3);
plot(t*60,M);
```

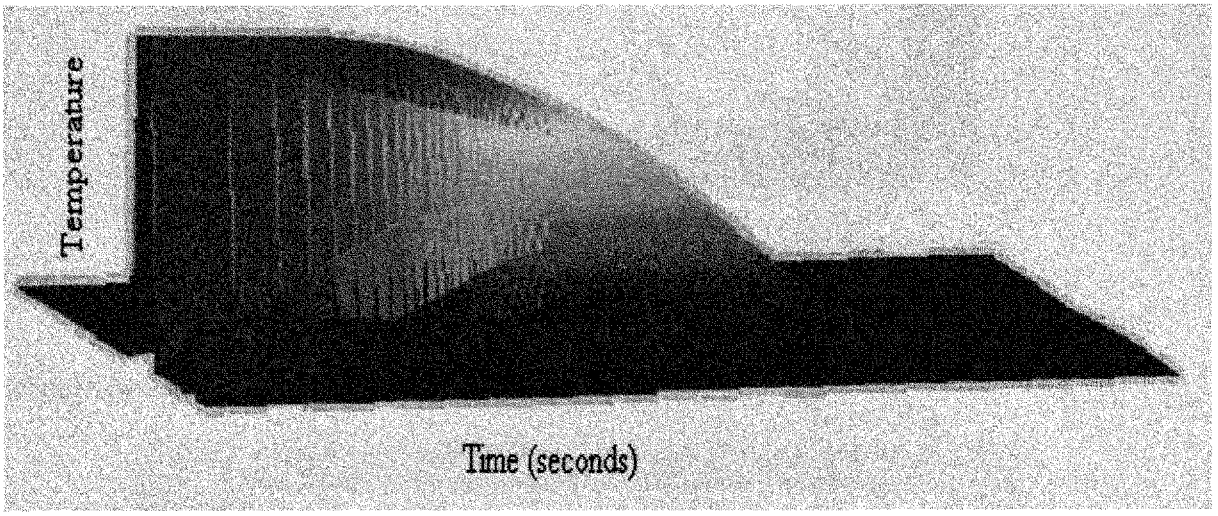

Fig.33. One-Dimensional Heat flow between the two wells of Twin -Well Calorimeter and its Envelope.

Fig.33 shows the one-dimensional heat flow, which is proportional to temperature between the two wells, maintained at T_1 and T_2 and the envelope temperature maintained at T_0 .As the time increases the temperature all the points on the one-dimensional space of Twin-Well tend to reach the envelope temperature. Fig.34 shows the flow of the heat between the two wells of the Twin-Well calorimeter as temperature counters. The counters show the flow of heat from the well at higher temperature to the well at lower temperature.

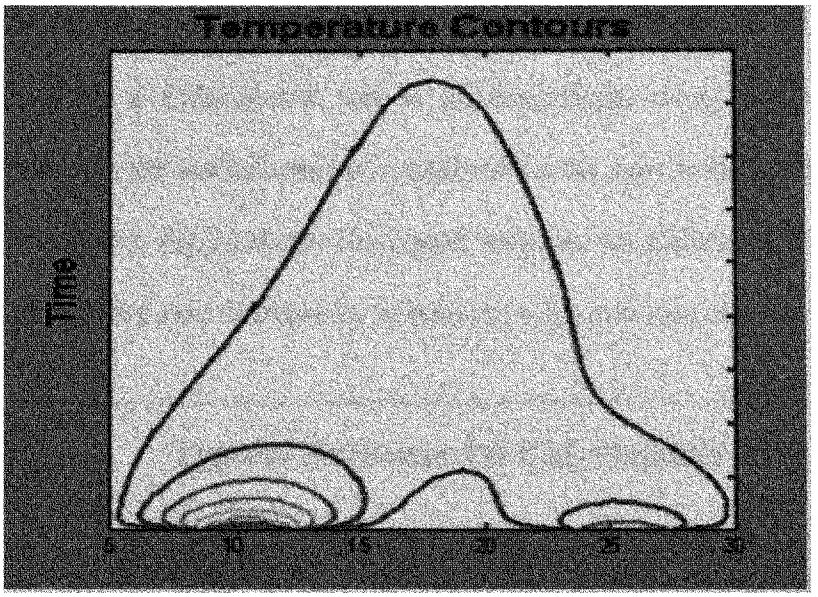

Fig.34. Temperature Contours for heat flow between the two wells.

The simulated response for the heat exchange between the wells in terms of voltage during a calorimetric test is shown in Fig.35.

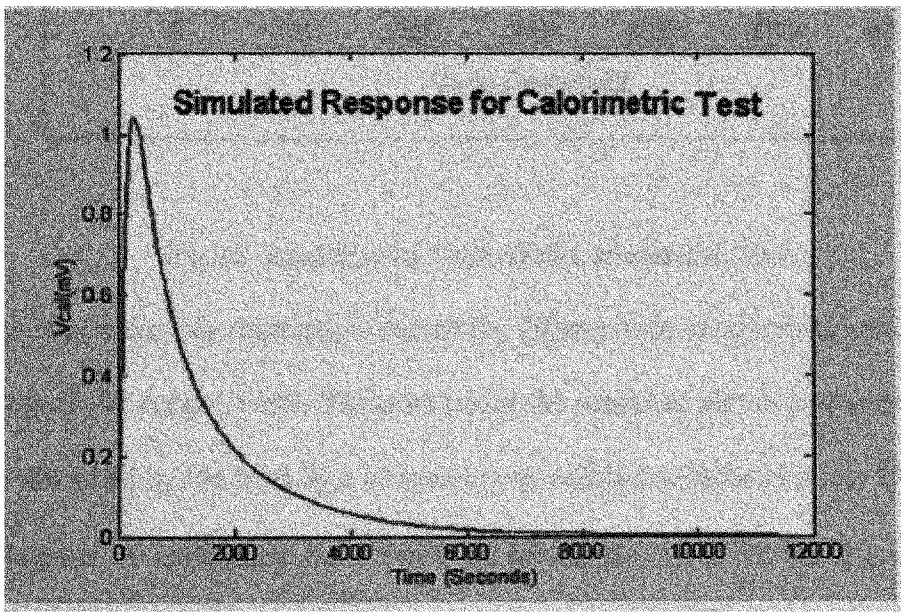

Fig.35.Simulated Response for a Calorimetric Test.

6.4 Calculation for Whole-Body SAR using Calorimetric Technique

Response for a Calorimetric test is an exponential decay when the voltage difference between is the thermocouples connected to the two wells of the Twin-Well calorimeter is measured. Fig.36 shows the typical response for Calorimetric test, which is similar to that of the response obtained by simulation in the previous section.

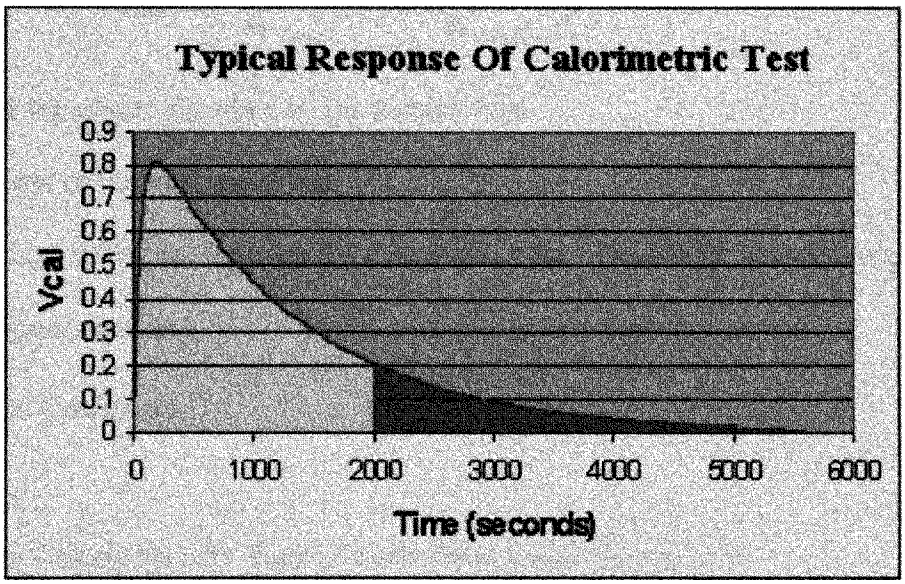

Fig.36. Response of Twin-Well Calorimetric Test.

The reason for this response is due to the difference in conductivity coefficients of loads to that of the copper wells. The area under the response plot is proportional to the RF energy absorbed by the load by a conversion or calibration factor $\gamma \cong 10$. The factor $\gamma \cong 10$ is obtained by calibrating the Twin-Well calorimeter with ice water and acetone. After a number of exposures and analyzing the heat transfer between the loads it is observed that the voltage difference between the wells follows an exponential decay around 1800 seconds. In order to increase the number of experimental measurements in a

day the area under the exponential decay is extrapolated, after stopping the test around 2000 seconds. Fig.36 shows the area under response curve is divided into two parts .The area shaded red is extrapolated using a time constant of 2492 seconds.

The Whole-Body SAR in a dummy of mass m used in the calorimeter can be:

$$SAR_{Load} = \frac{P_{Load}}{m_{Load}} = \frac{\gamma . \int_0^{\infty} V_{cal}(\tau) d\tau}{m_{Load} . \Delta t} \qquad (6.44)$$

where P_{Load} is the power absorbed by the dummy load,

m_{Load} is the mass of the load under test,

V_{cal} is the voltage difference between the two wells of the "Twin-Well" calorimeter,

Δt is the exposure duration,

γ is Calibration Coefficient.

6.5 Efficiency Calculation for Ferris Wheel from Calorimetric Tests

For efficiency calculation, we assume that all load positions at the wheel absorb the same amount of energy as the load position, so in order to get the total energy absorbed by all loads in wheel, we multiply energy absorbed by load times 40. The efficiency discussed here for a the load at a position is a relative term to the ideal load which absorbs fortieth of net power into the system, so sometimes this relative efficiency could be more than 100%.

On the other hand, the net power impinging the antenna is the difference between the forward and reflected power into the FW. The Lab View Data Acquisition program is used to collect the forward and reflected power data from their respective power meters.

The ratio in percentage of the power absorbed in the dummy bottle to that of the net power gives the efficiency of the Ferris Wheel. The relative efficiency of the Ferris Wheel at a position was estimated as follows:

$$e = (N_{Load} \cdot SAR_{WB} \cdot m_{Load}) / P_{Net} \tag{6.45}$$

where e is the relative efficiency of the Ferris Wheel at a particular position of Interest,

P_{Load} is the power absorbed by the loads in the FW,

P_{Net} is the total net power impinging on the loads in the FW

N_{Load} is the number of loads and is equal to forty,

SAR_{WB} is the Whole-Body SAR obtained from Calorimetric process,

m_{Load} is the mass of the load.

The average efficiency of the Ferris Wheel exposure system is found as

$$e_{FW} = (e_{Top} + e_{Bottom} + e_{Left} + e_{Right})/4 \tag{6.46}$$

where e_{FW} is the average efficiency of the system

and e_{Top}, e_{Bottom}, e_{Left} and e_{Right} are the average relative efficiency obtained at the positions of interest TOP, BOTTOM, LEFT, RIGHT positions respectively.

6.6 Calorimetric Test Procedure for loads

As already discussed, the types of loads used for the exposure experiments as loads are used in Calorimetric tests. They are dummy bottles filled with 37 g simulated tissue for the initial characterization. For the complete dosimetric characterization of Ferris Wheel mice cadavers of three weights 24 g, 32 g and 36 g are used.

6.6.1 Dummy Loads

1. Forty-two symmetrical bottles are filled with 37 grams of weight by volume of simulated tissue with +/- 0.1 g tolerance. The bottles are selected in such way that they easy fit into the Twin-Well calorimeter. Tie up three bottles with strings in a way that allows us to hold the bottles with the help of long strings during the exposure periods.
2. Place the three bottles in similar conditions and make sure both settle to room temperature.
3. Load the thirty nine bottles into the Ferris Wheel
4. Of the remaining three bottles, two are named A and B used as exposure loads alternatively at the position of interest and the third bottle named C is always used as sham.
5. Calibrate the Network Analyzer for the cable loss and tune the antenna for the load condition at and frequency of 915 MHz.
6. Ensure that the Lab View program is set up correctly. (i.e., General Purpose Interface Board (GPIB) Address 1 is set to Digital Voltmeter (DVM) reading the Twin-Well output, GPIB Address 2 and 3 for the power meters of Forward and Reflected powers respectively). Make sure that the gain is set to 30 dB for Instrument I (Twin-Well output) and 0 dB for power meters. Data should be collected from GPIB ports for every 2 seconds for at least 30 minutes or so.
7. Make sure that the power meters are calibrated with the offset value according to values on the bi-directional coupler (Forward and Reverse respectively) and the correction value according to the frequency of operation.

8. Make sure that reflected power meter reading is around 10% of the forward one.
9. Start data collection with the Lab View program.
10. Take A/B bottle place the sham one in a safe place at room temperature. Place the one to be exposed into plastic rocket and put all together into the selected carousel in the Ferris Wheel (i.e., Top, Left, Right or Bottom position)
11. Turn on the power amplifier and let it stabilize a few minutes. Determine the amount of exposure time (usually 30 seconds). Using a stopwatch toggle the switch to enable the RF exposure. At 30 seconds on the stopwatch toggle back the switch to disable the RF power.
12. Take the exposed bottle from the carousel and the sham with the help of the strings (make sure not to touch the bottles), and place them into the Twin-Well calorimeter at the same time.
13. Mark the well that contain the exposed and sham mice respectively and use always the same convention for different exposures.
14. Analyze Data.
15. Use the left over bottle for the next exposure after 45 minutes, which is sufficient time for the loads in the FW to reach room temperature.

6.6.2 Mouse Cadavers

1. Thaw forty-three mice of similar weight with +/- 0.5 g tolerance. Tie up two pairs of similar mice in a way that allows us to hold the mice with the help of a long string and also see that they will fit easily into the twin-well.
2. Place mice in similar conditions and make sure both settle to room temperature.

3. Ensure that the Lab View program is set up correctly. (i.e, GPIB Address 1 is set to DVM reading the Twin-Well output, GPIB Address 2 and 3 for the Power meters of Forward and Reflected powers respectively). Make sure that the gain is set to 30 dB for Instrument I (Twin-Well output) and 0 dB for power meters. Data should be collected from GPIB ports for every 2 seconds for at least 1800 seconds.
4. Make sure that the power meters are calibrated with the offset value according to values on the bi-directional coupler (Forward and Reverse respectively) and the correction value according to the frequency of operation.
5. After mice have been settled at room temperature, load thirty-nine mice into the Ferris Wheel with same orientation (i.e, all belly's of the mice downwards). The remaining two pairs are used as sham and exposed mice.
6. Calibrate the Network Analyzer for the cable loss and tune the antenna for that load condition at and frequency of 915 MHz.
7. Make sure that reflected power meter reading is around 10% of the forward one.
8. Start data collection with the Lab View program.
9. Take one pair of mice (mark the sham and exposed one); place the sham one in a safe place at room temperature. Place the one to be exposed into plastic rocket and put all together into the selected carousel in the Ferris Wheel (i.e., Top, Left, Right or Bottom position)
10. Turn on the power amplifier and let it stabilize a few minutes. Determine the amount of exposure time (usually 30 seconds). Using a stopwatch toggle the

switch to enable the RF exposure. At 30 seconds on the stopwatch toggle back the switch to disable the RF power.

11. Take the exposed mice from the carousel and the sham with the help of the strings (make sure not to touch the mice or the part of the rocket that touches the mice), and place them into the Twin-Well calorimeter at the same time.
12. Mark the well that contain the exposed and sham mice respectively and use always the same convention for different exposures.
13. Analyze Data.
14. Use the next pair of mice for the next exposure after 45 minutes, which is sufficient time for the loads in the FW to reach room temperature.

6.7 Data Analysis Procedure for Calorimetric Tests

1. Convert raw data file in .dat format into an excel spreadsheet (.xls). There should be four columns of data logged into the excel sheet, for the time T in seconds, the mV DC reading of calorimeter, Forward and Reverse power respectively.
2. Create a new column to calculate the net power, which is the difference of the forward and reflected power columns.
3. Integrate the area of the curve created by the data in the net power column to get the net energy supplied to the system.
4. From the column of the mV DC out put of differential calorimeter, integrate the area under this curve to get the total area under the curve of heat transfer between the wells.

5. Take the total area and divide by ten (Conversion Factor) to get a value (in Joules) of the heat dissipated in the load.
6. Take the above value and divide by the weight of that particular load to get the SAR value.
7. Compute the Efficiency of the FW.
8. To get the Normalized SAR, divide SAR with Net power per load (i.e. divide by 40).
9. Compute the 95% confidence interval level for the set of exposures.

CHAPTER VII

CALORIMETRIC RESULTS

Calorimetric experiments determine the SAR and efficiency to characterize the Ferris Wheel. Dummy loads were used for the initial characterization of the Ferris Wheel in order to get good repeatability. In order to simulate the life cycle of mice, the measurements were performed on 24 g, 32 g, 36 g mice. The Ferris Wheel is loaded with forty mice of similar weight with a deviation of +/- 0.5 g. Since we were using the dead mice and to compare with the live scenario, the mice elevated on a Styrofoam slab in order to place the collective center of mass in the center of the restrainer. As discussed in Chapter V a small offset of the collective mice center may introduce a large asymmetry, as the positioning of the mice in the restrainers is very critical.

Large numbers of exposures are done at each of four different positions of interest in the Ferris Wheel to attain repeatability. The positions of interest are the Left (9 :00 in clock) Top (12:00 in clock), Right (3:00 in clock) and Bottom (6:00 in clock) and the results of each position are as follows:

7.1 Dummy Bottles (Simulated Tissue)

7.1.1 Measurement of Normalized SAR

The below table shows the mean values of the Normalized SAR values obtained for different positions of interest and the mean Normalized SAR value for different for the whole set of loads.

Table 5. Calorimetric Results for Dummy Bottles as loads in terms of Normalized SAR

DATA FROM CALORIMETRIC TESTS FOR DUMMY LOADS			
TOP	BOTTOM	LEFT	RIGHT
0.45	0.62	0.52	0.56
Average Normalized SAR [W/kg/W]		0.54	

Lab View data acquisition program used for the collection of heat transfer between the loads in terms of voltage difference between the wells of Twin-Well calorimeter. The program collects the data at an instance and waits for 2 seconds to in collect for next data value. During the data collection for the exposure tests this software looses the heat content in a second for each minute because of the delay in collecting the data. So the error in heat can be acoounted by introducing a correction factor of 1.06667 for the loss in time.

Table 6. Normalized SAR after Correction Factor for Lab View Data Acquisition

CORRECTION FACTOR OF 1.06667 FOR LABVIEW INTEGRATION STEP			
TOP	BOTTOM	LEFT	RIGHT
0.46	0.63	0.53	0.57
Average Normalized SAR [W/kg/W]			0.55

There is some heat loss, which occurs during the time interval from the end of the exposure and the placement of loads into the Twin-Well calorimeter. As the above exposure tests are done in a very careful and repeatable process, the average time delay

for placing the loads into the Twin-Well is 5 seconds. In order to determine the percentage of heat loss in these 5 seconds, another set of measurements were carried out using the dummies with an intentional extending delay to 10 seconds and 15 seconds. Fig.37 shows the determination of the correction factor for the 5-second delay but for with the dummy bottles with 30 grams. The Normalized SAR might have higher values to the

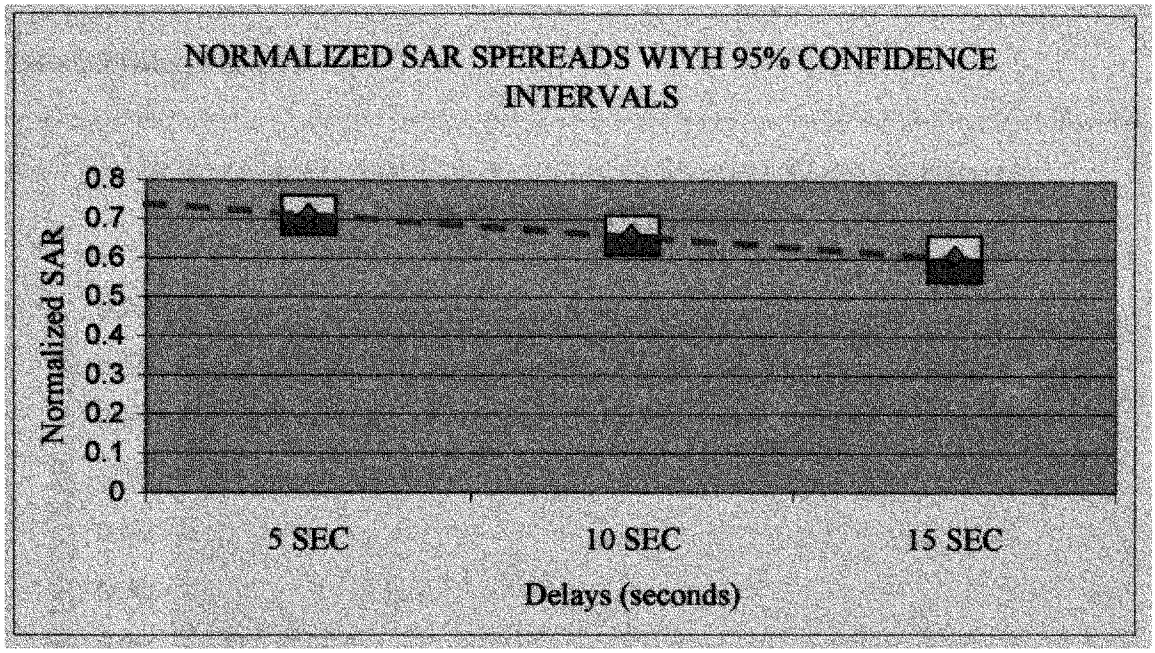

Fig.37. Extrapolation for the heat loss in 5-second delay.

Table 7. Correction factor for 5-second delay for Dummy Loads

Ratio of Normalized SAR for 5-second to 10- second Delay	1.08
Ratio of Normalized SAR for 10-second to 15- second Delay	1.12
Averaged Correction Factor	1.1

Table 8. Normalized SAR after Correction Factor for 5 second Delay

CORRECTION OF 1.1 FOR 5 SEC DELAY			
TOP	BOTTOM	LEFT	RIGHT
0.50	0.69	0.58	0.63
AVERAGE EFFCIENCY [%]			0.60

Also introducing the correction factor for transferring the loads form the wheel we have following Table 3.

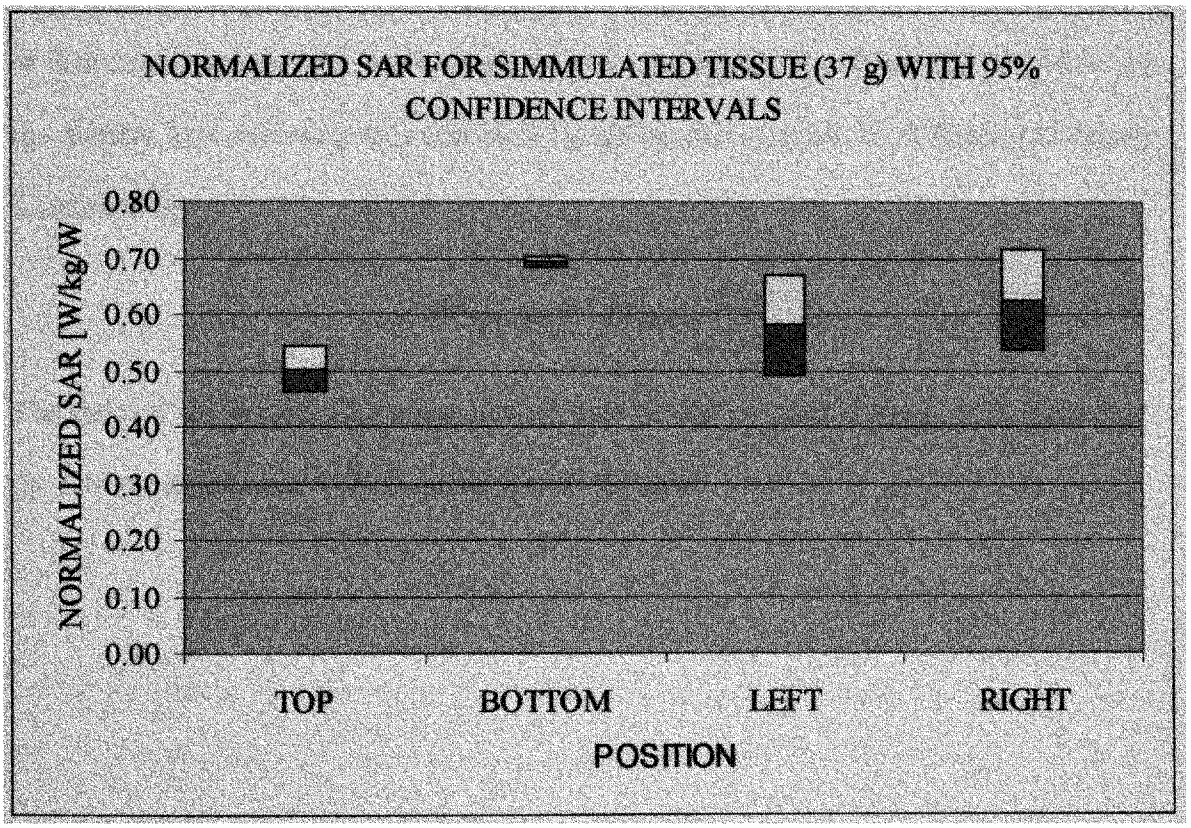

Fig.38. Normalized SAR (W/kg/W) Vs Position for the Dummy Loads.

The figure above shows the Normalized Whole-Body SAR averages to the net power at four different positions with their corresponding deviations for several

experiments using Calorimetric tests. Number of experiments ware repeated at that particular position until the standard error fall below 10% for that set of data.

The deviation of the average SAR is higher at the right and left positions is the positioning of the bottles is not always at the same in all exposures, but at top and bottom position the bottle seems to be resting at the same position with more consistency. In the Fig.29 it can be seen that change in displacement of 2.5 mm of the load from center has a large impact on the amount of energy absorbed by the body.

As discussed in Chapter IV the dummy load which is equivalent to mice in terms of dielectric properties but not in terms of average density. The Whole Body SAR in the the dummy load assuming as a real mice by taking into account the difference in density is obtained by

$$SAR_{WB-Mice} = SAR_{Dummy} \frac{\rho_{Dummy}}{\rho_{Mice}} \tag{7.1}$$

The ratio of the densities between dummy load to that of mice is about 1.25. Therefore, the average normalized SAR obtained is 0.75 W/kg/W.

7.1.2 Efficiency Measurements for the Exposure System

The following tables show the average efficiency at the respective positions and the

Table 9. Efficiency data from Calorimetric tests at different positions of interest on FW using Dummy Loads

EFFCIENCY DATA FROM CALORIMETRIC TESTS FOR DUMMY LOADS			
TOP	BOTTOM	LEFT	RIGHT
66.96	92.30	76.82	82.76
AVERAGE EFFCIENCY [%]			79.71

averaged efficiency of the wheel and equal to 79.71 %. This efficiency is based on the Calorimetric experimental results. The efficiency results from calorimetric tests also will have same correction factors as which are applicable for the Normalized SAR. Tables 9 and 10 show the efficiency results after the corrections factors are accounted for.

Table 10. Correction Factor for Lab View Data Acquisition Program

CORRECTION FACTOR OF 1.06667 FOR LABVIEW INTEGRATION STEP			
TOP	BOTTOM	LEFT	RIGHT
68.08	93.84	78.10	84.14
AVERAGE EFFCIENCY [%]			81.03

Table 11. Final Efficiency of FW using Dummy Loads including Correction Factor for 5-seconds delay

CORRECTION FACTOR OF 1.1 FOR 5 SECONDS DELAY			
TOP	BOTTOM	LEFT	RIGHT
78.88	103.22	85.91	92.55
AVERAGE EFFCIENCY [%]			89.14

So the final efficiency system is 89.14 %.

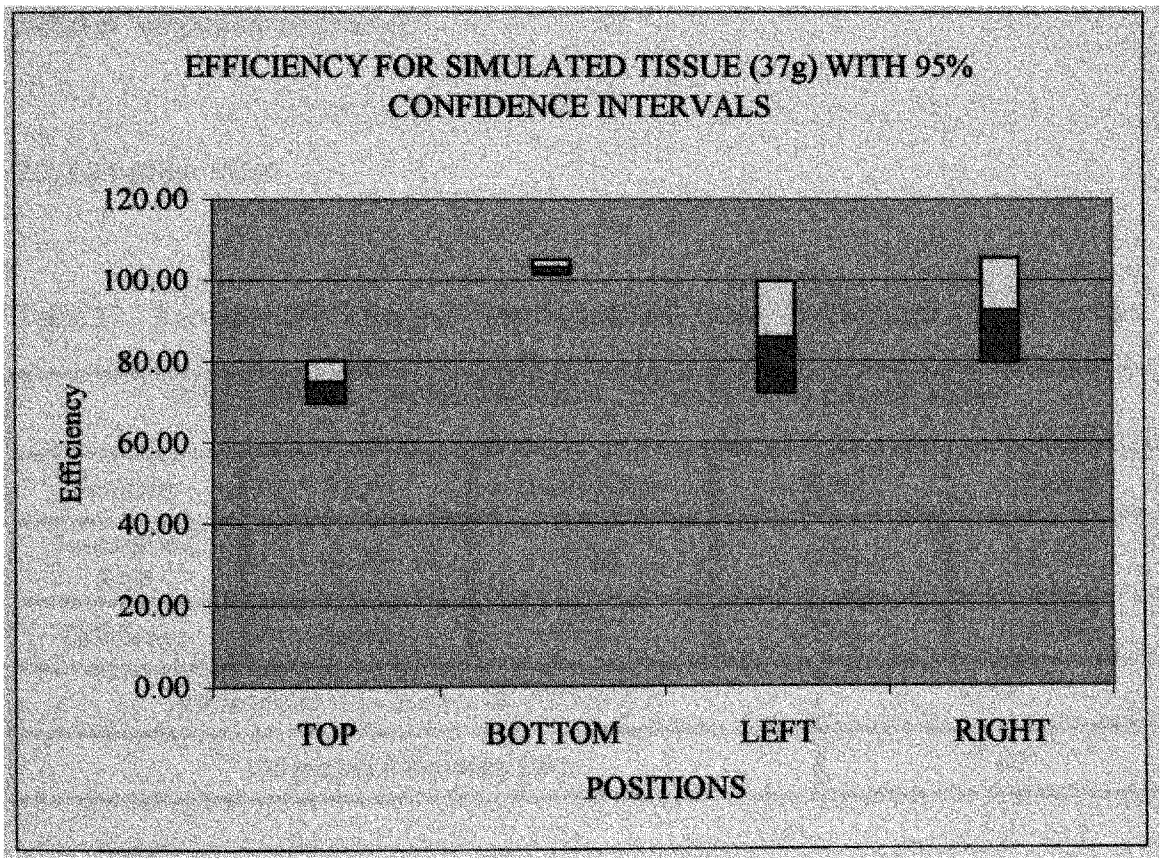

Fig.39. Efficiency Vs Position for the dummy loads.

7.2 Mice Cadavers

A number of Calorimetric tests on mice at different weights have been performed to refine the experimental techniques on mice and to achieve a good repeatability .The correction applied for the dummy bottles as loads will also apply for mice of the three different weights. But the correction factor for the 5 seconds delay in transferring the loads from the Ferris Wheel to Twin-Well calorimeter is not used because of this small delay in the case of mice cadavers is not so significant as the heat loss during the transfer of mice is very less when compared to the dummy loads. The results for the three different weights are as follows:

7.2.1 24-gram Mice

Table 12. Averaged Efficiency and Normalized SAR values for 24-grams mice as Loads

DATA FROM CALORIMETRIC TESTS FOR 24 GRAM MICE				
Position	TOP	BOTTOM	LEFT	RIGHT
Normalized SAR	0.71	0.85	0.79	0.75
Efficiency	66.52	77.77	72.8	69.38
Averaged Normalized SAR (W/kg/W):				0.78
Averaged Efficiency (%):				71.62

Table 13. Correction Factor for Lab View Data Acquisition Program

CORRECTION FACTOR OF 1.06667 FOR LABVIEW INTEGRATION STEP				
Position	TOP	BOTTOM	LEFT	RIGHT
Normalized SAR	0.72	0.86	0.80	0.76
Efficiency	67.63	79.07	74.01	70.54
Averaged Normalized SAR (W/kg/W):				72.81
Averaged Efficiency (%):				0.79

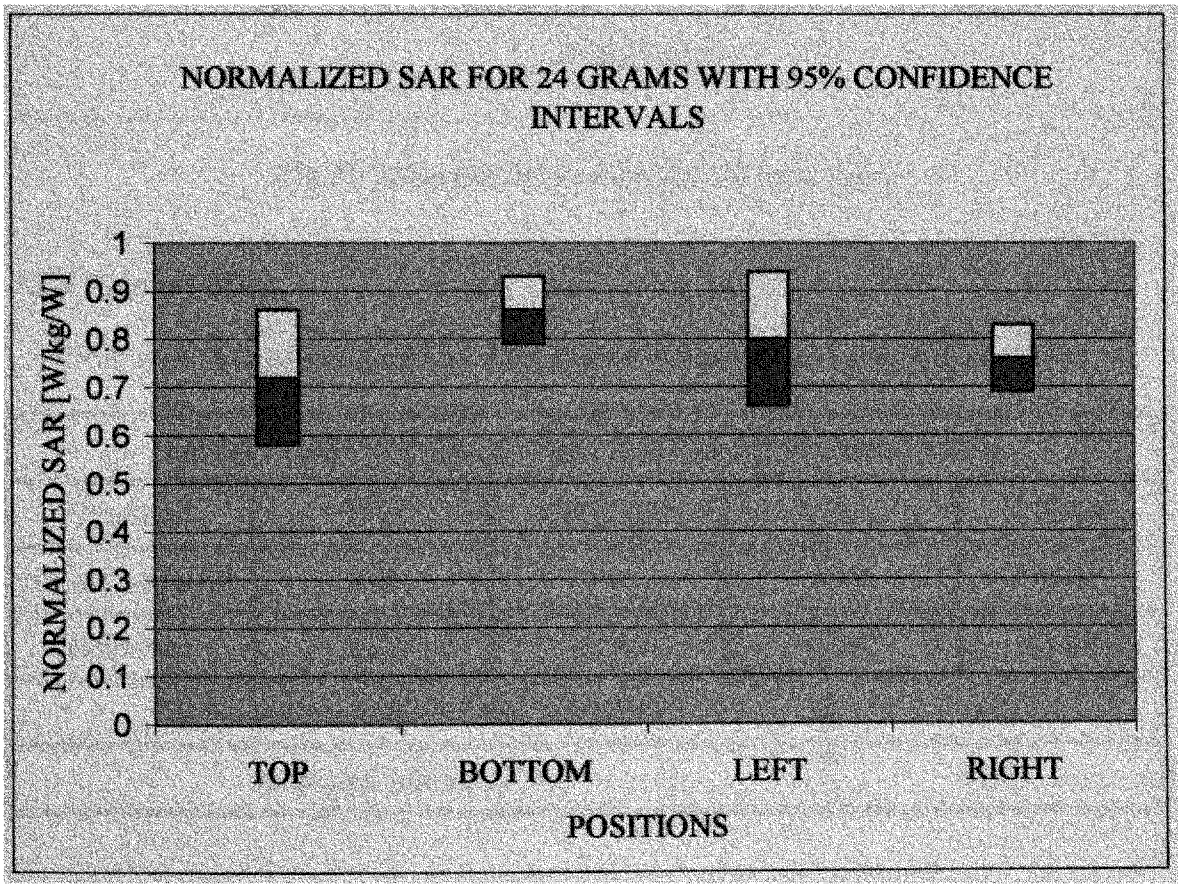

Fig.40. Normalized SAR (W/kg/W) Vs Position for the 24 g mice.

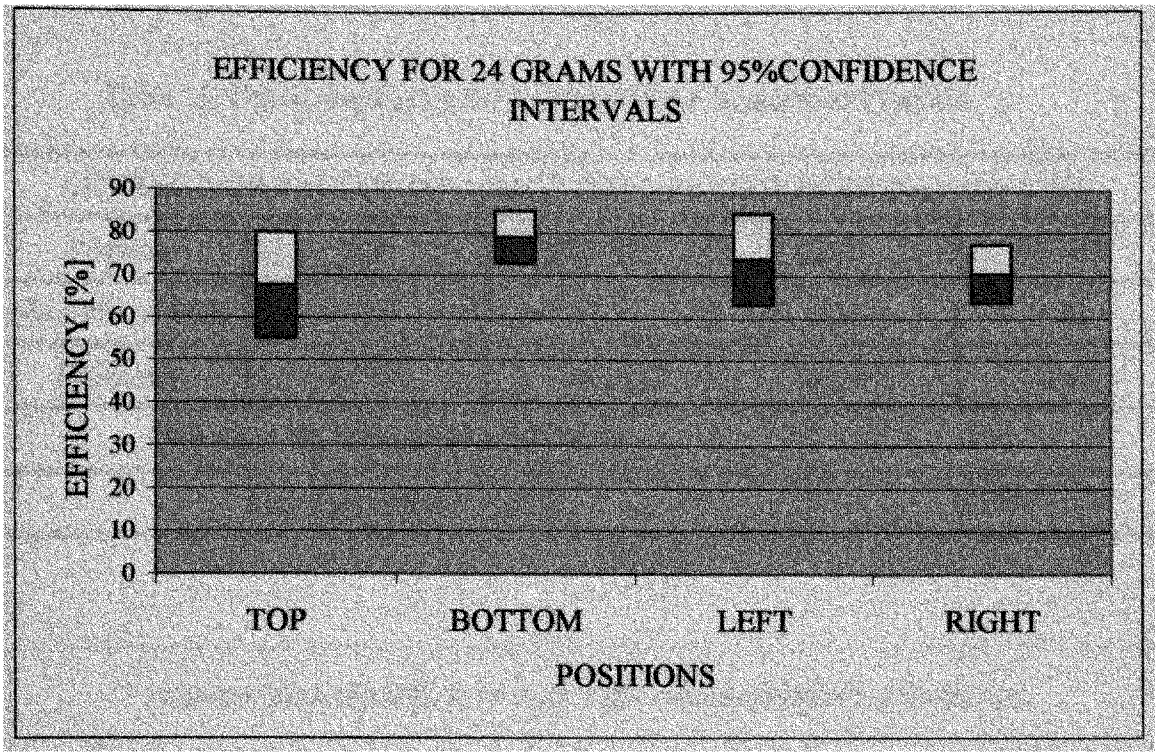

Fig.41. Efficiency Vs Position for the 24-g mice.

7.2.2 32-gram Mice

Table 14. Averaged Efficiency of the Ferries Wheel using 32 grams mice as load

DATA FROM CALORIMETRIC TESTS FOR 36 GRAM MICE				
Position	TOP	BOTTOM	LEFT	RIGHT
Normalized SAR	0.68	0.72	0.74	0.71
Efficiency	84.2	92.66	94.92	92.41
Averaged Normalized SAR (W/kg/W):				0.71
Averaged Efficiency (%):				91.05

Table 15. Correction Factor for Lab View Data Acquisition Program

CORRECTION FACTOR OF 1.06667 FOR LABVIEW INTEGRATION STEP				
Position	TOP	BOTTOM	LEFT	RIGHT
Normalized SAR	0.69	0.73	0.75	0.72
Efficiency	85.60	94.20	96.50	93.95
Averaged Normalized SAR (W/kg/W):				0.72
Averaged Efficiency (%):				92.56

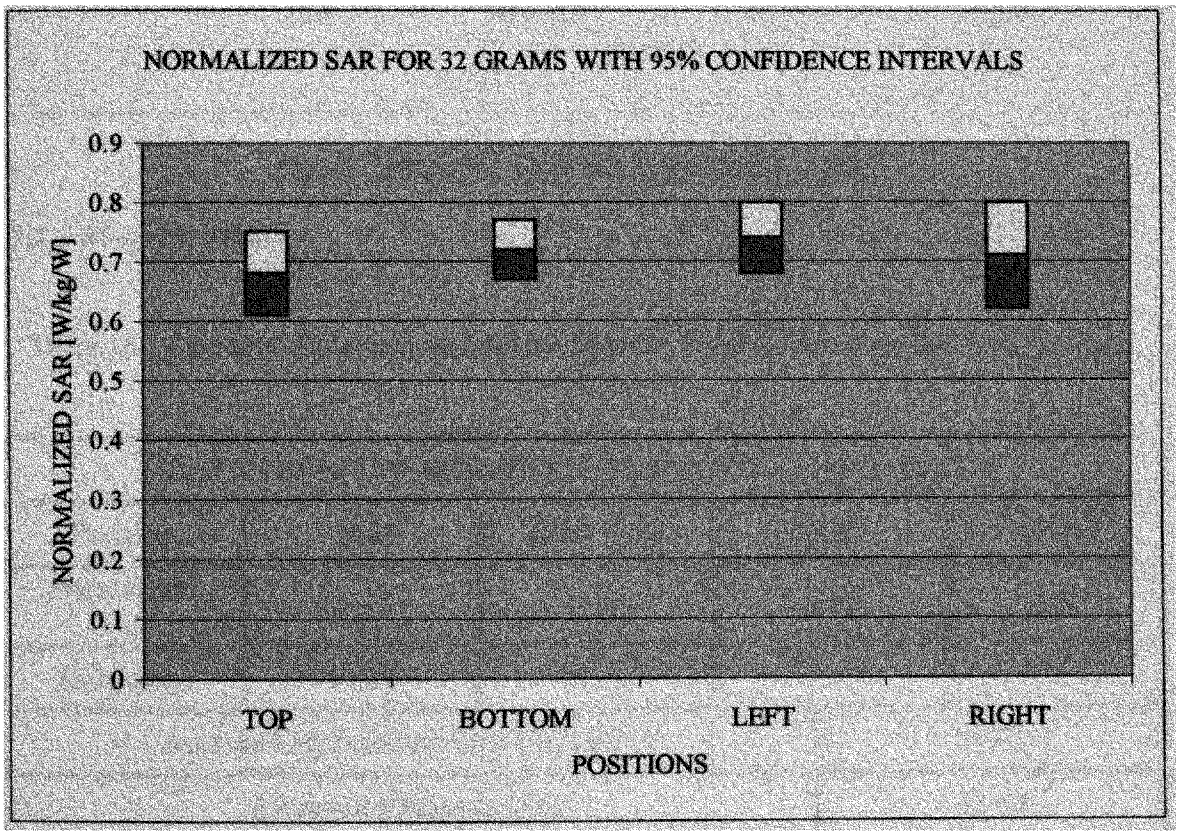

Fig.42. Normalized SAR (W/kg/W) Vs Position for the 32-g mice

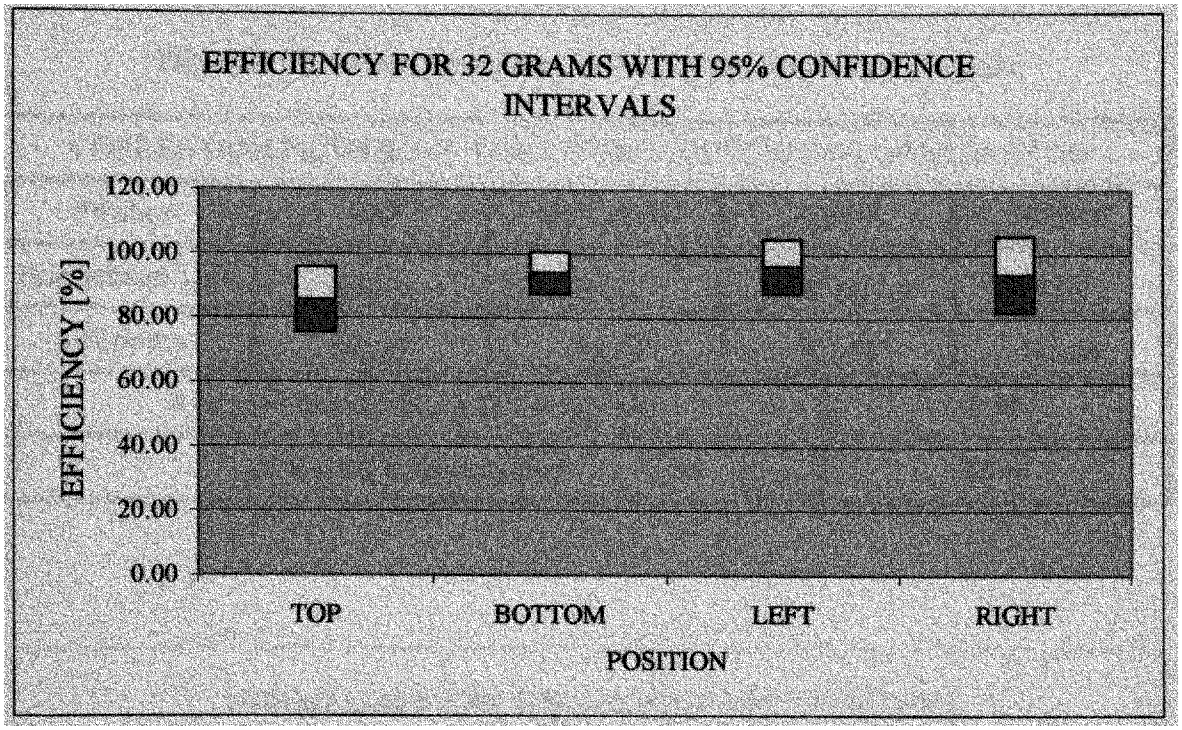

Fig.43. Efficiency Vs Position for the 32-g mice.

7.2.3 36-gram Mice

Table 16. Averaged Efficiency and Normalized SAR values for 36-grams mice as loads

DATA FROM CALORIMETRIC TESTS FOR 36 GRAM MICE				
Position	TOP	BOTTOM	LEFT	RIGHT
Normalized SAR	0.63	0.57	0.54	0.55
Efficiency	89.87	81.41	75.92	79.12
Averaged Normalized SAR (W/kg/W):				0.57
Averaged Efficiency (%):				81.58

Table 17. Correction Factor for Lab View Data Acquisition Program

CORRECTION FACTOR OF 1.06667 FOR LABVIEW INTEGRATION STEP				
Position	TOP	BOTTOM	LEFT	RIGHT
Normalized SAR	0.64	0.58	0.55	0.56
Efficiency	91.37	82.77	77.19	80.44
Averaged Normalized SAR (W/kg/W):				0.58
Averaged Efficiency (%):				82.94

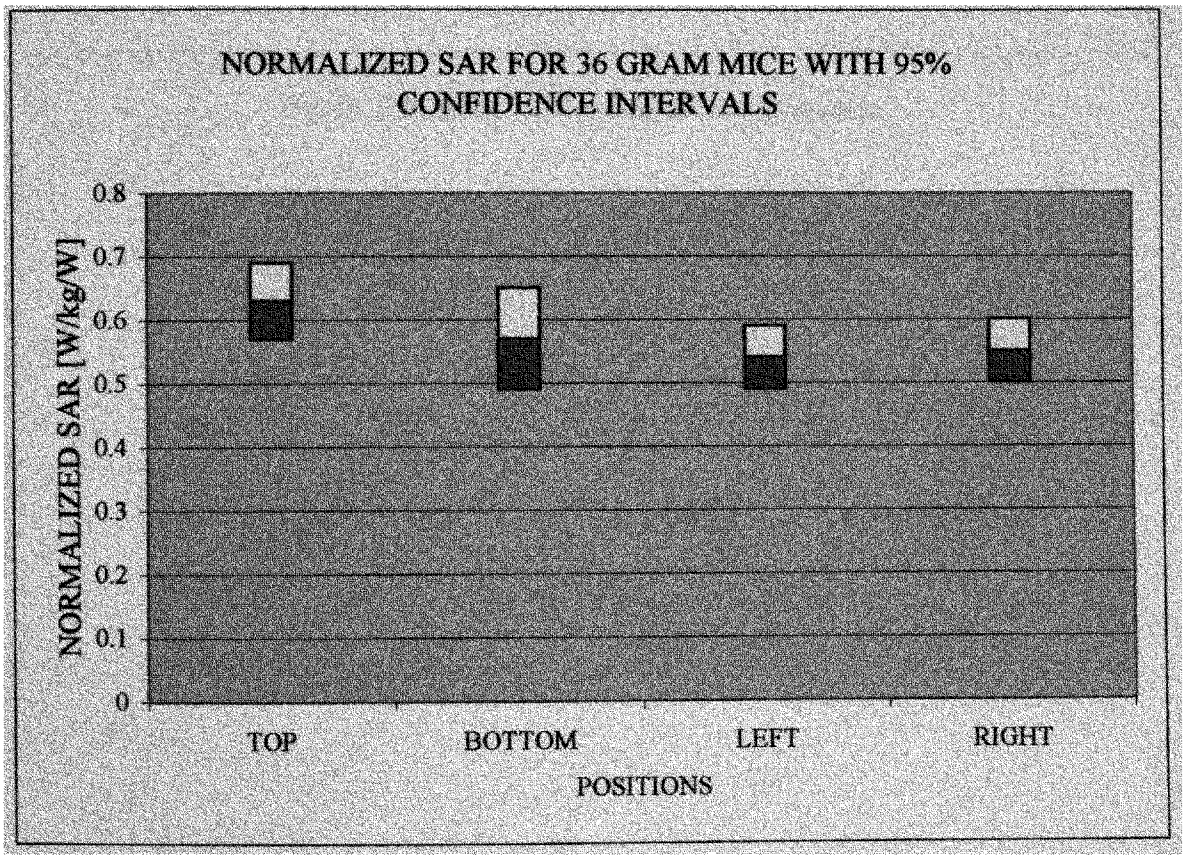

Fig.44. Normalized SAR (W/kg/W) Vs Position for the 36-g mice.

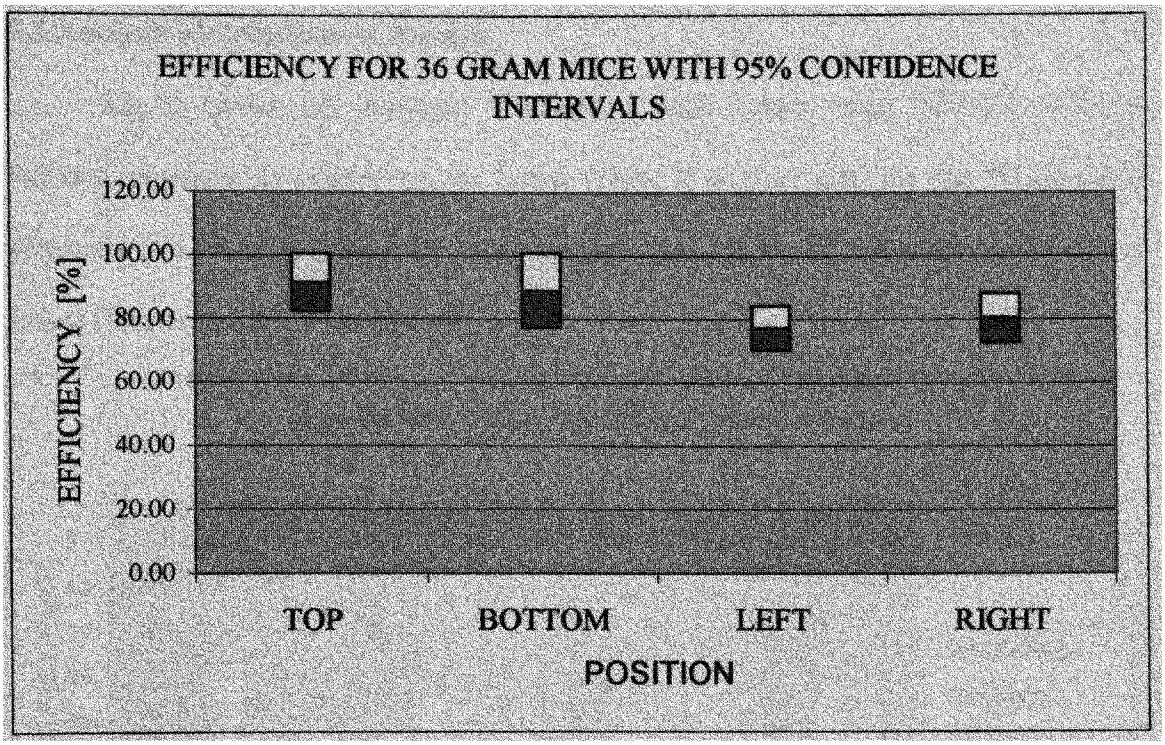

Fig.45. Efficiency Vs Position for the 36-g mice.

7.3 Analysis of Calorimetric Results

Fig.46 shows the averaged Normalized SAR values using different loads at different positions of interest on the Ferris Wheel It can be seen that the Whole-Body Normalized SAR is in 24-g mice is higher than that of the 32, 36 grams and Dummy Loads (Marked as ST in the figures).

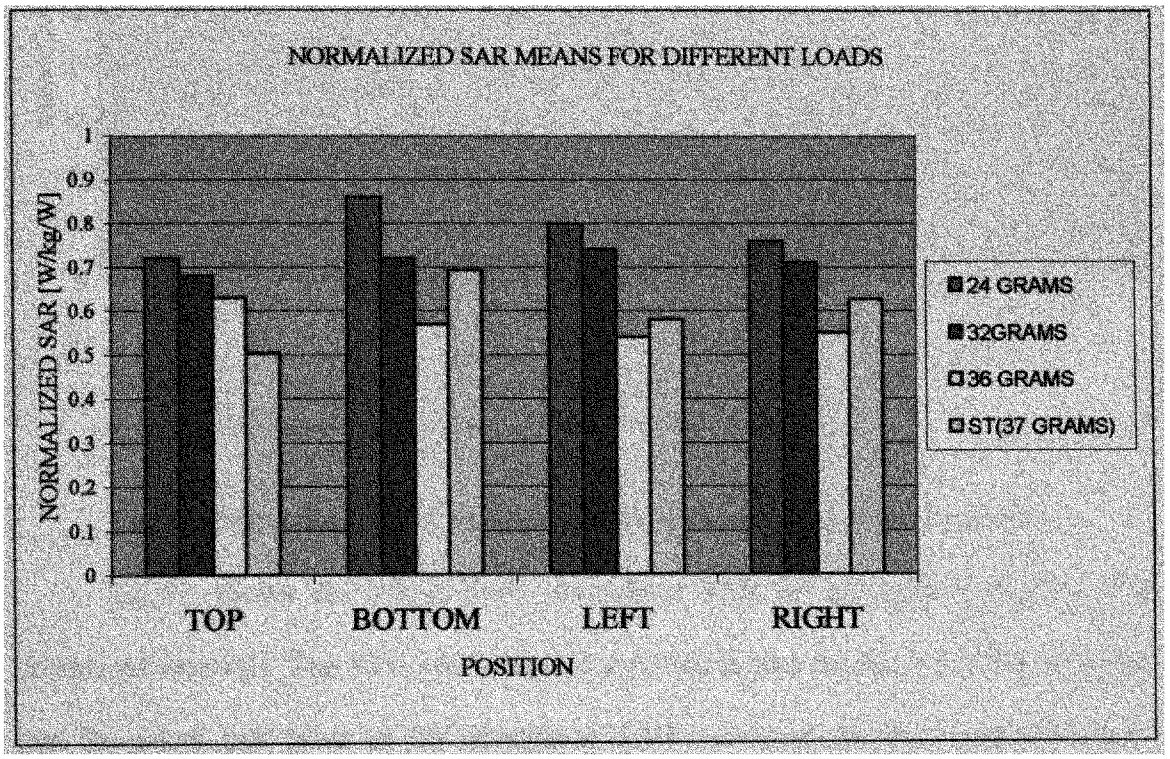

Fig.46. Whole- Body SAR values for Different weights versus Positions.

It can be also seen that the Normalized SAR values for three different mice weights and dummy loads at four positions on the Ferris Wheel lie between the 0. 50 - 0.85 W/kg/W.

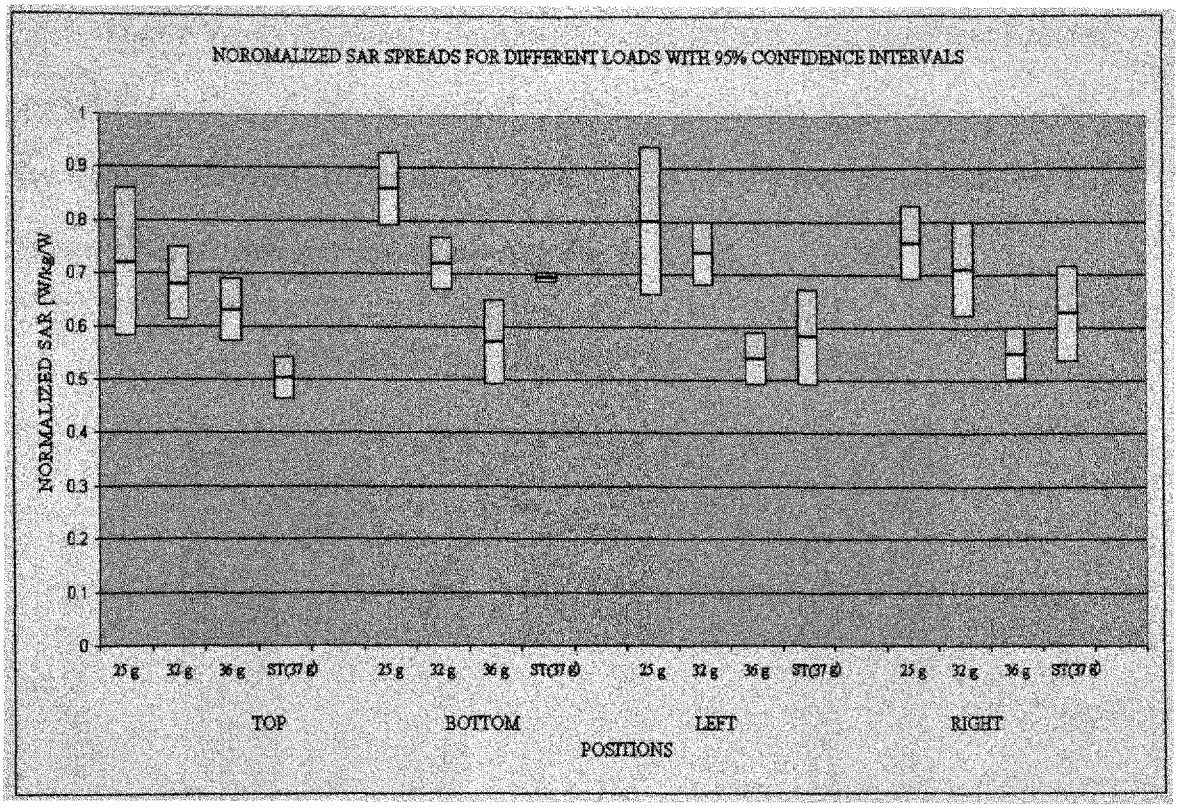

Fig.47. Whole-Body SAR values for Different Loads with their Deviations.

Fig.47. shows the Whole-Body normalized SAR for all loads with their 95% confidence intervals. The 95% confidence interval states that we have a 95% confidence that the actual true mean of the normalized SAR measurements lies in between these intervals. It's also seen that at position of interest the deviations from the mean are higher for the 24 g rather than the 32 and 36 g. The reason for the higher deviations in 24-g mice is due to the higher uncertainty in placing it not exactly at the center of the carousel as these mice very compared to 32, 36g. So chances of positioning the mice on the steep side of the curve shown in Fig.6 are higher in case of 24-g mice. This will lead to higher deviations in the case of 24 than the 32 and 36 g.

Fig.48. shows the average relative efficiency obtained at the positions of interest using different loads. It can be seen that the efficiency is lowest in the case of 24-g mice and highest in the case of 32-g mice. The average power efficiency of the system is found to be 84.4%, which is very high when compared to the earlier systems.

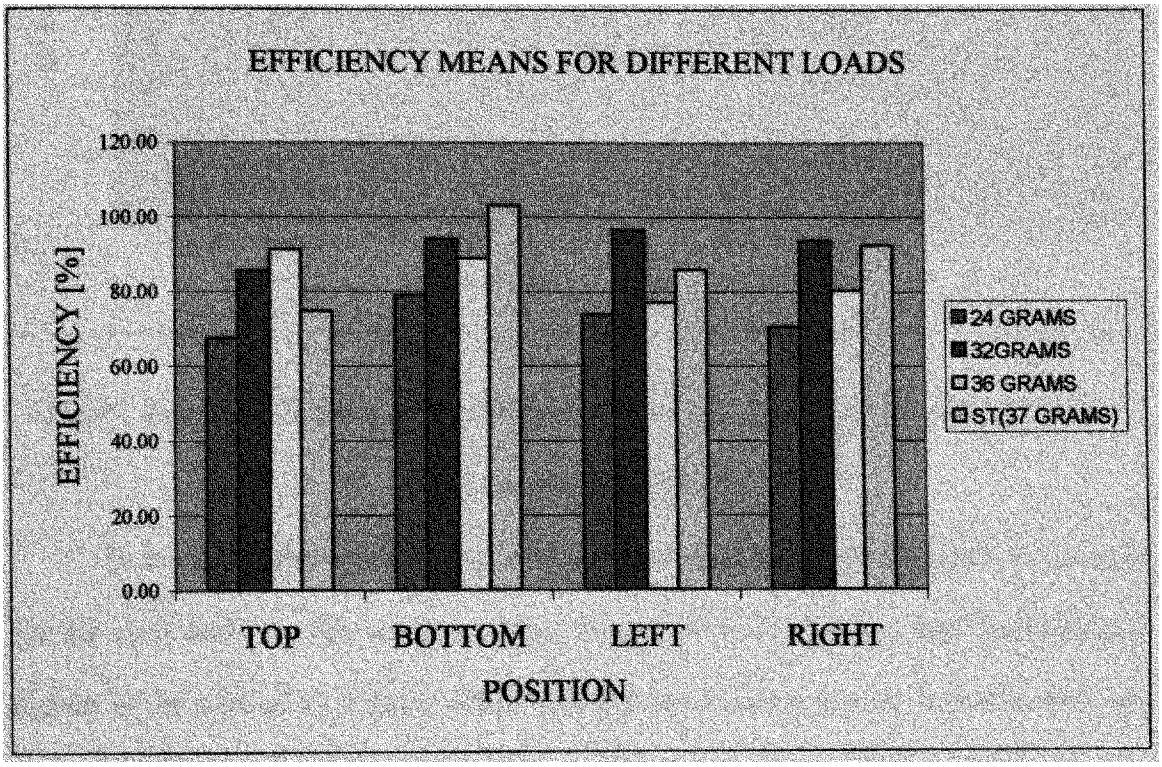

Fig.48. Relative Efficiency of the FW at Positions of Interest using Different Loads.

It is also seen that the highest deviations of the relative efficiency between the Top and Bottom positions for any type of load is 0.69 dB and the Left and the Right positions is 0.32 dB, which shows that the system is very symmetrical about the positions of interest.

Fig.49 shows the relative efficiency spreads at the positions of interest for different loads with their 95% confidence intervals.

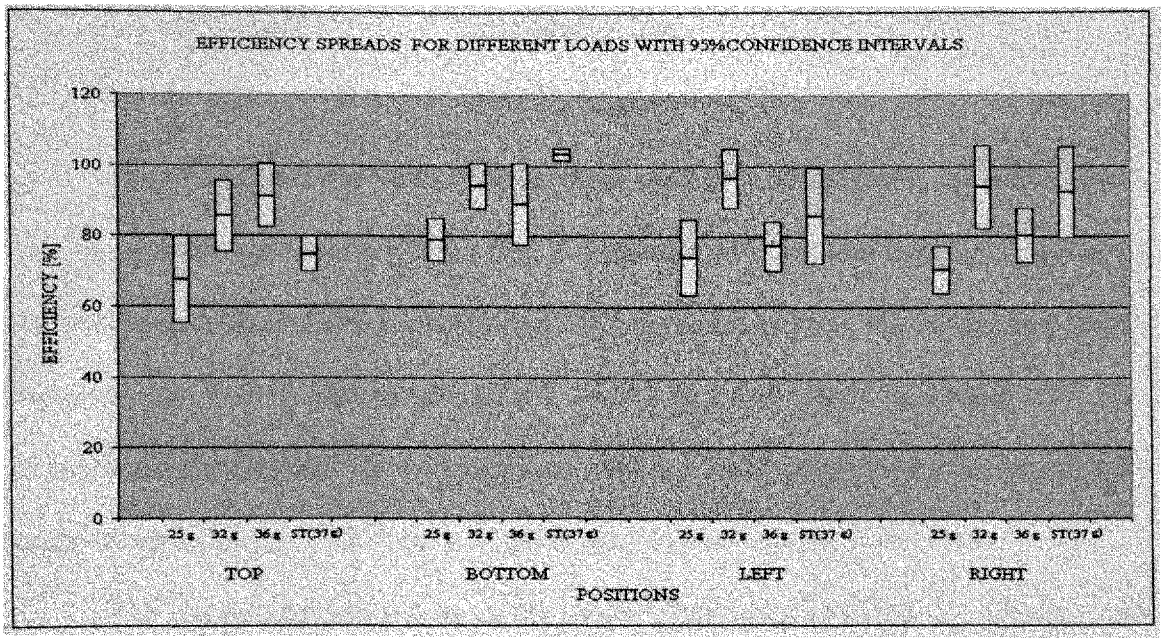

Fig.49. Relative Efficiency at the Positions of Interest for Different Loads with their 95% Confidence Intervals.

In the Australian study it is seen that mouse weighs around 32-grams for most of the life cycle and very few weeks at 25-g. As seen from the Ferris wheel is operating at highest in the case of 32-g mice, which says that the systems used in Australia study are working at their highest efficiencies for most of the time in the two year period.

CHAPTER VIII

CONCLUSIONS

The measured E-field distributions inside the Ferris Wheel along the ρ-axis and z-axis i.e., (inside the restrainer) by using E-field measurement probes have an excellent correlation with that of the simulated ones. The simulations have shown that the system preserves the E-field distribution pattern even when the system is loaded with four different weights of loads in a symmetrical fashion. Small displacement in the effective Barry-center of the load will induce an asymmetry in distribution of the fields.

The characterization results of the Ferris Wheel using calorimetric technique with dummy loads and mice cadavers Chapter 5 shows that the obtained Normalized SAR values are very consistent in all positions of interest and has a range from 0.5 to 0.9 W/kg/W. The average efficiency obtained from these experiments using different loads (dummy and mice cadavers) is 84.4%, which shows that the system is efficient in transferring the energy into its loads. The highest deviation in efficiency between top and bottom positions is 0.69 dB. The left to right difference is about 0.32 dB for any type of load, which shows that the system in symmetrical distributing power into the loads.

The tunable antenna of the FW exposure has good tuning capability over the wide range of loading conditions during characterization of the FW using calorimetric technique. The system was used for a huge number of exposure experiments and it has shown good reliability and consistency.

The Ferris Wheel Exposure system provides an efficient means for conducting long-term animal studies of Whole-Body RF exposure.

REFERENCES

[1] Michael H. Rapacholi, Anthony Basten, Val Gedski, Denise Noonan, John Finnie and Alan W. Harris "Lymphomas in Eμ-*PIM 1* Transgenic Mice Exposed to Pulsed 900 MHz Electromagnetic Fields," Radiation Research, Vol.147, pp.631-640, 1997.

[2] Tammy D. Utteridge, Val Gebski, John W. Finnie, Barrie Vernon-Roberts and Tim R. Kuchel "Long-Term Exposure of Eμ- Pim1 Transgenic Mice to 898.4 MHz Microwaves does not Increase Lymphoma Incidence," Radiation Research, Vol.158, pp.357-364, 2002.

[3] Q. Balzano, C.K. Chou, A. Faraone, Renato Cicchetti an d Roger Y. Tay "An Efficient RF Exposure System with Precise Whole-Body Average SAR Determination for vivo Animal Studies at 900 MHZ," *IEEE Trans. On Microwave Theory and Techniques*, vol.48, no.11, pp-2040-2049, Nov 2000.

[4] A.W.Guy, "Miniature anechoic chamber for chronic exposure of small animals to plane-wave microwave fields," *J. Microwave Power*, vol. 14,no. 4, pp. 327–338, 1979.

[5] C.K.Chou and A.W.Guy, "Systems for exposing mice to 2,450-MHz electromagnetic fields," *Bioelectromagnectics*, vol. 3, no. 4, pp. 401–412,1982.

[6] V.W. Hansen, A. K. Bitz, and J. R. Streckert, "RF exposure of biological systems in radial wave guides," *IEEE Trans. Electromagnetic Compatibility*, vol. 41, pp. 487–493, Nov.1999.

[7] P.Russo and A.Faraone " Numerical Analysis of the " Ferris Wheel" Mice exposure system using an efficient cylindrical FDTD Scheme".

[8] C.K.Chou, H. Bassen, J.Osepchuk, Q. Balzano, R.Petersen, M.Meltz, R. Cleveland J.C. Lin, and L.Heynick "Radio frequency electromagnetic exposure: Tutorial review on experimental dosimetry," *Bioelectromagnectics*, vol.17, pp.195-208, 1996.

[9] *IEEE Standard for Safety Levels with Respect to Human Exposure to Radio Frequency Electromagnetic Fields, 3 kHz to 300 GHz*, IEEE Standard C95.1, ICNIRP, 1991.

[10] "Evaluating compliance with FCC guidelines for human exposure to radio frequency electromagnetic fields," Federal Communications Com-mission, Washington, D.C, OET Bull. 65, Aug. 1997.

[11] "Radio frequency electromagnetic fields; properties, quantities and units, biophysical interaction, and measurements," National Council on Radiation Protection and Measurements, Bethesda, MD, NCRP Rep. 67, 1981.

[12] Durney CH, Massooudi H, and Iskander MF (1986): " Radio frequency Radiation Dosimetry Hand book, 4th Edition (Report TR-85-73)."Brooks Air-force Base, TX: USAF School of Aerospace Medicine.

[13] Durney CH, Johnson CC, Barber PW, Massooudi H, and Iskander MF, Lords JL, Ryser DK, Allen SJ, Mitchell JC (1978): " Radio frequency Radiation Dosimetry Hand book, Second Edition (Report TR-78-22)."Brooks Air-force Base, TX: USAF School of Aerospace Medicine.

[14] Gandhi Op, Hunt EL and D'Andrea JA (1977): Deposition of electromagnetic energy in animals and in models of man with and without grounding and reflector effects. Radio Sci 12(6s): 39-47.

[15] Charles Polk and Elliot Postow, *CRC Handbook of Biological Effects of electromagnetic fields.* Boca Raton, Florida: CRC Press, Inc.

[16] Luengas Wilson, "Determination of Localized SAR by Thermography and Thermometric processes using Ferris Wheel as an Exposure System" Master's Thesis in Preparation, Florida International University, Electrical and Computer Engineering, 2002.

[17] K.S.Yee, "Numerical Solution of Initial Boundary Value Problems Involving Maxwell's Equations in Isotropic Media," *IEEE Transactions on Antennas and Propagation*, Vol.14, No.4, pp.302-307, 1966.

[18] H. Bassen, M. Swicord, and J. Abita, "A Miniature Broad-Band Electric Field Probe," *Annals New York Academy of Sciences*, vol. 247, pp.481-493, 1975.

[19] A.Faraone," Preliminary report on the Ferris Wheel Exposure System dosimetry". Motorola internal Report, July 2002.

[20] Renato Cicchetti. "Mathematical Model for Twin-Well Calorimeter". Motorola Internal report, September 2002.

[21] Stanley Humpheies, Jr., *Field Solutions on Computers* Boca Raton, Florida: CRC Press, Inc.

FLORIDA INTERNATIONAL UNIVERSITY

Miami, Florida

DETERMINATION OF WHOLE-BODY SPECIFIC ABSORPTION RATE (SAR) AND CHARACTERIZATION OF FERRIS WHEEL RADIO FREQUENCY (RF) EXPOSURE SYSTEM USING CALORIMETRIC TECHNIQUES

A thesis submitted in partial fulfillment of the

requirements for the degree of

MASTER OF SCIENCE

in

ELECTRICAL ENGINEERING

by

Subbarao V. Chebrolu

2002

To: Dean Vish Prasad
College of Engineering

This thesis, written by Subbarao V. Chebrolu, and entitled Determination of Whole-Body Specific Absorption Rate (SAR) and Characterization of Ferris Wheel Radio Frequency (RF) Exposure System using Calorimetric Techniques, having been approved in respect to style and intellectual content, is referred to you for judgment.

We have read this thesis and recommend that it be approved

Subbarao V. Wunnava

Malcom Heimer

Chung-Kwang Chou

Antonio Faraone

Tadeusz M.Babij, Major Professor

Date of Defense: November 22 , 2002

The thesis of Subbarao V. Chebrolu is approved.

Dean Vish Prasad
College of Engineering

Dean Douglas Wartzok
University Graduate School

Florida International University, 2002

DEDICATION

To my parents and sister, for their support and encouragement.

ACKNOWLEDGMENTS

Several people have helped me to conduct and complete the research presented here. First and foremost, I would like to thank Dr. C.K.Chou and Dr. Antonio Faraone for their patience, understanding and moral support. I was fortunate in having the opportunity to discuss ideas with both of them, whose deep perception and constructive criticism helped to focus and refine myself. Their suggestions and constant encouragement gave me a boost of confidence and stimulation.

I am also grateful to Dr. Renato Cicchetti and Dr. Giorgi Bit-Babik for their support in deriving the mathematical model for the twin-well calorimeter and simulations on Ferris Wheel respectively. This thesis would have not been possible without the help and support from Wilson Luengas, Maurice Ballen, John McDougall, George Han, Andy Greesner and Mike Kanda for their technical contribution at the Motorola Florida Research Labs during this research.

I wish to thank Motorola for sponsoring my study, providing the laboratory and equipment for doing this research. I also want to thank the Electrical and Computer Engineering Department of FIU for the tuition waiver and teaching assistantship given to me.

My special thanks to my major professor and advisor Dr. T.M. Babij for his continued guidance and support during the preparation of this thesis and for Dr. Babij's opting me to work for Motorola's project was truly invaluable. I would also like to thank Dr. Subbarao Wunnava and Dr. Malcom Heimer who also served in my graduate committee for their valuable cooperation and priceless time throughout my Master's program at the Department of Electrical and Computer Engineering.

ABSTRACT OF THE THESIS

DETERMINATION OF WHOLE-BODY SPECIFIC ABSORPTION RATE (SAR) AND CHARACTERIZATION OF FERRIS WHEEL RADIO FREQUENCY (RF) EXPOSURE SYSTEM USING CALORIMETRIC TECHINQUES

by

Subbarao V. Chebrolu

Florida International University, 2002

Miami, Florida

Professor Tadeusz M. Babij, Major Professor

The "Ferris Wheel" RF Exposure System was designed by Motorola Inc. to study the long-term biological effects due to RF exposure [3]. The main goal of this research project was to characterize the "Ferris Wheel" to know how efficient and symmetrical was the exposure system in distributing the RF power among its loads. The characterization of the system was done in terms of power efficiency, SAR, Whole-Body SAR and Localized SAR.

Exposure to RF sources is quantified in terms of SAR which defines the rate of electromagnetic deposition per unit mass. Determination of Whole-Body averaged SAR requires to have the actual amount of energy absorbed where as the temperature increase in the tissue material yields the Localized SAR. Calorimetric Techniques were used to characterize the "Ferris Wheel" exposure system in terms of Whole-Body SAR and efficiency. Microwave Studio and XFDTD simulation programs based on *Finite Difference Time Domain* method were also used to determine the Whole-Body SAR and

E-field distribution in the "Ferris Wheel." The E-field distribution inside the FW was measured by using E-field probes and result was compared to that of simulated.

TABLE OF CONTENTS

LIST OF TABLES

TABLE PAGE

LIST OF FIGURES

FIGURE PAGE

CHAPTER I

INTRODUCTION

Over the past several decades a large number of scientific studies have been published worldwide on biological effects from exposures to extremely low frequency (ELF) fields and radio frequency (RF) fields such as emitted by radars and telecommunication transmitters. Some of these studies have reported a number of hazards from electromagnetic fields (EMF) exposures, but these are generally at very high exposure levels. International exposure guidelines have been developed to protect against them.

There are several important considerations when evaluating possible health effects of RF fields. One is the frequency of the radiation. By virtue of their frequencies, the photon energies associated with RF are insufficient to cause ionization in matter such as body tissue. Because of this, RF fields are called non-ionising, which unlike X-rays and gamma radiations can cause ionisation leading to the breakup of the molecular structure of matter.

Mobile telephones, often called cell phones, are now an integral part of modern telecommunications. The technology of the mobile phone system necessitates the installation of a large number of antennas or base-stations in order to accommodate the large number of users, and to provide the necessary coverage. Many of these antennas and base-stations are installed on top of high-rise buildings. Because of the large number of users, there is now considerable public concern about possible health hazards from EMF exposures from mobile phones or their base stations.

Mobile phone handsets and base stations present quite different exposure situations. Mobile phone handsets are low-powered RF transmitters, emitting maximum powers in the range of 0.13 to 0.6 watts. The RF field strength (and hence RF exposure to a user) falls off rapidly with distance from the handset. Therefore, the RF exposure to a user of a mobile phone located tens of centimeters from the head using a "hands free" appliance is far lower than to a user who places the headset against the head. RF exposures to nearby people from these devices are very low.

Base stations transmit power levels typically from a few watts to less than 100 watts, depending on the size of the region or "cell" that they are designed to service. The antennas emit RF beams that are typically very narrow in the vertical direction but broad in the horizontal direction. Because of the narrow vertical spread of the beam, the RF field intensity at the ground directly below the antenna is low. The RF field intensity increases slightly as one moves away from the base station and then decreases for greater distances from the antenna. Paging and other communications antennas used by fire, police and emergency services, operate at similar power levels as cellular base stations, and often at a similar frequency. Television and radio broadcast antennae commonly transmit much higher RF levels than mobile base stations.

RF fields penetrate exposed tissues to depths that depend on the frequency, usually up to a centimeter at the frequencies used by mobile phones. RF energy is absorbed in the body and produces heat, but the body's normal thermo-regulatory processes carry this heat away. Health effects due to RF exposure have shown to be related to heating. RF energy which interacts with body tissues at levels used by mobile

phones are too low to cause any significant heating. No consistent studies have shown adverse health effects at exposure levels below international guideline limits.

Current scientific evidence indicates that exposure to RF fields, such as those emitted by mobile phones and their base stations, is unlikely to induce or promote cancers. Several studies of animals exposed to RF fields similar to those emitted by mobile phones found no evidence that RF causes or promotes cancer. Epidemiological studies found no convincing evidence of increase in risk of cancer or any other disease with use of mobile phones.

A study was conducted at Royal Adelaide Hospital lead by Dr. Michael Repacholi exposing lymphoma prone mice to digital Global Systems Mobile (GSM) 900 Megahertz fields over a 9 to 18 month period [1]. The mice were divided into two groups of 100 each and placed in the cages, housed in identical conditions in two different chambers and subject to the same amount and type of handling. The match extended even to having a sham antenna hanging over the control group.

One of the two groups was subject to GSM pulsed signal at a power-density roughly equal to a cell-phone transmitting for two half-hour periods each day [1]. The only difference between the "shams" (controls) and the exposed mice, was that one group had an antenna which was radiating cell phone-type RF signals (at handset powers) for two hours a day, while for the other group, power was never switched to the antenna.

The study found that the exposed mice had more than two fold increase in lymphoma as compared to the controls. This study provoked concern worldwide, because it was the first reputable research to point to a positive link between mobiles and cancer.

Dr. Repacholi et al study was criticized since the RF exposure dose used is poorly defined and only one RF exposure dose level was used, so that the nature of the dose-response was unknown. The mice used were *Pim1* mice, so there was no way to determine whether the effect was unique to the animals that had been genetically engineered to make them lymphoma prone. Hence, the study is being considered more like a pilot study than a comprehensive bioassay

Because of its findings, the Australian government funded a follow up study to establish whether or not the same results could be produced once again with natural and lymphoma prone mice at different dosage levels. A different type of exposure system was required so that RF exposure doses could be more tightly defined and in a more controlled environment in order to give a precise dose of exposure. The RF exposure System used in this study was the "Ferris Wheel (FW)"exposure system [3] designed by Motorola Florida Research Labs, which provides a Whole-Body exposure for mice. A detailed explanation regarding construction and design of this system is discussed in Chapter II.

The result of this new study lead Dr. Tammy Utteridge using 600 normal and 600 lymphoma-prone mice were exposed to 898 MHz GSM-modulated RF energy for 1 hour per day for 24 months. Four different exposure levels of 0.25, 1.0, 2.0 and 4.0 W/kg were tested. The results show no significant increase in lymphoma and no significant dose-response trend [2].

The main goal of this research is to have a detailed dosimetric characterization of the "Ferris Wheel" RF exposure system designed for mice to know how efficient and symmetrical is the exposure system in distributing the RF power into the mice. The

dosimetric parameter used for the dosimetric characterization of the system is Specific Absorption Rate (SAR) that is widely used in the research will be discussed in Chapter III.

There are a number of Techniques used for the SAR measurements. Chapter IV discusses the various techniques used for the measurement of the Whole- Body SAR and Localized SAR with examples using the Ferris Wheel as an exposure system.

In Chapter V the electric field distributions inside the FW cavity using cylindrical FDTD code developed at Motorola are simulated and compared to that of the measured electric fields using E-field probes. Effects in the field distributions due to some intentional geometrical asymmetries are analyzed using simulation software Microwave Studio.

Chapter VI deals with the Whole-Body SAR characterization of FW using Calorimetric technique. Mathematical modeling and simulations in MATLAB for the Twin-Well calorimeter used for measurement of Whole-Body SAR is described as well. Detailed description of calorimetric test procedure used for different types of loads is also provided.

Chapter VII lists the results for the calorimetric tests performed for different types of loads.

CHAPTER II

THE "FERRIS WHEEL" AS AN EXPOSURE SYSTEM

As discussed in Chapter I, biological effects due to the RF exposure can be studied by carrying out long-term exposure to animals. The exposure environment used in Dr. Repacholi et al for the mice was not well controlled i.e., all the mice didn't had the same nominal levels and Whole-Body exposure to the RF fields as they were allowed to move freely inside their cages [1].

The RF system called "Ferris Wheel" developed at the Motorola Florida Research Labs allows a Whole-Body exposure to mice and provides symmetrical distribution of RF fields to the mice located around the transmitting antenna [3]. The earlier Whole-Body animal exposure to (locally) plane waves has been accomplished in the past by means of circular or rectangular wave-guides, radial wave-guides, and rectangular horns. In these structures, the matching of the antenna to the RF source is fairly insensitive of the loading, e.g., animal orientation with respect to the incident field [4-6]. Electromagnetic cavities have been employed with tuning, as they are very sensitive to load changes. By forcing the animals into restrainers will allow a Whole-Body exposure of the animals, as well as an efficient use of the available RF power. One of the basic advantages of this exposure system is that, being a closed electromagnetic structure; straightforward power balance can be employed to assess the average Whole-Body SAR of the mice [3].

2.1 Design and Construction of the "Ferris Wheel" Exposure System

The Ferris Wheel exposure system shown in Fig.1 is made up of a radial electromagnetic cavity formed by two parallel circular plates mounted on a polycarbonate frame. The two circular plates are single-side copper-clad laminate printed circuit boards (PCBs), and are mechanically supported by a 10 cm hollow Teflon ring long and about 10 cm in radius and 1.8 cm thick. The circular plates are joined around the perimeter by an array of shorting posts to form the radial cavity. Forty mice are placed at 9 cm apart at 44 cm from the center, co-polarized with respect to the incident TEM wave. The cavity is fed at the center by an internal tunable transition from the coaxial feed line [3]. The Ferris Wheel is loaded with forty mice periodically distributed around the perimeter.

Fig.1. Ferris Wheel Exposure System [3].

A tunable transition from a 50-ohm coaxial feed line excites a cylindrical TEM wave that impinges on 40 symmetrically arranged mice, which are equidistant from the exciter. The mice, restrained in plastic tubes inserted through circular holes in the plates, as shown in Fig.2, are held co-polarized with the incident electric field (E-polarization) to maximize the absorption of RF energy [3].

The symmetric arrangement provides uniform exposure to the mice, while the Whole-Body TEM illumination induces fairly uniform RF absorption within each mouse. Depending on the position of a mouse in the Ferris Wheel, the wave impinges from different directions.

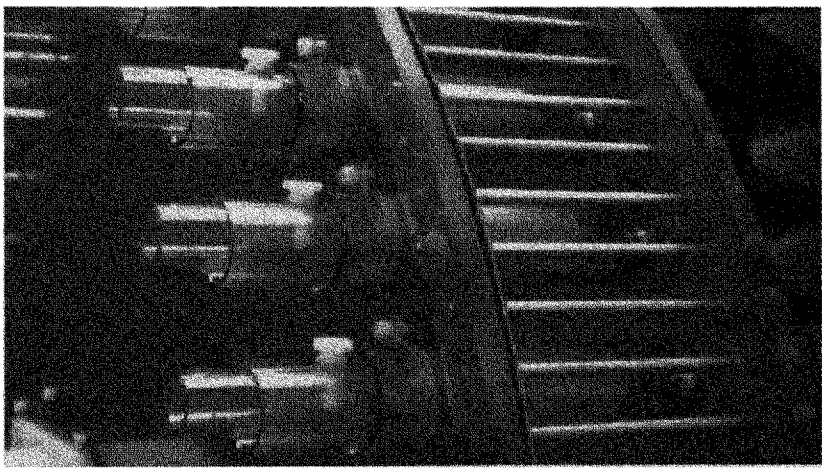

Fig.2. Mouse restraining mechanism [3].

Fig.2 shows the mouse holder that slides and locks to a plastic sleeve attached to the cavity frame. A pusher is held to the restrainer by means of a thumbscrew to keep the mouse exposed inside the "Ferris Wheel"[3].

An array of 120 shorting posts is preferred to a solid electric wall since it lets light into the cavity, which is needed for the mice. The posts are 10 cm long and 6.35 mm in diameter. They are symmetrically distributed around the perimeter of the cavity at 48 cm from the center, co-polarized with the electric field of the impinging TEM wave, and less than one-tenth of a wavelength apart to ensure low RF leakage. Return-loss measurements of the unloaded cavity shown that appreciable radiation would not result, which was confirmed by radiation measurements of the loaded cavity [3].

2.2. Field equations for the Ferris Wheel system

Since the Ferris Wheel exposure system is radial wave-guide has a cylindrical structure as shown in Fig.3. The electromagnetic fields inside in the cylindrical reference frame are derived in the following way [7].

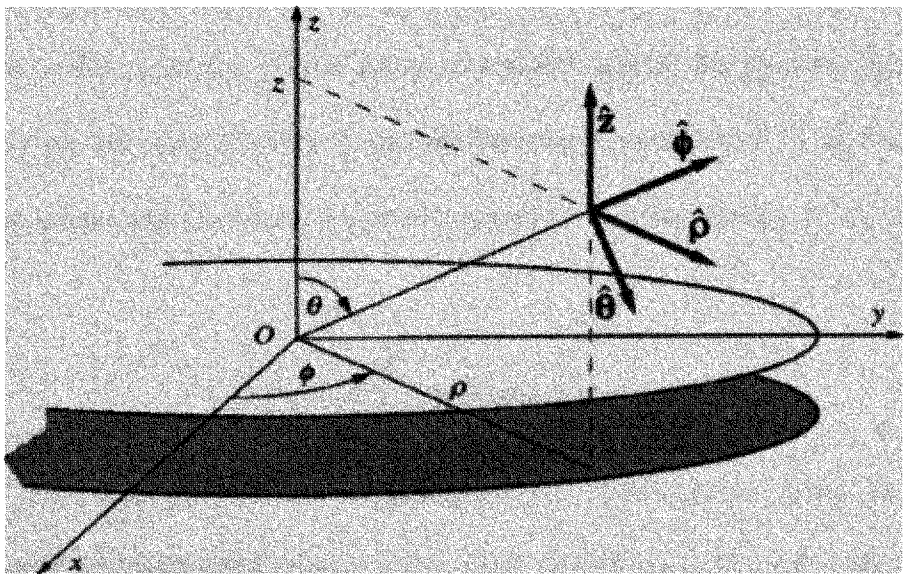

Fig.3. Reference cylindrical coordinates for Ferris Wheel Exposure system [7].

Assuming no vertical variation i.e. $\partial / \partial z = 0$ and perfect metal conductors, it yields

$$E_t = \hat{\rho} E_\rho + \hat{\varphi} E_\varphi = 0 \tag{2.1}$$

and

$$\nabla . E = 0 \tag{2.2}$$

in the field domain.

Assuming the impressed current is uniformly distributed on a vertical cylinder of radius a

$$J = \hat{Z} \frac{I_o}{2a\pi} \delta(\rho - a), \qquad 0 \le z \le h \tag{2.3}$$

where h is the thickness of the cylindrical cavity.

The Maxwell's equations yield

$$\nabla_t^2 E_z + k^2 E_z = j\omega\mu \frac{I_o}{2a\pi} \delta(\rho - a) \qquad 0 \le z \le h \tag{2.4}$$

with $k^2 = -j\omega\mu(\sigma + j\omega\varepsilon)$

where σ is the dielectric conductivity.

Due to the symmetry of the structure and the source, the electromagnetic fields depend only on the radial variable ρ and the boundary condition of E_z on the source is obtained by integrating the above Maxwell's equation over the surface $\rho' \le \rho$ as $\rho \to a$, resulting

$$\lim_{\rho \to a} 2\pi\rho \frac{\partial E_z}{\partial \rho} = j\omega\mu I_0 \tag{2.5}$$

As the incident field is a free-space-like TEM plane wave, as long as circumferential or longitudinal higher order mode excitation is not very significant, the field components in the cylindrical reference frame can be expressed as follows,

Applying the above condition to equation (2.4) results in

$$E_z(\rho) = A_r H_0^{(1)}(k\rho) + A_f H_0^{(2)}(k\rho) \tag{2.6}$$

where $H_0^{(1)} and\ H_0^{(2)}$ are the zeroth order Hankel functions that describe the inward and outward cylindrical waves respectively [7].

The magnetic field is simply derived from the relation

$$\boldsymbol{H} = -\nabla \times \boldsymbol{E}/j\omega\mu \tag{2.7}$$

and is expressed as

$$H_\phi(\rho) = \frac{1}{j\omega\mu}\frac{\partial E_z}{\partial \rho} = \frac{1}{-j\eta}\left[A_r H_1^{(1)}(k\rho) + A_f H_1^{(2)}(k\rho)\right] \tag{2.8}$$

where $\eta = \sqrt{j\omega\mu/(\sigma + j\omega\varepsilon)}$ is the wave impedance and k is the wave number of the medium.

Even at a short distance, the cylindrical wave impedance approaches the plane-wave impedance, therefore an exposure in the radial waveguide is very similar to free space, provided the cross section of the exposed body is much smaller than its distance from the center so that the impinging wave front can be considered locally flat and uniform.

2.3 Tunable Coax-to-Radial Cavity Transition

Tuning ability of the cavity exciter is desired to ensure proper matching to the RF source over a relatively wide range of possible loading conditions. A tunable transition from the coaxial feed line to the radial cavity was designed with the objective of

maximizing the modal conversion to the fundamental cavity mode by keeping the exciter's current as uniform as possible.

As depicted in Fig.4, the transition is formed by a top-loaded monopole antenna, which is capacitively coupled with a passive counterpoise. In this way, the accumulation of electric charges is concentrated in the small region comprising the capacitive loads so that the current along the monopole as well as the counterpoise is kept fairly uniform.

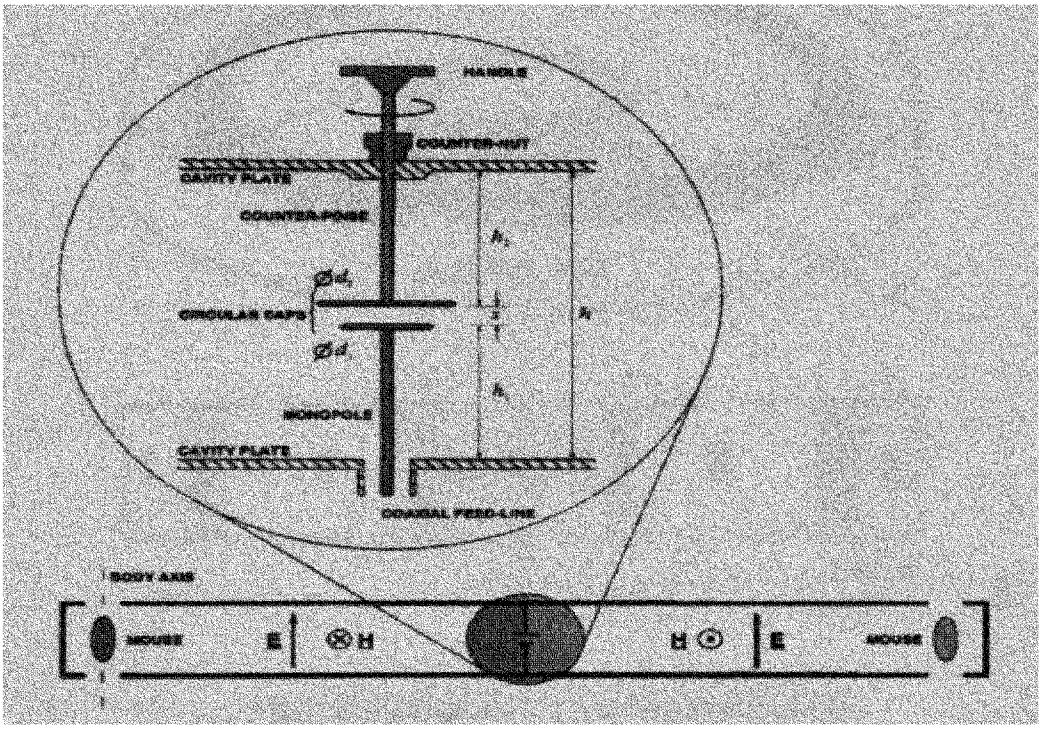

Fig.4. Schematic of Tunable Transition from the coaxial feed [3].

Tuning of the loaded cavity is performed through adjusting the capacitive coupling by moving the counterpoise closer or farther from the monopole, which is easily accomplished by threads on its arm. A plastic counter-nut ensures good electrical contact

of the counterpoise with the cavity plate. The actual implementation of the tuning element is shown in Fig.4 [3].

The Fig.5 shows the electric wall formed shorting posts and the loads. In the figure δ is the distance between the position of the center of the carrousel and the electric short post and, λ_o is the wavelength of the incident wave.

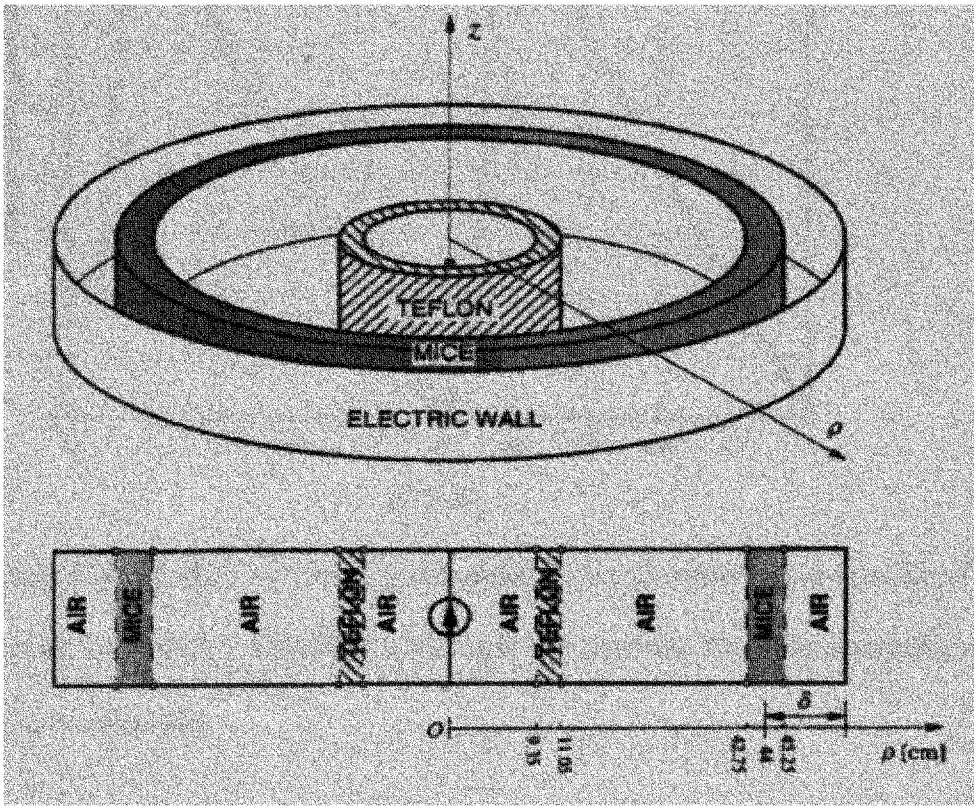

Fig.5. Horizontal view of the Ferries Wheel [3].

The distance δ is determined by using a prototype cavity where the shorting poles are placed at different distances from 48 to 50 cm from the center. On the base of return loss the optimal distance is determined to be at 48 cm from the center. At this distance the

ratio of δ/λ_0=0.12 is where the peak of the efficiency curve exists as shown in the Fig.6. Any slight variations may result in the fall of step region and the efficiency drops sharply.

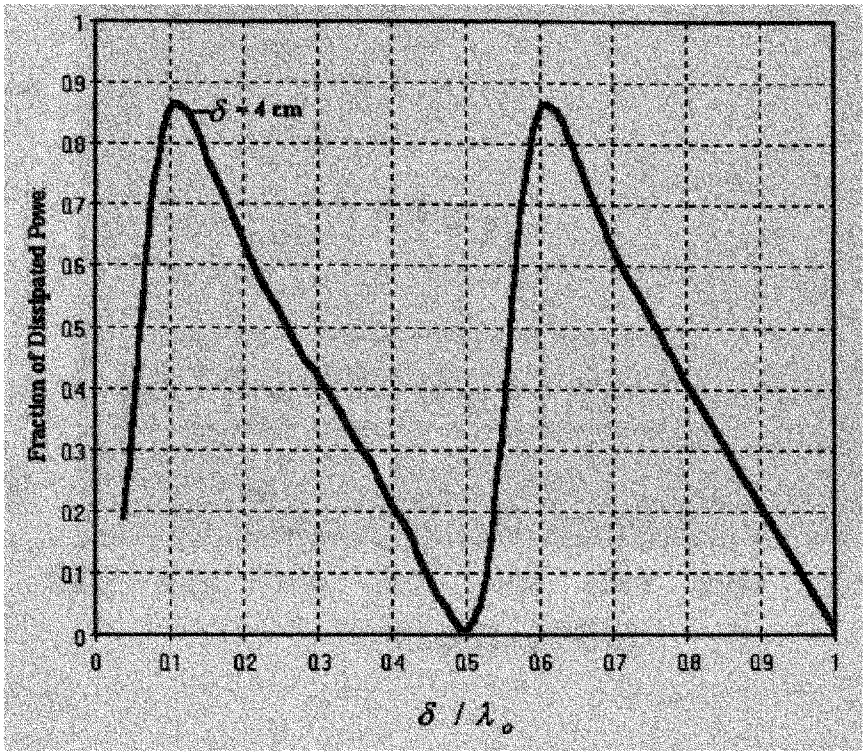

Fig.6. Fraction of the incident RF power that is dissipated in the mice versus distance of the shorting wall, according to the radial-transmission-line model. The optimal distance is shown to be at $\delta \approx 4$ cm [3].

The wide band tuning capability of the exciter is shown in the Fig.7. This figure shows good matching to the source at 900 MHz with relatively low percent of power is reflected back into the cavity. At 915 MHz the separation between the caps of the passive counter poise to the cap of the monopole antenna is around 8 mm and the return loss is around 9 dB.

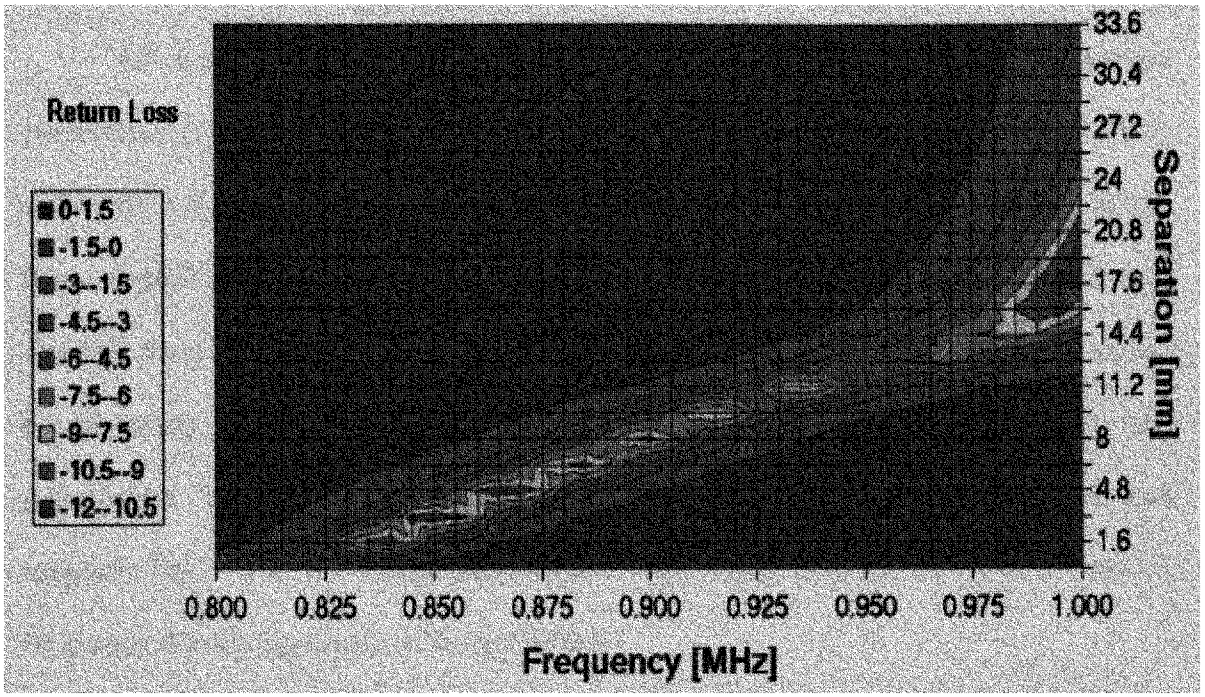

Fig. 7. Return loss of the "Ferris Wheel," achieved by using the tunable exciter to optimize the impedance match to the 50- feed line [3].

CHAPTER III

RF DOSIMETRY

RF interactions with biological materials are complex functions of numerous parameters [8]. These interactions produce highly non-uniform distributions of EM fields within the object, which are related to the dielectric properties and the density of the tissue regardless the external exposure field uniformity. Dosimetry studies are done to quantify these electromagnetic interactions. Radio waves in free space are characterized by frequency, intensity of electric (E) and magnetic (H) fields, their direction, and polarization. The internal fields and currents are related to the incident external and magnetic fields in a very complicated manner. The results obtained from animals cannot be always directly applicable to human beings.

The RF interactions as well as the resultant deposition of microwave power in the body are measured in terms of Specific Absorption Rate (SAR). The mass normalized rate of energy absorption or dose rate was introduced to microwave research in the late 1960s formerly known as "absorbed power density". This parameter was officially designated Specific Absorption Rate (SAR) by the National Council on Radiation Protection and Measurements [11].

Definition

Specific Absorption Rate (SAR): the time derivative of the incremental energy *(dW)* absorbed by an incremental mass *(dm)* contained in a volume element *(dV)* of given mass density (ρ)[11].

SAR is measured in Watts per kilogram (W/kg) of body mass, which represents the RF absorption rate in body tissue [8]. SAR is the parameter used by government regulatory agencies to determine compliance with non-ionizing radiation hazard standards.

The power absorption usually takes place in a confined body region, as in the case of the head exposed to a cellular phone, even if the (SAR_{WB}) is well below the basic limit, the local SAR can assume rather high values. In the frequency range of 100 kHz to 6-10 GHz, SAR is the relevant dosimetric quantity. SAR is a quantity that describes the amount of absorbed energy for a specific material at a certain frequency. For the purpose of radiation protection, dosimetric quantities are needed to estimate the absorbed energy and its distribution inside the body. Regulatory agencies have established Specific Absorption Rate guidelines, standards and test procedures to define SAR levels that can be safely absorbed by the body.

The value of 4 W/kg Whole-Body SAR is accepted worldwide as the threshold for the induction of biological harmful effects [9]. Up to now, the most recognized RF exposure standards adopt the SAR, averaged over the Whole-Body (SAR_{WB}), as the basic parameter to establish the safety of an exposure [10]. According to the ANSI/IEEE (*American National Standard Institute/Institute of Electrical and Electronics Engineers*) standard the maximum SAR averaged over 1 g should not exceed 1.6 W/kg and that the Whole-Body mass averaged SAR should not exceed 0.08W/kg for uncontrolled environments.

3.1 Equations Relating Specific Absorption Rate (SAR)

The Specific Absorption Rate limits have been defined in different ways but all of them are related to the same basic principle of transferring energy from electromagnetic fields to an absorbing object. The quantity can also be derived from either the temperature gain or from an electric field.

SAR defined in terms of energy as the time derivative of the incremental energy absorbed by (dissipated in) an incremental mass contained in a volume of a given density

SAR is simply defined as the mass averaged rate of energy absorption in tissue

$$SAR = \frac{d}{dt}\left(\frac{dW}{dm}\right) = \frac{d}{dt}\left(\frac{dW}{\rho dV}\right) \tag{3.1}$$

and is related to the internal E-Field by

$$SAR = \frac{\sigma}{\rho}E^2 \tag{3.2}$$

where σ is the conductivity of the tissue in S/m,

ρ is the mass density in kg/m^3,

and E is the rms electric field strength in V/m.

Thus, SAR is a measure of the electric field, and indirectly the magnetic field and current density at the point of interest [11].

Also SAR is a measure of the local heating rate *dT/dt*, which in terms of relation is

$$\frac{dT}{dt} = \frac{SAR}{c} \quad °C/s \tag{3.3}$$

where *c* is the specific heat capacity of the tissue in J/kg/°C.

ΔT is the temperature change in °C,

Δt is exposure time in seconds

This assumes "ideal" thermodynamic circumstances, i.e., no heat loss by thermal diffusion, heat radiation, or thermoregulation (blood flow, sweating, etc.). The SAR distributions are quite complicated even when resulting from plane-wave exposure. Depending upon the size and orientation of the animal and the frequency, it is possible that one or more SAR peaks ("hot spots") could occur.

3.2 Localized and Whole-Body SAR

There are two types of SAR measurements:

1. Localized SAR
2. Whole-Body SAR

Localized SAR is a measure of the rate of energy absorbed by (dissipated in) an incremental mass contained in a volume element of dielectric materials such as biological tissue [12].

$$Localized \quad SAR = \frac{d}{dt}\left(\frac{dW}{dm}\right) = \frac{d}{dt}\left(\frac{dW}{\rho dV}\right) \tag{3.4}$$

It is called the Localized SAR because it changes from point to point according to the dielectric properties of the absorbing object and the distribution of dissipated RF energy.

Average SAR is defined as the rate of change of total energy stored in the volume integral of the absorbing object divided by the total mass of the body [10]. This Average SAR is also commonly known as Whole-Body SAR

$$Average \ SAR = \int_v PdV / M \tag{3.5}$$

Both Whole-Body and Localized SAR's are expressed in terms of watts per kilogram (W/kg) or milliwatts per gram (mW/g).

3.3 Factors that Determine the Value of SAR

The following factors and conditions have an influence in heat absorption of a biological object, which determine the value of SAR [8].

Dielectric Properties

The magnitude and special distribution of EM fields within the biological tissues depend on the dielectric properties of the tissue (dielectric constant and conductivity).

Tissue Structure

The highest local SAR is usually at or near the surfaces of an externally exposed object. In general absorbing tissue material is a complex biological system consisting of multiple layers of tissue. When exposed to the field propagates thorough these layers of tissue, a portion of energy is reflected from each boundary, and a portion is transmitted into the next layer. The amount of transmission and reflection at each boundary depends on the difference in dielectric properties of the tissues at that layer.

Tissue Orientation and Field Polarization

It has been shown both theoretically [13] and experimentally [14] that the SAR in a exposed object is maximal when the long axis of the body is parallel to the direction of a uniform external electric field. For some cases the average SAR in a human body is about 20 times higher than that occurring when the electric field is perpendicular to the long axis of the model.

Field Frequency

Dielectric properties, the field strength and spatial distribution of internal fields also vary with frequency.

Source Configuration

The most important conditions of the exposure field is whether it is a *far field* or *near field.* The far field extends from a certain minimum distance from the source to infinity. In this region the field has predominantly plane–wave character i.e., E fields and H fields are spatially uniform and mutually perpendicular. The far field typically begins at a distance of $(2D^2/\lambda)$ from the radiating source, where D is the longest dimension of the radiating structure.

Exposure Environment

The quantity of energy absorbed by a body in the RF field depends on environmental factors like free space, on ground plane, near metal reflectors, metallic conductive structures like waveguides. Metal implants can cause intense modifications in SAR distribution in the exposed object.

Time-Intensity Factors

Exposure duration and external field strength are very important parameters that determine the total amount of energy absorbed.

Specific heat capacity (c)

The amount of heat absorbed by a tissue material depends on the specific heat capacity of the tissue.

Methods for Determination of SAR

The SAR measurement is very important in terms of dosimetry. Different procedures were used to measure SAR in terms of heat absorbed and temperature raise and E-fields according to the equations in section 2.2. The methods employed for dosimetry studies are as follows [12]:

1) Calorimetric technique to quantify the average or Whole-Body SAR in the whole object.
2) Power balance methods to quantify Whole-Body SAR.
3) Measurement of Localized SAR using Thermometric or Temperature probes.
4) SAR distribution patterns in biological object by Thermography.
5) Implanting E-field probes to measure the Local SAR.
6) Simulations in an electromagnetic simulation codes like Microwave Studio and XFDTD.

CHAPTER IV

SAR MEASUREMENT TECHNIQUES

This Chapter discusses some other methods that help in determining the Whole-Body SAR and Localized SAR. Whole-Body SAR can also be measured by the help of differential power technique which is a very simple straight forward measurements of forward and reflected power into the system also known as the power balance method for SAR measurements.

SAR distribution patterns and the Localized SAR in biological object can be analyzed by the SAR thermography and thermometric techniques. Both these procedures are employed to determine the SAR distribution in the sagittal plane of the mice. It also helps in making the absolute SAR in some organs of interest like the brain, belly etc.

In a thermography procedure the SAR distribution patterns are analyzed using an infrared camera that scans the temperature reading on flat surface. Thermometric measurements are made on the biological tissue to observe the temperature variation inside the load by using temperature probes. A Luxtron fiber optical temperature probe, which is transparent to the electromagnetic field, is placed between the two halves to sense the temperature. For both procedures the mouse is encapsulated in a Styrofoam holder where it is frozen after that and cut along the sagittal plane. E-field probes are also used to measure SAR values from point-to-point in a simulated phantom.

4.1 Differential-Power Technique

The Whole-Body SAR in the loads of the Ferris Wheel can be obtained by dividing the power dissipated in the loads by their mass. A directional coupler and two power meters to read forward and reflected powers into the port of the Ferris Wheel exposure system. This method is based on the power balance of the system and thus, it is important to obtain these power readings precisely.

The power balance equation is,

$$P_{loads} = (P_{inc} - P_{ref}) - (P_{\Omega} - P_{rad}) \tag{4.1}$$

states that the power dissipated in the mice can be found by measuring the incident P_{inc} and reflected P_{ref} power at the cavity port, and estimating the ohmic losses in metal and dielectric losses in plastics P_{Ω} and the radiated power P_{rad}. The first two contributions are measurable throughout the exposure using a bi-directional coupler. The ohmic and dielectric losses have been estimated measuring the return loss and the power radiated by the unloaded cavity at 900 MHz in an anechoic chamber and the missing power accounted for is about 1% of the incident power [3].

Assuming that the loss of energy due to ohmic effects and radiation do not vary significantly over relatively wide changes of the loading conditions [3]. Therefore, the amount of power dissipated in the loads can be determined just by monitoring bi-directional power flow, so that the collective Whole-Body average SAR is

$$SAR_{Dummy} = \frac{P_{Dummy}}{m_{Dummy}} = \frac{P_{inc} - P_{ref} - (\alpha_{\Omega} + \alpha_{rad})P_{inc}}{m_{Dummy}} \tag{4.2}$$

where, $\alpha_{\Omega} \approx 0.01$, $\alpha_{rad} \approx 0.01$ and m_{Dummy} is the total mass of the 40 loads.

The dummy load was a 30 cm^3 plastic bottle filled with tissue-simulated liquid (water: sugar: salt: hydroxethylcellulose ~53.5:44.25:1.15:1 weight wise) of 37 grams, which is equivalent to 30g mice, are used as loads [3].

The determination of the Whole-Body SAR using this technique is quite accurate but mainly relies on power measurements. The assumption here is that the dissipated RF power is equally spread among the dummy loads, which may not be the case due to some asymmetry in positioning of these dummy loads. The accuracy of these measurements can be improved by collecting the forward and reverse power meter reading with the help of Lab View data acquisition software. Controlling temperature of the couplers and power meter heads also improves the stability of the measurements. A number of experiments were done using the simulated tissue bottles as loads at different positions on the FW. The average normalized SAR obtained is 0.66 W/kg/W.

But since we are using a dummy load which is equivalent to mice in terms of dielectric properties but not in terms of average density. Assuming the dummy load as real mice, the Whole-Body SAR in the mice by taking into account the difference in density is

$$SAR_{WB-Mice} = SAR_{Dummy} \frac{\rho_{Dummy}}{\rho_{Mice}} \tag{4.3}$$

where ρ_{Dummy} and ρ_{Mice} are the average density of dummy load and mice respectively [3]. The ratio of the densities between dummy load to that of mice is about 1.25. Therefore, the average normalized SAR obtained is 0.8 W/kg/W.

4.2 Thermography

The SAR distributions in the biological objects are complex. A scanning infrared thermographic camera can be used to provide detailed SAR distribution or temperature distribution in tissue equivalent phantom models or animals exposed to the high RF radiation fields in a short time. Suitable material to separate sections of the phantom or cadaver must be used, and readout after termination of exposure must be rapid. If the output of the thermographic camera is put into a computer, average SAR can be easily computed using special software codes [15].

A model of an animal or other object is made of tissue equivalent materials and cut along planes whose two-dimensional SAR (temperature) distribution is to be determined. To avoid water loss from the material, the open surfaces are covered with a very thin (0.05 mm or less) polyethylene film [15]. A frozen animal is cast a Styrofoam block, bisected, covered with polyethylene film and equilibrated to the room temperature. During exposure, the bisected halves are joined. The model or cadaver is then exposed under specific test conditions for a pre-determined limited time to a high-intensity field. The parts quickly are separated and the internal surface of one of the halves is immediately scanned with an infrared thermal camera. To obtain the temperature or SAR information undistorted by thermal conduction, the exposure time and the delay between taking thermal scan must be minimized. The delay and the recording time must be no longer than 10 seconds [8]. Large temperature gradients should be avoided, as they will result in thermal conduction; gradients of 5 to 10 degrees C are normal.

This technique has proven valuable in assessing SAR distribution for laboratory animals and models of man and was first introduced by A.W. Guy and has gained worldwide acceptance [8]. The procedure involves using a thin sheet of plastic to facilitate separating the halves of the phantom; thus the procedure was limited to top and bottom slots in the Ferris Wheel to have a exposure to linearly polarized field (E-field parallel to the interface) in order to avoid interrupting induced currents that would normally flow perpendicular to the median plane of separation.

Thermographic Imaging Procedures:

1. For thermographic procedure it is needed to prepare the mice for taking the thermo graphic pictures using a thermal camera. This process is called `Foaming & Cutting`. The Styrofoam mixture is prepared using equal quantities of A & B solutions. The thawed mouse is properly aligned with reference axis in a cylindrical mould with open top and closed bottom. The mixture is poured into the mould so that the foaming takes place. The obtained mouse with the foam is allowed to solidify and then refrigerated so that it can be cut easily using an electrical saw [16].
2. Now it is ready to test the mice by wrapping each half of the mouse with silk screen/plastic wrap. Place both halves of the mouse (the two slides) on their flat surfaces and are allowed to thaw to room temperature. Now they are ready for taking thermal pictures. One of the halves is placed on the apparatus made up of styrofoam, which allows the flat surface of the mice half facing parallel to the thermal camera.

3. Take a picture by connecting the thermographic camera's processing unit to a PC loaded with Lab View data acquisition software created for collecting data from this camera through the General Purpose Interface Board (GPIB) card slot. Start up the Lab View software and run the data acquisition software. Turn the data acquisition on and capture an image. This first image data file that will be used in post-processing.
4. During the exposure, the bisected halves are joined and are placed in top or bottom slots of the Ferris Wheel exposure system. The exposure inside the Ferris Wheel is done at high RF power (300 W) for determined amount of time (30 seconds) and one of the halves (used before) is place back onto apparatus immediately. The data acquisition is started immediately as above outlined to take the picture of the exposed mouse. This will be the second image. Fig.8 shows an illustrative example of mice and the gradients of temperature are shown as different colors.
5. Since the image files are in terms of temperature measurements of each pixel of the image files, the differential of the above two taken picture files or picture should result in the temperature gradients in the mouse. A special software written in FORTRAN code helps in making the differential can run program to process the before and after shots into one picture that shows the differential. Fig.9 shows the resultant differential picture and different color lines show the temperature increase in the tissue of the mice.

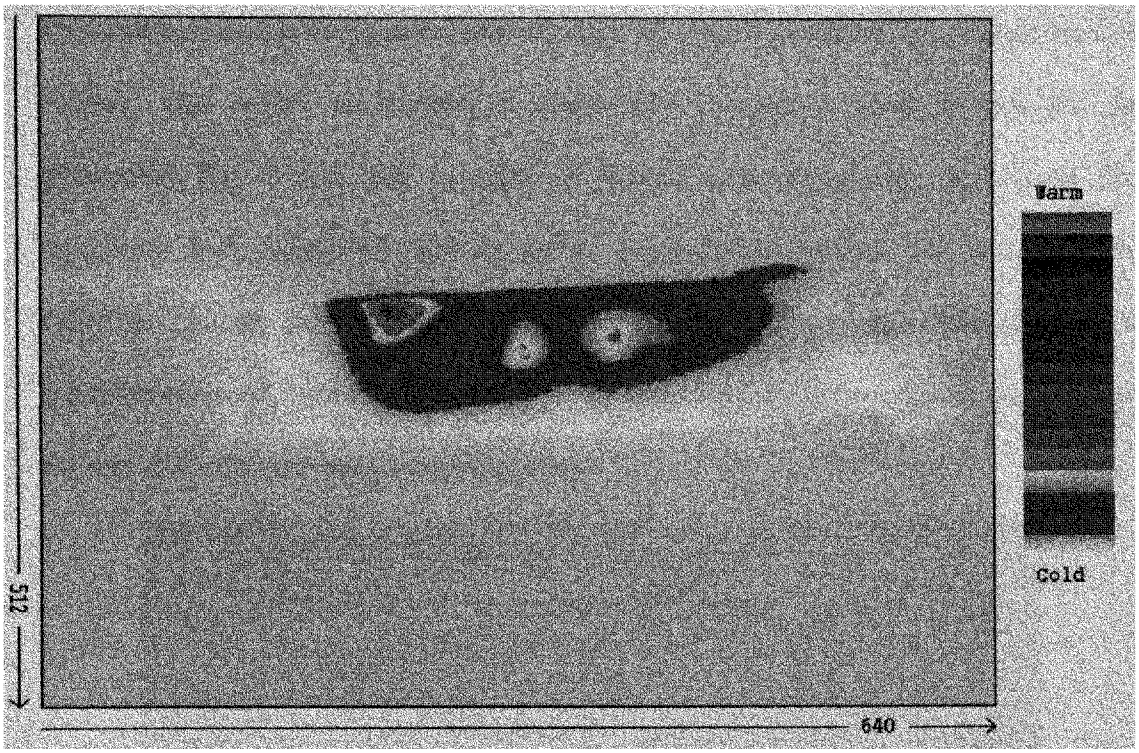

Fig.8. Thermal image showing the temperature distribution after exposure [16].

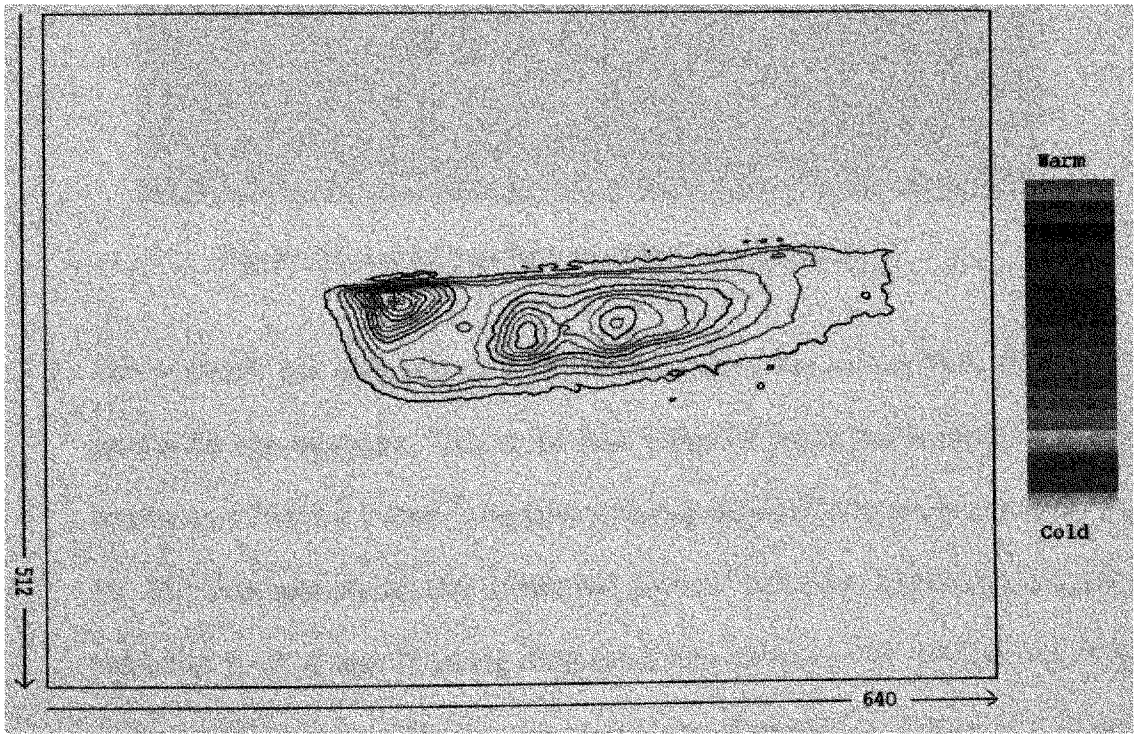

Fig.9. Differential image showing the heat counters and hot spots inside mouse [16].

This software can process many sets of image files into corresponding differential files (ofiles). The "ofile" designation is simply the designation used to describe the differential file. These will be used in further data processing. A colored line represents each degree of variation across the collected images. The increments of color line can also be set to half or quarter degree. Fig.10 shows the heat counters of the mice obtained from the differential picture overlapped on the original picture taken for one of the halves using a digital camera.

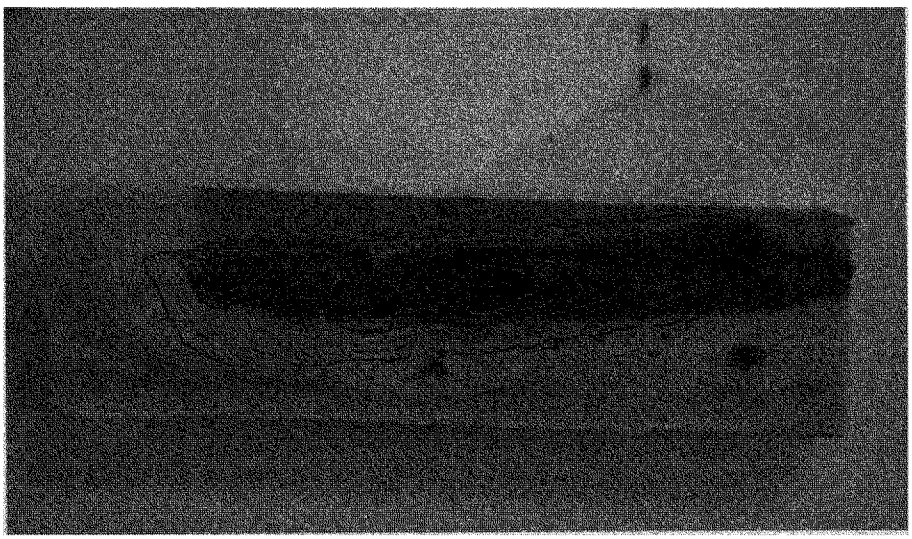

Fig.10. Mouse picture with the Thermal contours [16].

6. The software not only makes a differential picture but also a SAR distribution profile for the exposure. This is the final stage of the software program is also known as "The Big Picture", because it has six different plots as shown in the Fig 11. The first plot shows the differential picture with four reference axes points named as A, B, C and D on the differential thermal scan. The software according to the temperature raises in the picture allocates the locations of these axes on the scale.

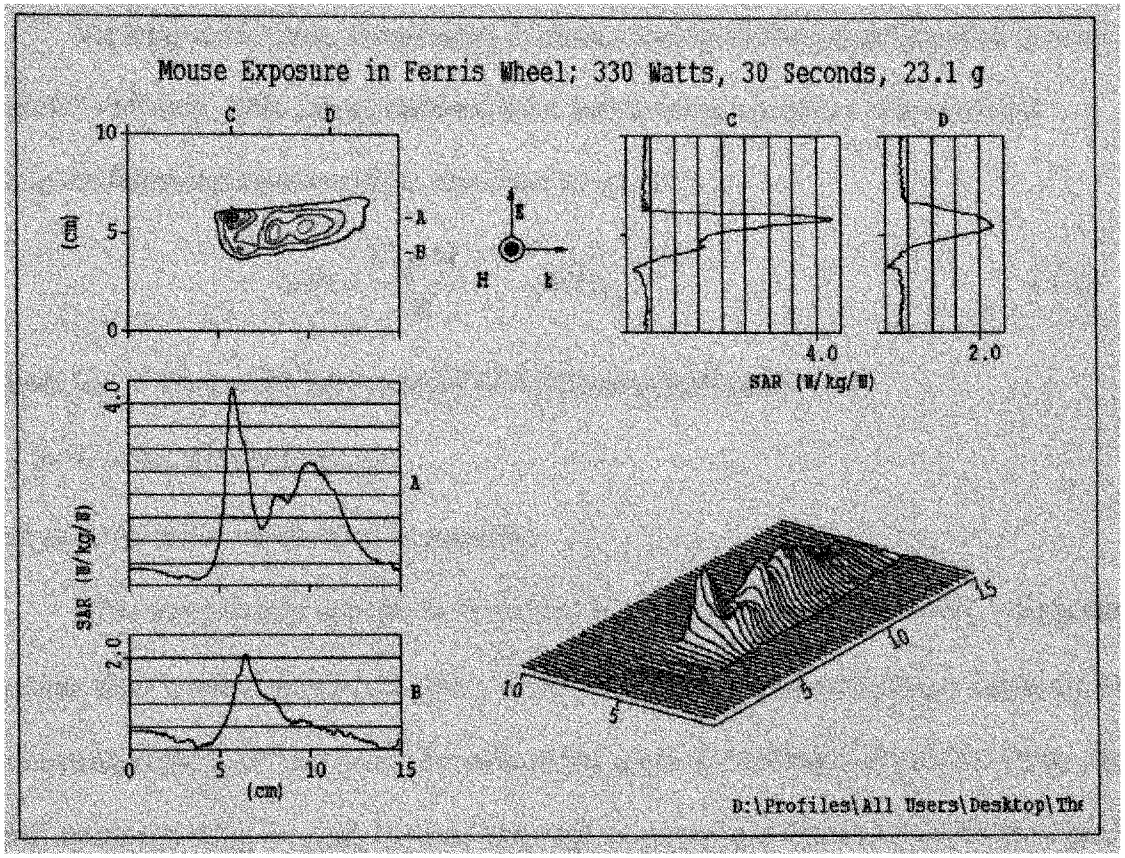

Fig.11. SAR Distribution Profile [16].

The four small graphs show the one-dimensional SAR distribution pattern about their respective axis. The last graph is a two-dimensional SAR distribution pattern obtained by a simple combination of two of these four graphs. The cross hair in the picture shows the highest hot spot location in the mouse. SAR values obtained from the thermographic procedure are normalized to the input power. The peak Normalized SAR at head for the above example is 4.0 W/kg/W.

4.3 Thermometry

As long as the tissue temperature increases linearly during short-term exposure to high-RF radiation, SAR can be obtained from thermal or temperature measurements using the following equation [8] as discussed in section 2.2

$$SAR = \frac{C_H \Delta T}{\Delta t} \qquad (W/kg) \tag{4.4}$$

where C_H is the specific heat capacity of the tissues (kcal/kg °C)

ΔT in °C is the temperature rise

and Δt is the exposure duration in seconds

The temperature rise can be measured at a particular point of interest, taking into account heat conduction for the time period Δt. Thus, by employing above equation we can calculate the SAR that would be assessed by a non-perturbing probe at that point. The term non-perturbing is used here as opposed to the conventional temperature probes, which not only might interact with the electromagnetic field but also measure the mean temperature of a discrete volume, introducing further errors in the experimental assessment of SAR [15].

SAR measurements with Temperature Probes

The difficulty of measuring temperature in electromagnetic fields with many conventional thermometers stems form three types of interaction between the thermometer and the field. They are electromagnetic interference (EMI); direct heating of temperature sensor, and perturbation of the field by the thermometer. Placing the leads of the sensor perpendicular can minimize the interference and induction pick-up to the E-field. Magnetic induction pick-up is reduced when the leads are slightly twisted [12]. Out

of several types of non-perturbating temperature probes have been developed Vitek probe [BSD Company, Salt Lake City, Utah] and Luxtron probes [Luxtron Corporation, Santa Clara, California] are used.

4.3.1. Thermal SAR Measurements on Dummy Loads

The experimental setup comprises of the "Ferris Wheel" loaded with dummy equivalents, with one of the dummies encapsulated in a styrofoam shell as shown in Fig.12.

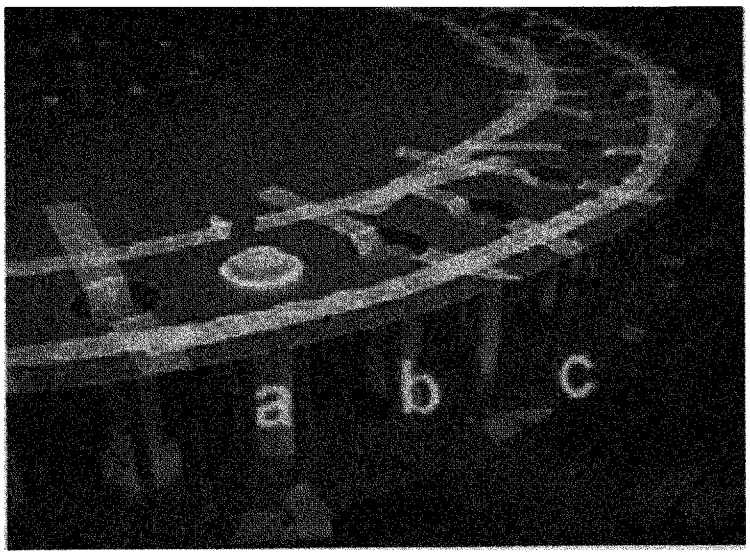

Fig.12. Experimental setup for thermal SAR measurements using Vitek thermistor probe [3].

A Vitek-101 thermistor probe is inserted through a small hole into the solution of the dummy bottle containing the tissue equivalent solution. A short high-power RF exposure of 30 W for 2 min induces a temperature rise in the dummy. The dummy is vigorously shaken after exposure to equalize the temperature throughout so that the average temperature increase reading can be recorded regardless of the actual position of

the thermistor inside the dummy [3]. Assuming the heat loss exchange to the external environment is negligible due to of the styrofoam enclosure, the difference between the final and initial average temperature in the dummy is proportional to the dissipated RF power, therefore,

$$SAR_{Dummy} = \frac{C_{Dummy} \cdot \Delta T}{\Delta t} \qquad (W/kg) \qquad (4.5)$$

where C_{Dummy} is the specific heat of the particular tissue-equivalent solution used and is equal to 2.8 J/g/K that was employed, and Δt is the exposure duration.

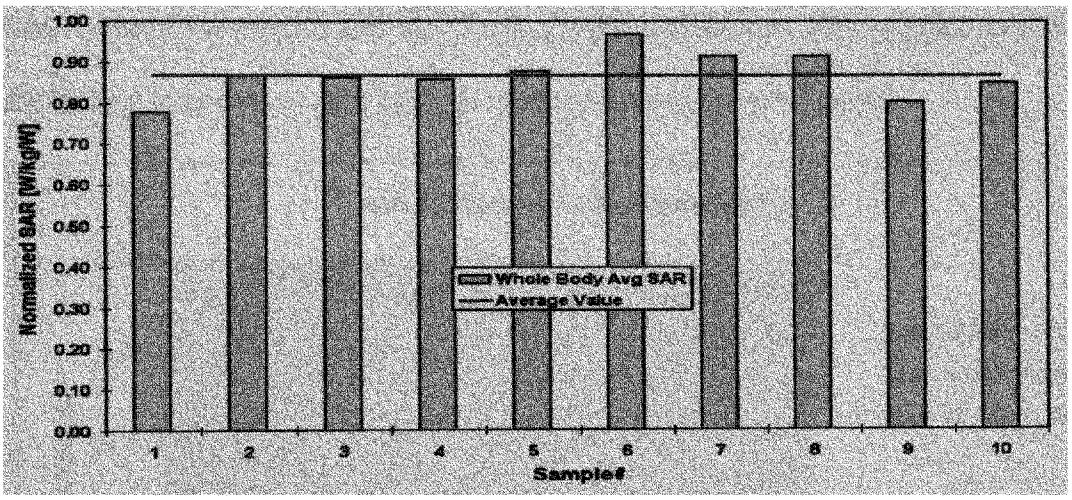

Fig.13. Normalized thermal SAR measurements of dummy Loads using Vitek probe [3].

Fig.12 shows the details of the experimental setup, while Fig.13 reports the results of ten thermal measurements performed on dummy equivalents, given in terms of the fraction of the incident power.

The Normalized thermal SAR is the Fraction of the incident RF power that is dissipated or absorbed in the dummy load. The obtained Normalized thermal SAR measurements are performed on 30-g dummy equivalents. Averaged Normalized SAR is about 0.85 W/kg/W.

4.3.2. Thermal SAR Measurements on Mice

As discussed in the previous section, the mice used thermography is also used for making thermal measurements during the exposure time. Three temperature probes (Vitek/Luxtron) were placed at position of interest like the brain, neck and belly where the local hot spot locations are usually found using thermography. The thermography process helps in recognizing the hotspot locations so that the probes are placed at that point approximately. The Localized SAR in these regions is calculated from the rate of temperature rise during the exposure as per the above equation (4.4). Fig.14 shows the linear raise of the temperature raise at the position of interests. The equation and slope for the highest temperature raise at the position of interest were computed.

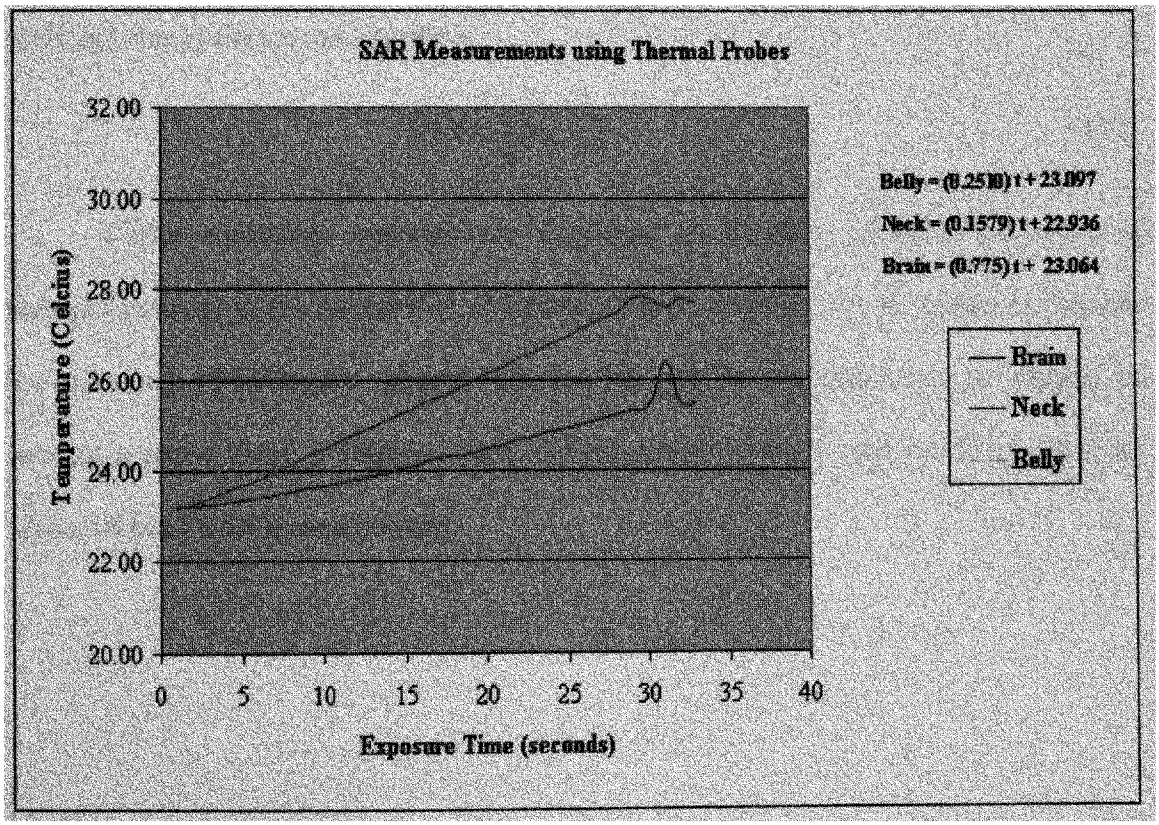

Fig.14. Linear raise in temperature at the positions of interest [16].

The Normalized SAR is obtained as follows

$$N - SAR = (C_{Mice} \cdot Slope) / P_{Net} \tag{4.6}$$

where C_{Mice} is the specific heat of mice and is equal to 3.2 J/kg/°C,

Slope is the ratio of ΔT raise in temperature and t is the time of exposure.

P_{Net} is the net power applied during the exposure period.

In this particular case the temperature raise is high in belly with a slope of 0.2510. Normalized SAR value at this point of interest is 2.41 (W/kg/W) [16].

4.4 E-field probe

An E-field can be measured at a point or points with in the tissue equivalent "phantom" model or a biological system by an E-field probe [8]. The equation relating SAR and rms E-field measurement is

$$SAR = \frac{\sigma}{\rho} \left| E_{rms}{}^{2} \right| \tag{4.7}$$

Tissue equivalent materials are developed to simulate dielectric properties of biological tissues at the frequencies of interest. These materials can be shaped to simulate the geometry of biological objects. The E-field with in the object can be mapped by moving a probe along a selective path. E-field probes provide most sensible and direct means of local SAR measurements.

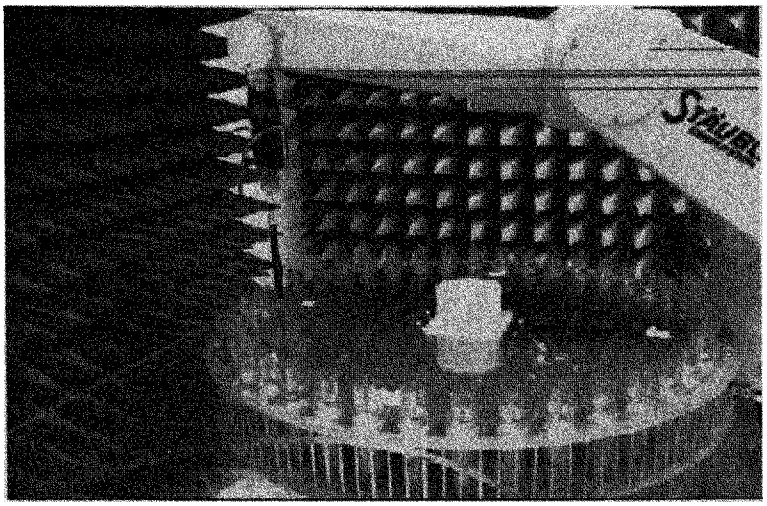

Fig.15. Experimental setup for E-field measurements inside the restrainer.

The E-field probes usually use three small orthogonal dipole antennas to provide isotropic measurements to determine the SAR using E-field probes accurately the probes must be calibrated. The E-field measurements through the middle of the dummy load at four different positions i.e., Top, Bottom, Left and Right of the "Ferris Wheel" are measured by using E-field probes with small 1-mm tip diameter. The arrangement for the measurements using the DASY Robot is shown in Fig.15.

The E-field distribution along the Z-axis through the middle of the dummy is found to be symmetrical at all the positions of interest. It is found that the distributions at open end is small and increases to the peak in the middle of the cavity as shown in Fig.16. The deviation in the peak SAR obtained between Top and Bottom positions is 1.25 dB and to that of the Left and Right is about –0.5dB.

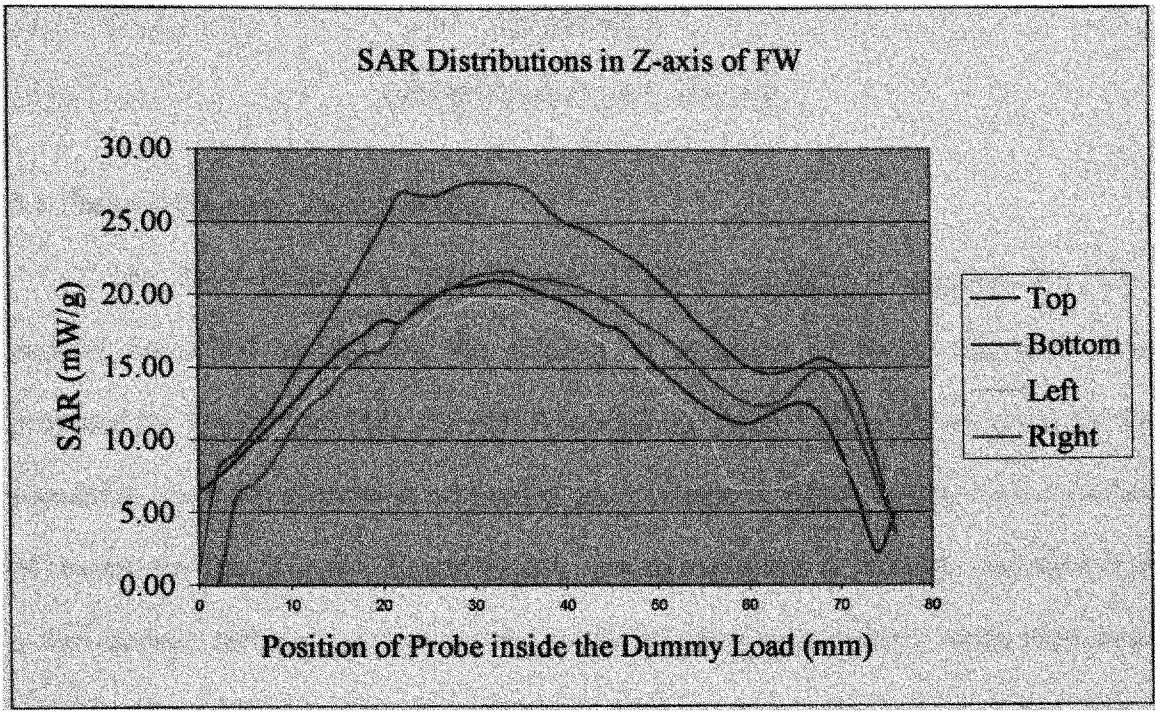

Fig.16. E-field distribution through the dummy along z-axis in the FW reference plane.

CHAPTER V

COMPUTER SIMULATIONS

5.1 Finite-Difference Time Domain

The Finite-Difference Time-Domain (FDTD) technique is arguably the most popular numerical method for the solution of problems in electromagnetics. First proposed by Yee in 1966 [17], the FDTD method has existed for nearly 30 years, and its popularity continues to grow as computing cost continue to decrease. There are a number of reasons for this; it is easy to understand, easy to implement in software, and since it is a time-domain technique, it can cover a wide frequency range with a single simulation run.

The Yee cell is the basis of the FDTD numerical method and usually is a three dimensional cube in which the permittivity, permeability and conductivity of the material surrounded by the perimeter of the cube is defined. For the Ferris Wheel exposure system the Yee unit cell is defined in terms of cylindrical coordinates [17]. Any electromagnetic field (E and H vectors) that impinges on one face of the unit will be scattered or absorbed within the cell depending upon the characteristics of the cell, the remainder of the field will be propagated to other faces. When two or more cells are neighbors, the propagated field on the face of one cell becomes the impinging field of the next cell ie., becomes the boundary conditions for next cell.

Maxwell's (differential form) equations are simply modified to central-difference equations, discretized, and implemented in software. The electric field is solved at a given

instant in time, then the magnetic field are solved at the next instant in time, and the process is repeated over and over again [17].

A simple description on the operation of this method is discussed. When Maxwell's differential form equations are examined, it can be seen that the time derivative of the E field is dependent on the Curl of the H field. This can be simplified to state that the change in the E field (the time derivative) is dependent on the change in the H field across space (the Curl). This results in the basic FDTD equation that the new value of the E field is dependent on the old value of the E field (hence the difference in time) and the difference in the old value of the H field on either side of the E field point in space.

Naturally, this is a simplified description with the constants omitted. The H field is found in the same manner. The new value of the H field is dependent on the old value of the H field (hence difference in time), and also dependent on the difference in the E field on either side of the H field point. This description holds true for 1D, 2D and 3D, FDTD techniques.

However, when multiple dimensions are considered, the difference in space must be considered in all appropriate dimensions. In order to use the FDTD, a computational domain must be established. The computational domain is simply the 'space' where the simulation will be performed. The E and H fields will be determined at every point within the computational domain. The material of each cell within the computational domain must be specified. Typically, the material will be either free-space (air), metal (perfect electrical conductors), or dielectrics; any material can be used, as long as the permeability, permittivity, and conductivity can be specified.

Once the computational domain and the grid material are established, a source is specified. The source can be an impinging plane wave, a current on a wire, or an electric field between metal plates (basically a voltage between the two plates), depending on the type of situation to be modeled. Since the E and H fields are determined directly, the output of the simulation is usually the E or H field at a point or a series of point within the computational domain.

Since the Ferris Wheel system has a cylindrical geometry, as shown in Fig.3 the FDTD code is developed in cylindrical coordinates. The below figure shows the FDTD cell used in cylindrical co-ordinates.

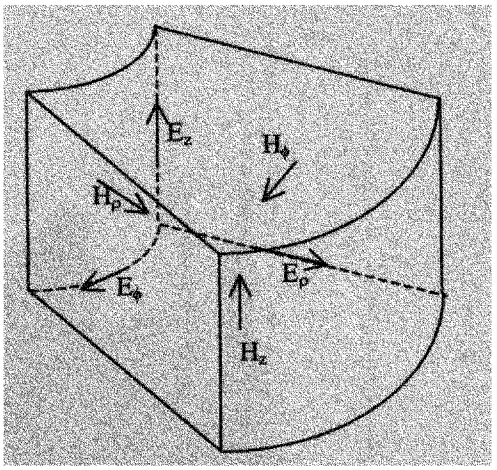

Fig.17. FDTD Cylindrical unit cell [7].

Inside the empty cavity, the TEM field components can be expressed in the cylindrical reference as from the above equations; we notice that when the mice are placed inside the cavity, they can be considered exposed to an incident TEM-like wave. The mice are placed with their body axis at 44 cm from the "Ferris Wheel" center, so their axis is co-polarized with the incident electric field. Such a position enhances the efficiency of the cavity [7].

As the mice tissue is complex, heterogeneous and has a non-uniform body they change the incident field characteristics and alter its uniformity. Equations (2.6) and (2.8) cannot be employed to assess SAR uniformity inside the animal. On the other hand, SAR measurements everywhere inside the animal are extremely difficult, if not impossible. For this reason an FDTD simulation code is necessary developed to perform the analysis. The analysis is performed at 900 MHz with dummy loads into the cavity.

5.1.1 Simulation for Radial E-field for Ferris Wheel at 900 MHz

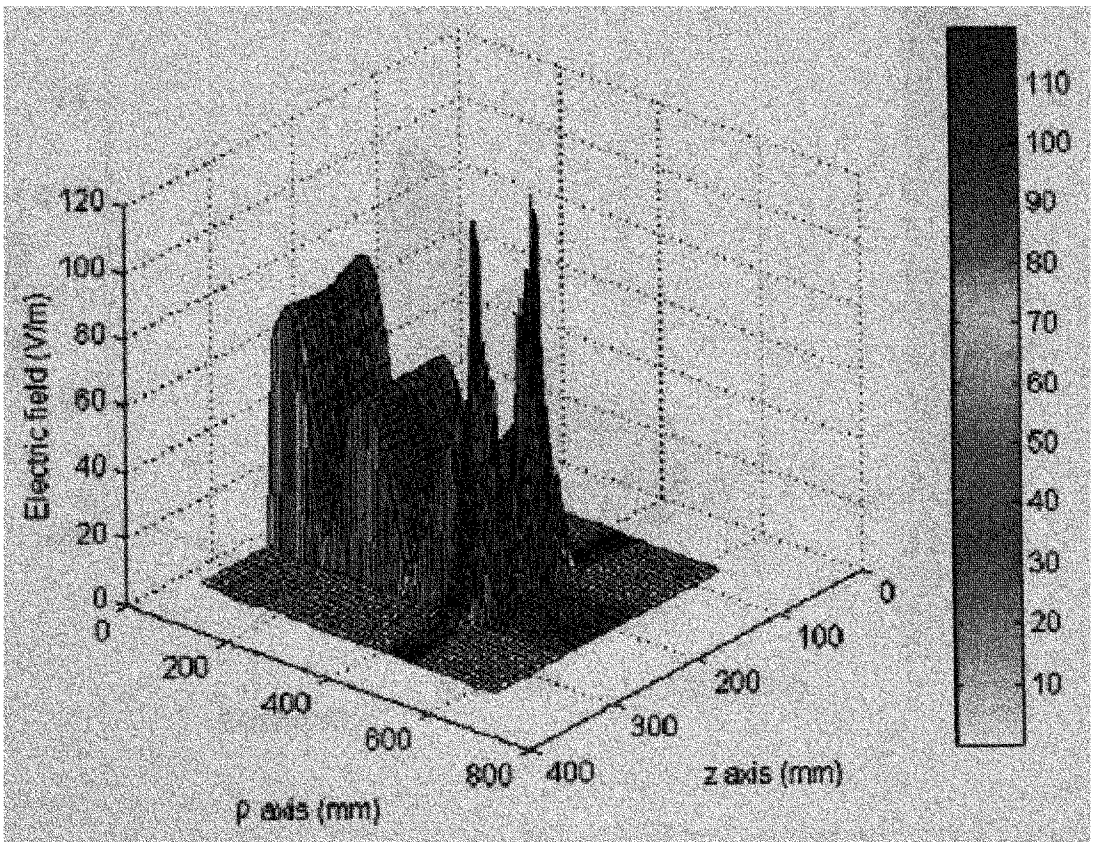

Fig.18. Distribution of the total electric field inside the cavity for the ρ-z cut through the middle of the dummies at 900 MHz [7].

Fig.18 shows the E-field distributions inside the loaded cavity along the ρ-Z cut through the middle of the dummy. The figure also shows the standing wave formed inside the loaded cavity due to the shorting posts. The field amplitude decreases as it penetrates the dummy but increases gain at the other side of the dummy because of wave reflection at the shorting posts. The input power is about 50 mV in this simulation.

5.1.2 Simulation for SAR Distribution Inside the Dummy Load at 900 MHz

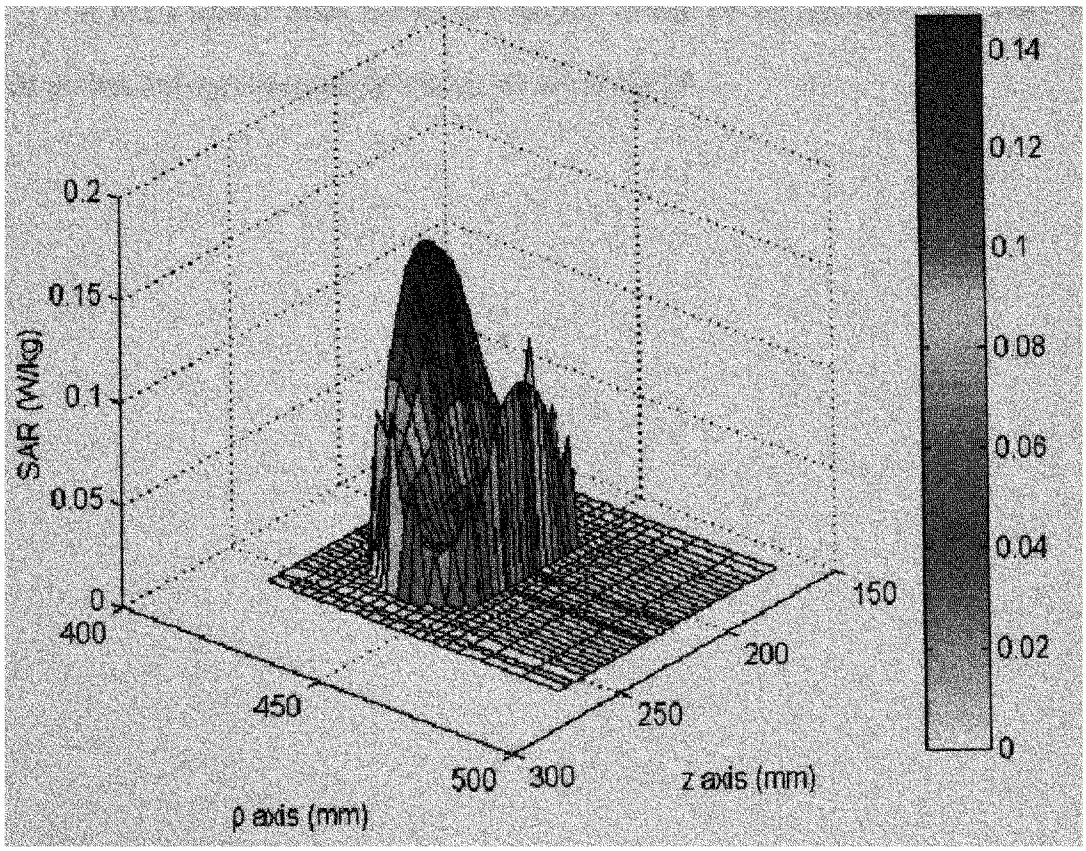

Fig.19. SAR distribution inside the dummy for the ρ-z cut through the middle of the dummies at 900 MHz [7].

Fig.19 shows the simulation for the SAR distribution inside the dummy load at 900 MHz. It can seen that SAR at the open ends is smaller and increases to the maximum at the center. This increase in the SAR distribution at the center is due to the shorting posts placed at 40 mm from the center of the restrainer. The center of the dummy load is at 440 mm and the shorting posts are placed at 480 mm from the exciter of the Ferris Wheel respectively. The maximum peak SAR inside the dummy is 0.145 W/kg and the Whole-Body average SAR is 0.041 W/kg.

It has a similar SAR distribution pattern to that of the measured with help of E-field probes through the dummy load as shown in Fig.16.

5.2 Experimental validation for XFDTD Simulations

In order to validate the FDTD code, experimental measurements are done by loading "Ferris Wheel" with forty dummy bottles with dielectric parameters of the dummies bottles are ε_r=52 and σ=1 S/m [17]. A miniature field probe is inserted between the shorting posts and measuring the radial E-field distribution. The miniature probe features three small dipole sensors with rectifying diode detectors placed along three orthogonal directions in the so-called I-beam arrangement as shown in the Fig.20 below [18].

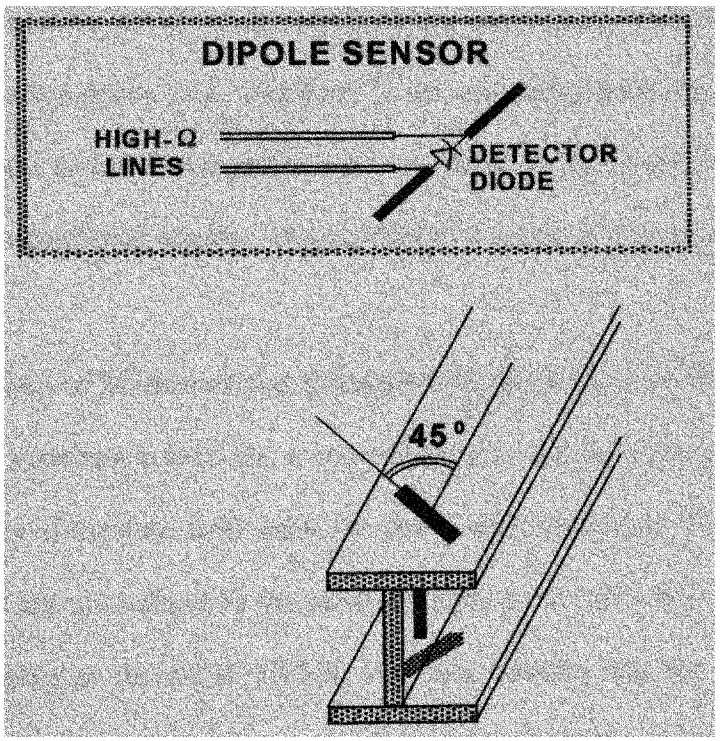

Fig.20. Sketch of the miniature electric field probe, realized in the I-beam configuration, used for the measurements inside the "Ferris Wheel" at 900 MHz [7].

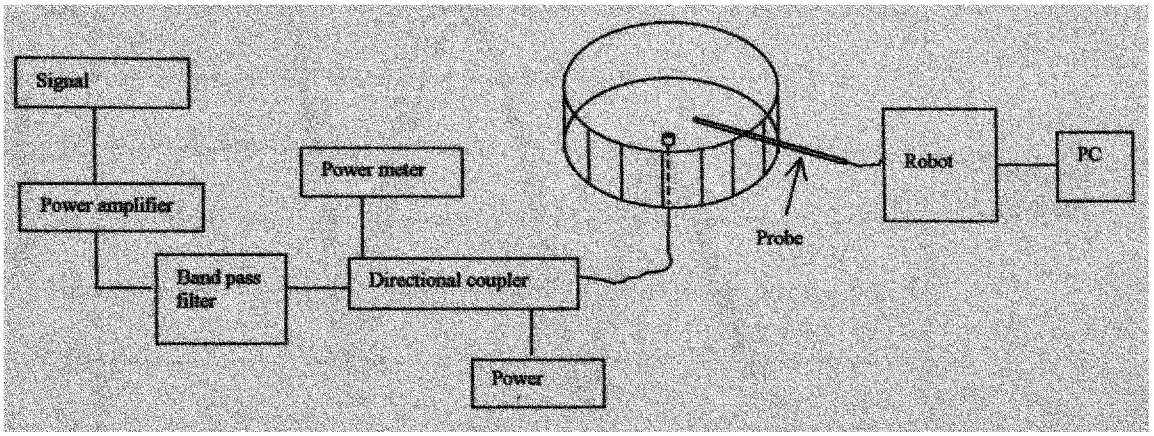

Fig.21. Measurement set-up for the radial distribution of the E- field at 900 MHz. [7]

The miniature probe was connected to an automated data acquisition system by IDX, Inc. Forward and reflected power were measured at the "Ferris Wheel" feed-point by means of a bi-directional coupler. The experimental set-up is sketched in Fig.21.

5. 2.1. Comparison of Measured and Simulated Radial E-field at 900 MHz

For best matching conditions, a comparison between the measured and calculated radial distribution of the total field inside the cavity were performed. The results reported in Fig.22, which are normalized to the same net input power (0.3 W), show a very good agreement. Looking at the radial VSWR, they also indicate that the structure stores a good amount of reactive energy, as confirmed by its relatively narrow impedance bandwidth.

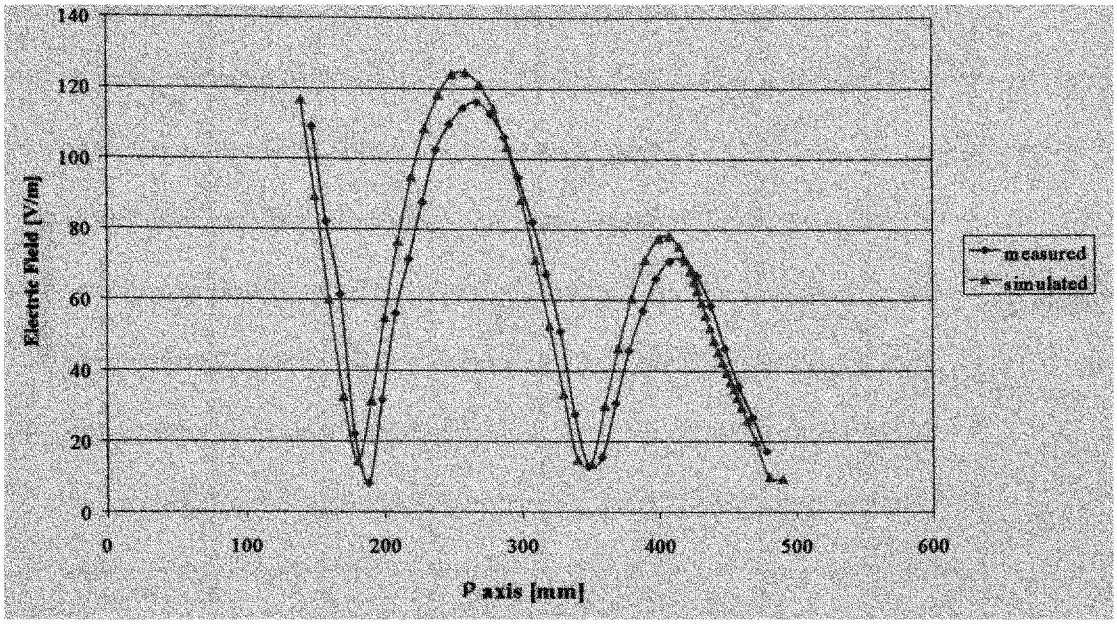

Fig.22. Comparison between the simulated and measured total electric field radial distribution at 900 MHz [7].

5.2.2. Comparison between Measured and Simulated Return Loss

The Simulations computed for cavity's return loss at 900 MHz to a 50-ohm source, for different positions of the tuning counterpoise show good correlation with the measured return loss. In Fig. 23, a comparison between measured and simulated return loss versus counterpoise position shows good agreement [7]. The offset is just 1 *mm*, which is probably due to uncertainty of distance measurement and neglecting of the two small caps thickness.

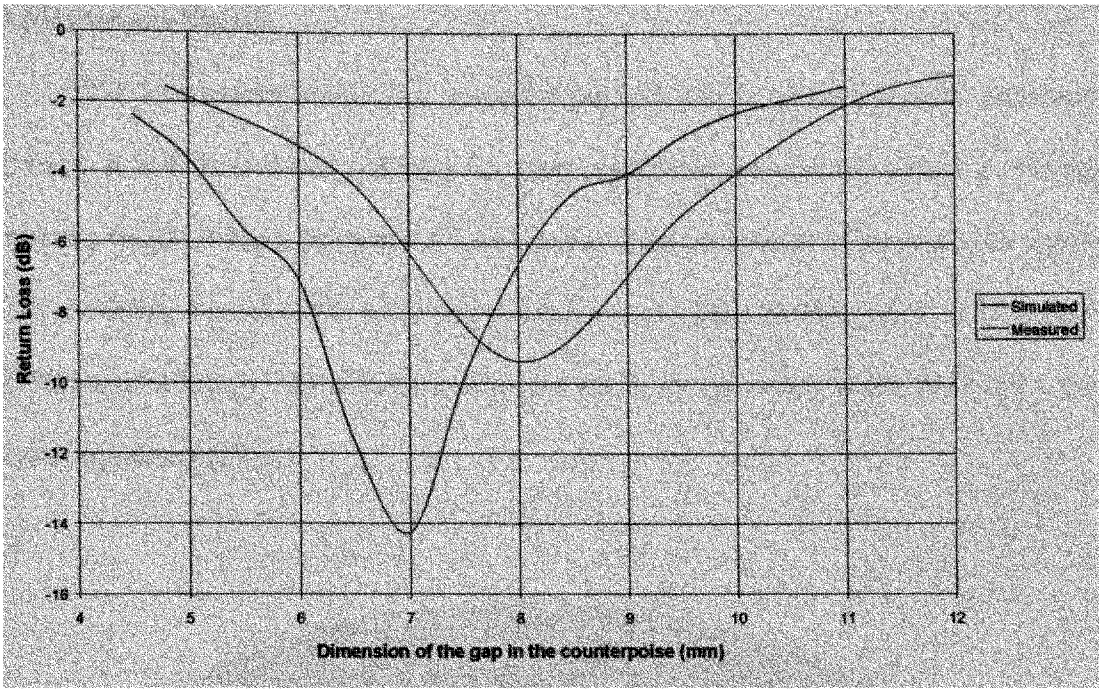

Fig.23. Comparison between the measured return loss of the cavity and the simulated one versus counterpoise distance at 900 MHz [7].

The prediction accuracy of the return loss value is satisfactory, since the net input power difference amounts to less than 15% at the best match. Such a small discrepancy could be due to the ideal materials considered in the simulation and to uncertainties of the dummies dielectric parameter. Another source of uncertainty could be associated with the description of the region where the coaxial feed-line enters the cavity.

5.3 Microwave Studio

CST Microwave Studio is a powerful and easy to use electromagnetic simulation software. It is fully featured software for electromagnetic analysis and design in the high frequency range. It has a powerful solid modeling front-end which is based on the famous ACIS modeling kernel. CST Microwave Studio uses Finite-Difference in Time Domain (FDTD) methodology based on fine adaptive mesh for geometry using Maxwell's time varying equations [19].

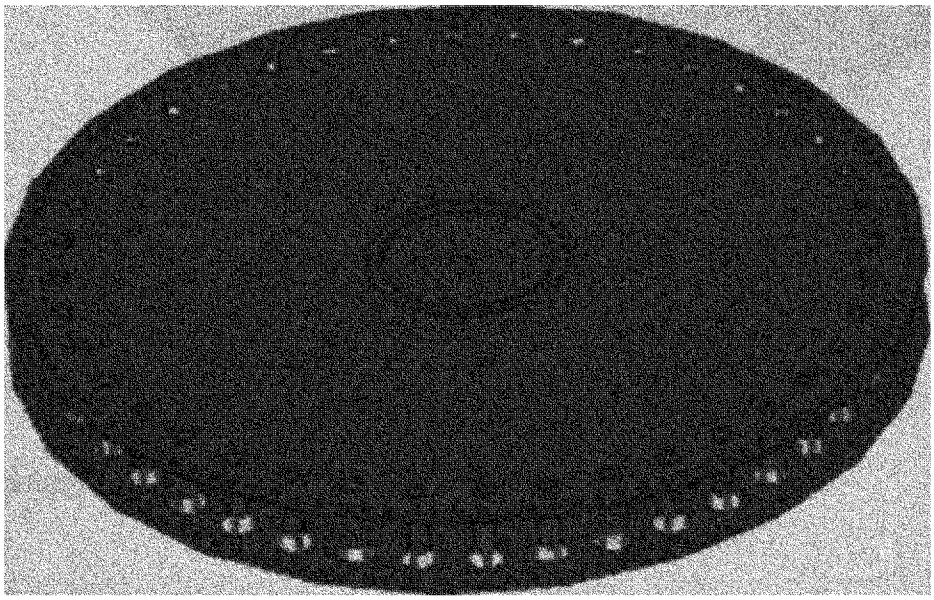

Fig.24. Model of FW in Microwave Studio [19].

Fig.24 shows the computational model of Ferris Wheel created in Microwave Studio loaded with forty identical cylinders that simulate the electrical load by the mice. A number of numerical simulations of the FW system are performed to identify the

condition upon which the geometrical asymmetries might have produced severe unbalance in the RF energy distribution.

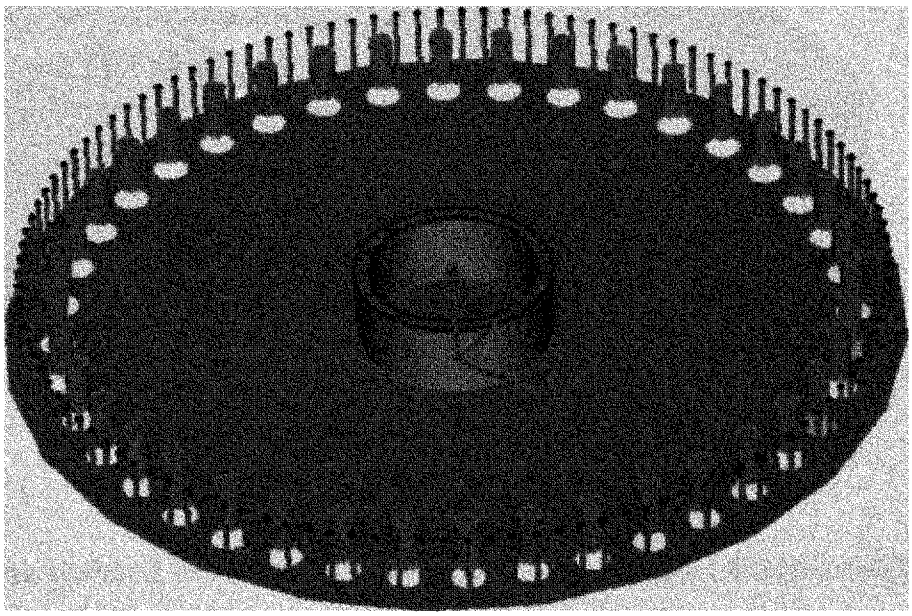

Fig.25. Internal details of the Ferris Wheel [19].

Fig. 25 shows the internal details about the Monopole antenna (field exciter), Teflon ring, holes for inserting the mice and the shorting poles.

Asymmetries in the Ferris Wheel.

The Ferris Wheel exposure system is simulated for the following geometrical asymmetries:

1. Different mouse weight: In the mouse model the length of the mouse phantoms is kept constant and varied along the diameter [19].

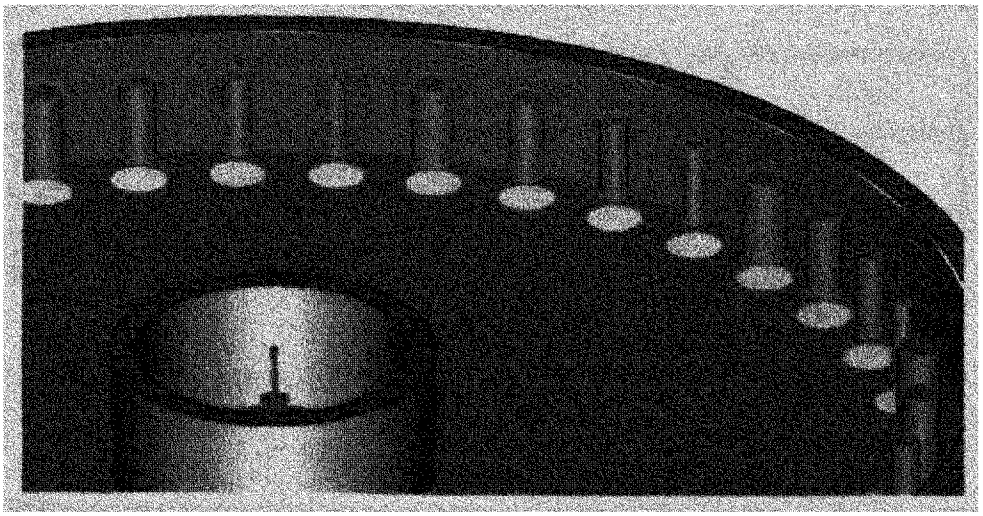

Fig.26. Ferris Wheel loaded with four different loads [19].

Two cases were analyzed, one with two weights and other with four different weights as shown in the Table 1.

Table 1. Asymmetric weight loading is repeated several times to fill the FW [19].

CASE #1 (Two weights)			CASE #2 (Four weights)		
H [mm]	D [mm]	Mass [mm]	H [mm]	D [mm]	Mass [mm]
60	10	18.8	60	7.5	10.6
60	15	42.4	60	10	18.8
60	10	18.8	60	12.5	29.5
60	15	42.4	60	15	42.4

Case#1: The following table shows the results for two different mice for 1 W net input power. The larger mouse exhibits larger peak 1-g to Whole-Body SAR ratio.

Table 2.Case#1 Results [19].

Mass [g]	SAR WB	SAR 1-g	1-g/WB
18.8	0.65	1.29	1.98
42.4	0.86	2.17	2.51

Case#2: Table: 3 Shows the results for four different mice for 1 W net input power.

Table 3:Case#2 Results [19].

Mass [g]	SAR WB	SAR 1-g	1-g/WB
10.6	0.88	1.28	1.45
18.8	0.71	1.40	1.98
29.5	.84	2.02	2.40
42.4	1.13	2.82	2.51

The most important results of the simulations are that the ratios of the 1-g and Whole-Body averages are insensitive to the asymmetries introduced in the FW [19]. The SAR distribution with in the mice is negligibly affected by rather significant, thus indicating small mutual coupling between the mice.

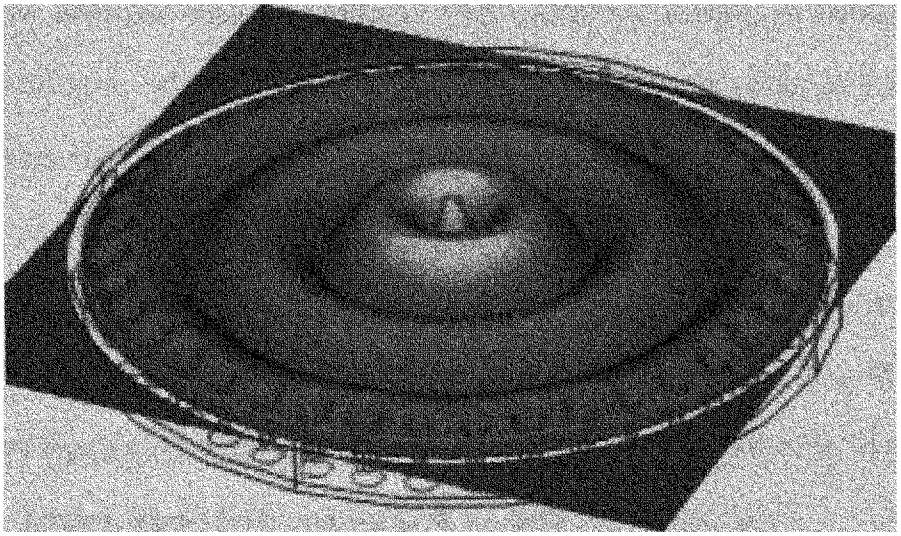

Fig.27. Electric field distribution for FW using four different weight mice [19].

In practice, the nearby mice minimally affect the mechanism of energy absorption. The total electric field plot over the bisecting cut plane shown in Fig.27. The electric distribution preserves an excellent azimuthally symmetry.

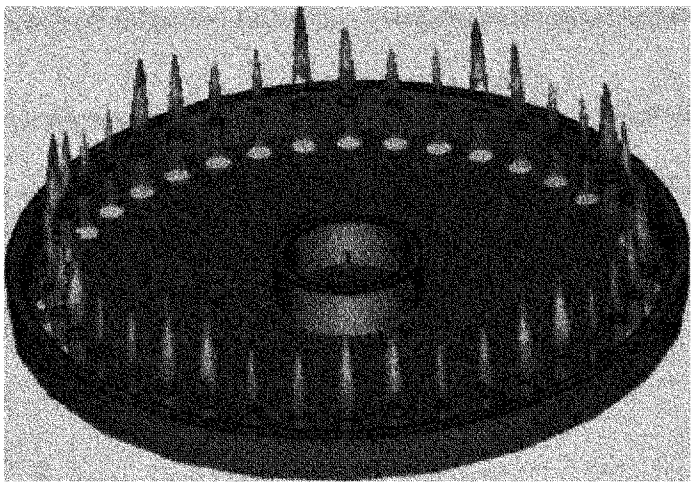

Fig.28. SAR distribution over a cut-plane bisecting the FW loaded with four different weights [19].

2. Offset of the collective mouse barycentre: This asymmetry consists in shifting the center of mass of mice, which ideally coincides with the geometrical center of the FW. All mice are assumed (H=60 mm, D =12.5, Mass =29.5) for three cases of offset of 2.5,10,10 mm respectively.

The below table shows the asymmetry resulting from an offset of the center of mass of the mice with respect to the geometrical center of the FW can potentially introduce a very high degree of non-uniformity in the Whole-Body and peak 1-g SAR.

Table 4.Whole-Body and 1-g SAR for different Offsets [19].

Offset [mm]	SAR WB	SAR 1-g	1-g/WB
0.0	1.0	1.0	2.38
2.5	2.6	2.4	2.39+/-10%
5.0	4.2	3.7	2.37+/-11%
10.0	24.9	20.4	2.36+/-20%

In the Fig.29.a shows the marked asymmetry in the total electric field distribution is caused by the 10 mm offset, which is responsible for the dramatic non-uniformity in the SAR distribution across the mice.

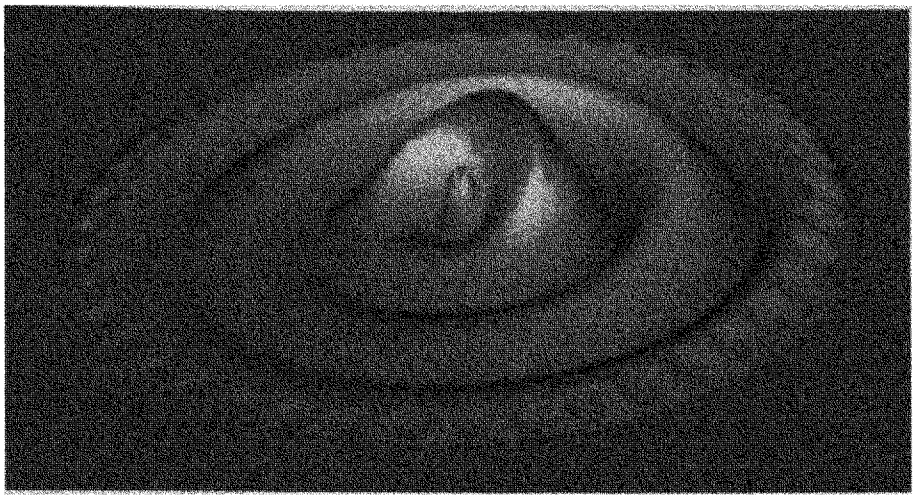

Fig.29.a

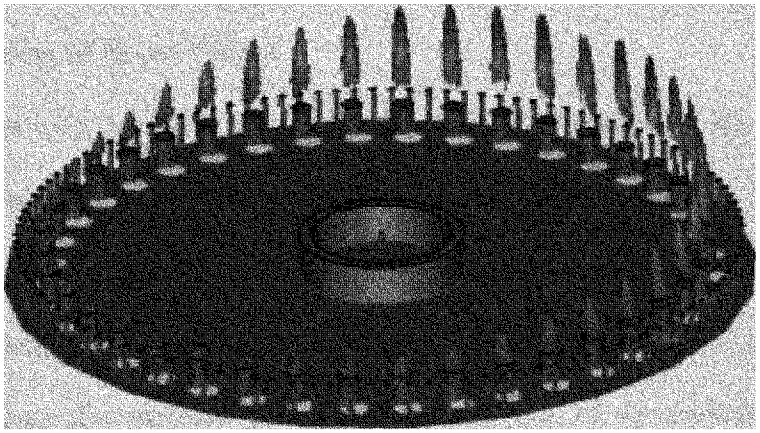

Fig.29.b

Fig.29. Total electric field simulation (a) and SAR distribution (b) in a FW loaded with 29.5 g mice arranged witha10mm offset between the collective mass and the geometrical center of FW [19].

In general it is found that the SAR is lower for the samples closer to the lateral wall, which is intuitive since the electric field associated to the dominant mode vanishes.

CHAPTER VI

DETERMINATION OF WHOLE-BODY SAR AND CHARACTERIZATION OF FERRIS WHEEL USING CALORIMETRIC PROCESS

As already discussed in the previous Chapters it is necessary to characterize the behavior of the Ferris Wheel in terms of symmetry and efficiency. In order to confirmation the reliability of the exposure system the results obtained in terms of SAR and efficiency should be of good repeatability. For SAR measurements the actual power absorbed by the load must be measured very precisely. This chapter discusses the calorimetric process, which helps in precise determination of Whole-Body SAR.

6.1 Characterizing of Ferris Wheel

The most ideal condition to start the initial characterization on the "Ferris Wheel" exposure system is to have symmetrical loading structure, which can be achieved by using dummy bottles filled with simulated tissue material as loads, discussed in Chapter IV. The net energy radiated from the radiating element will be assumed to be equally distributed among the symmetrical loads, as they are of approximately equal and equidistant from the center. As already discussed the simulated tissue material doesn't have the any complexity in terms of shape and dielectric properties. Since the Ferris Wheel has forty slots and it is impractical to test every position for the amount of power absorbed by each load, four different position of interest are chosen as shown in Fig.30.

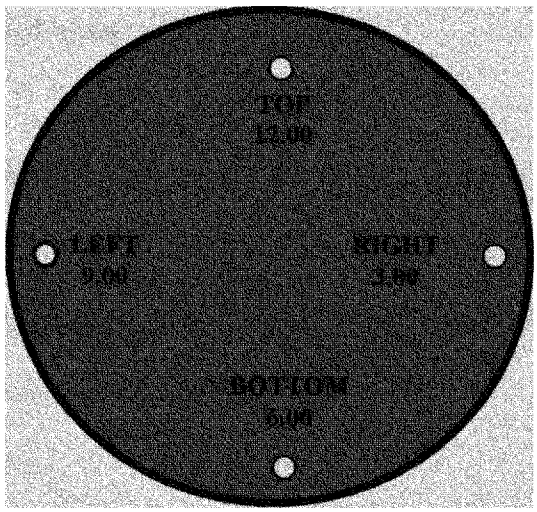

Fig .30. Four different positions of interest on the wheel

Several exposures were done using simulated tissue at the four different locations (TOP, BOTTOM, LEFT, RIGHT) on the Ferris Wheel to measure the amount of energy absorbed by the dummy bottles for each of one these locations. These four locations TOP, BOTTOM, LEFT, RIGHT are also known as 12.00 clock, 6.00 clock, 9.00 clock and 3.00 clock respectively. For the specific Left Position, an intentional delay time was introduced in between end of exposure and putting the mice into the calorimeter, This delays were 5, 10 and 15 seconds which will be explained in next sections.

Since the Ferris Wheel is designed for the exposure of mice and to replicate the Australian experiment in terms of loading, the actual characterization should be done with experiments containing realistic type of loads i.e., mice into the "Ferris Wheel".

In order to replicate the Australian study in terms of the loading, it was chosen to use mice of three different weights to simulate the life cycle of a mouse. The weights used to simulate the life cycle of a mouse are 25 g, 32 g and 36g respectively. The

experimental procedure using the mice is almost the same as that of the dummy bottles containing the simulated tissue.

6.2 Experimental setup for the Ferris Wheel exposure system

The following schematic shows the RF setup for the Ferris Wheel exposure system, comprising of the signal generator at 915 MHz, Bi-directional coupler and power meters to measure the forward and reflected powers.

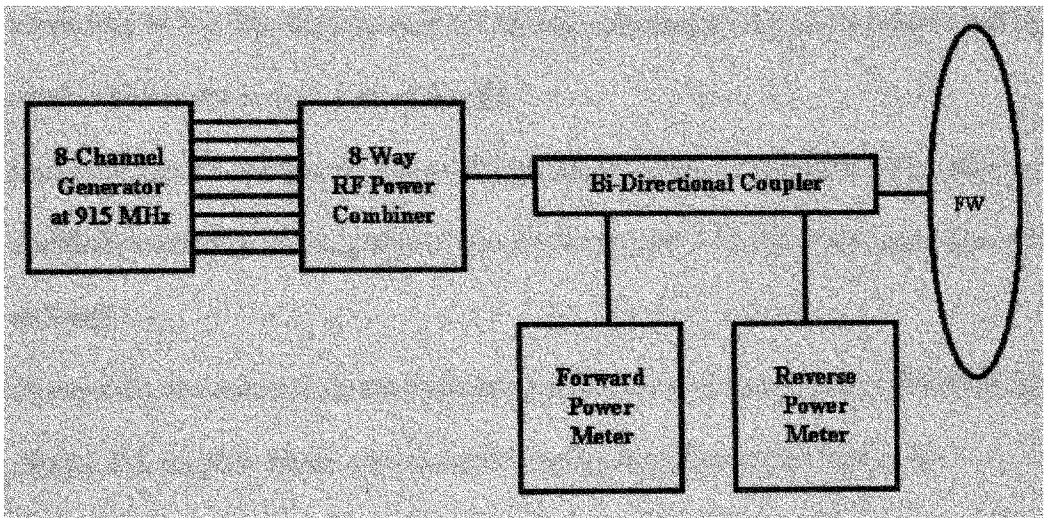

Fig.31. Schematic of RF setup for "Ferris Wheel" Exposure System

Before an exposure is performed the "loaded" exposure system should be tuned in order to maximize the energy transferred to the loads. The following tuning procedure should be followed whenever new loads are used, which change the loading conditions

1. Calibrate the network analyzer to take account the losses of the cable and connectors used. The standard S11 calibration procedure should be performed for

short, open and load conditions. Make sure the frequency range is adjusted from 850 MHz to 950 MHz.

2. Disconnect the cable from the directional coupler and connect the network analyzer to the feeding point in the "Ferris Wheel" through the cable used for calibration. Check for the single dip on network analyzer screen. Enable the marker to be shown in the screen and set it up at 915 MHz.
3. Inside the part of the Teflon ring outside the cavity a long shaft (counter-poise) is seen. Loose the plastic screw to release the shaft. Let it rotate to right or left according to the dip displacement in the analyzer screen. Adjust the shaft until the marker points the lowest part of the dip.
4. Carefully tighten the plastic nut to disable any rotation of the shaft. The reflection coefficient reading in the analyzer should be around –11 dB when mice are used as loads.
5. Disconnect the cable from the network analyzer and reconnect the cable from the directional coupler. Make sure to have a tight connection at the feed point.
6. It's advisable to check the internal components of the connector from time to time to evaluate their integrity.
7. After the above steps were done, the load position (Top, Left, Right, and Bottom) should be chosen.

6.3 Twin-Well Calorimeter for Whole-Body SAR Measurements

A calorimeter helps us in determining the RF dosage in the absorbing objects. Whole-Body SAR of a biological object can be determined by using a "Twin-Well" Calorimeter. It consists of two identical cylinders large enough to contain the objects. Each cylinder is surrounded by a thermopile, an array of thermocouples connected in series (voltage additive). The thermopiles of the two cylinders are connected in opposite polarities so that the voltages are subtracted. Therefore when both cylinders are at the same temperature, the resulting voltage from the thermopiles is zero.

The amount of heat energy absorbed during an exposure in an object is determined by using two similar bodies, but at different temperatures $T_1(t)$ and $T_2(t)$, in the wells of the calorimeter. It was given the name "differential Twin-Well" calorimeter because it measures the difference in heat between the bodies that are placed in two copper wells.

During Ferris Wheel exposure tests using loads, twin-well calorimeter allows to make differential heat measurements between loads used as exposed and sham of similar weight. Due to the difference in temperature or heat content between exposed and sham, the heat flows from higher temperature well to the lower temperature. The process of heat transfer is very slow as a low conductive material separates the wells and surrounds the envelope.

6.3.1 Mathematical Modeling for the "Twin-Well" Differential Calorimeter

Twin-Well is employed to determine the RF dose variation verses load position in the carousel. It helps in determining the Whole-Body SAR in dummy bottles or mice cadavers. Highly precise measurements are made of the quantity of microwave energy absorbed by models or bodies of exposed animals. A reference or non-exposed

target is placed in one well, an exposed target in the other well; the difference in thermal loading is then detected by sensitive thermocouples. The difference in heat exchanged between the wells having a reference constant temperature T_0 (usually Room temperature at 23°C) is determined by monitoring the output voltage from the calorimeter, which is proportional to the temperature difference between the wells. The amount of energy absorbed by the sample tissues in terms of temperature changes is used for determination of SAR value.

Under this hypothesis the amount of the heat flowing by the first body in the time interval $(t, t+dt)$ can be approximated as follows [20]

$$dq_1 = \{R_{10}[T_1(t) - T_0] + R_{12}[T_1(t) - T_2(t)]\}dt \tag{6.1}$$

with

$$dq_1 = -m_1 c_1 \, dT_1 \tag{6.2}$$

where m_1 is the mass of the body, while c_1 is its specific heat. Equating (6.1) and (6.2) it results

$$-m_1 c_1 \frac{\partial}{\partial t} T_1(t) = \{R_{10}[T_1(t) - T_0] + R_{12}[T_1(t) - T_2(t)]\} \tag{6.3}$$

Proceeding in the same way for the second body we obtain

$$-m_2 c_2 \frac{\partial}{\partial t} T_2(t) = \{R_{20}[T_2(t) - T_0] + R_{21}[T_2(t) - T_1(t)]\} \tag{6.4}$$

The differential equations governing the twin-well calorimeter are then

$$\begin{cases} m_1 c_1 \dfrac{\partial}{\partial t} T_1(t) = -\{R_{10}[T_1(t) - T_0] + R_{12}[T_1(t) - T_2(t)]\} \\ m_2 c_2 \dfrac{\partial}{\partial t} T_2(t) = -\{R_{20}[T_2(t) - T_0] + R_{21}[T_2(t) - T_1(t)]\} \end{cases} \tag{6.5}$$

To obtain the solution of the above differential equations we employ the Laplace transform obtaining

$$\begin{cases} m_1 c_1 [s T_1(s) - T_{10}] = -\left\{R_{10}\left[T_1(s) - \dfrac{T_0}{s}\right] + R_{12}[T_1(s) - T_2(s)]\right\} \\ m_2 c_2 [s T_2(s) - T_{20}] = -\left\{R_{20}\left[T_2(s) - \dfrac{T_0}{s}\right] + R_{21}[T_2(s) - T_1(s)]\right\} \end{cases} \tag{6.6}$$

After some simple mathematical manipulations the following system of linear equations are derived

$$\begin{cases} [m_1 c_1 s + R_{10} + R_{12}] T_1(s) - R_{12} T_2(s) = m_1 c_1 T_{10} + R_{10} \dfrac{T_0}{s} \\ [m_2 c_2 s + R_{20} + R_{21}] T_2(s) - R_{21} T_1(s) = m_2 c_2 T_{20} + R_{20} \dfrac{T_0}{s} \end{cases} \tag{6.7}$$

or in a more compact form

$$\begin{bmatrix} m_1 c_1 s + R_{10} + R_{12} & -R_{12} \\ -R_{21} & m_2 c_2 s + R_{20} + R_{21} \end{bmatrix} \cdot \begin{bmatrix} T_1(s) \\ T_2(s) \end{bmatrix} = \begin{bmatrix} m_1 c_1 T_{10} + R_{10} \dfrac{T_0}{s} \\ m_2 c_2 T_{20} + R_{20} \dfrac{T_0}{s} \end{bmatrix} \tag{6.8}$$

The Laplace transforms of the terms $T_1(t)$ and $T_2(t)$ are then determined by solving the above system of linear equations. Solving (6.8), we obtain

$$T_1(s) = \frac{\begin{bmatrix} m_1 c_1 T_{10} + R_{10} \dfrac{T_0}{s} & -R_{12} \\ m_2 c_2 T_{20} + R_{20} \dfrac{T_0}{s} & m_2 c_2 s + R_{20} + R_{21} \end{bmatrix}}{\begin{bmatrix} m_1 c_1 s + R_{10} + R_{12} & -R_{12} \\ -R_{21} & m_2 c_2 s + R_{20} + R_{21} \end{bmatrix}} \tag{6.9}$$

$$T_2(s)=\frac{\begin{bmatrix} m_1 c_1 s+R_{10}+R_{12} & m_1 c_1 T_{10}+R_{10}\dfrac{T_0}{s} \\ -R_{12} & m_2 c_2 T_{20}+R_{20}\dfrac{T_0}{s} \end{bmatrix}}{\begin{bmatrix} m_1 c_1 s+R_{10}+R_{12} & -R_{12} \\ -R_{21} & m_2 c_2 s+R_{20}+R_{21} \end{bmatrix}} \tag{6.10}$$

from which it results

$$T_1(s)=\frac{\left[m_1 c_1 T_{10}+R_{10}\dfrac{T_0}{s}\right]\left[m_2 c_2 s+R_{20}+R_{21}\right]+R_{12}\left[m_2 c_2 T_{20}+R_{20}\dfrac{T_0}{s}\right]}{\left[m_1 c_1 s+R_{10}+R_{12}\right]\left[m_2 c_2 s+R_{20}+R_{21}\right]-R_{12}R_{21}} \tag{6.11}$$

$$T_2(s)=\frac{\left[m_2 c_2 T_{10}+R_{20}\dfrac{T_0}{s}\right]\left[m_1 c_1 s+R_{10}+R_{21}\right]+R_{21}\left[m_1 c_1 T_{10}+R_{10}\dfrac{T_0}{s}\right]}{\left[m_1 c_1 s+R_{10}+R_{12}\right]\left[m_2 c_2 s+R_{20}+R_{21}\right]-R_{12}R_{21}} \tag{6.12}$$

or

$$T_1(s)=\frac{\left[s m_1 c_1 T_{10}+R_{10}T_0\right]\left[m_2 c_2 s+R_{20}+R_{21}\right]+R_{12}\left[s m_2 c_2 T_{20}+R_{20}T_0\right]}{s\left\{\left[m_1 c_1 s+R_{10}+R_{12}\right]\left[m_2 c_2 s+R_{20}+R_{21}\right]-R_{12}R_{21}\right\}} \tag{6.13}$$

$$T_2(s)=\frac{\left[s m_2 c_2 T_{10}+R_{20}T_0\right]\left[m_1 c_1 s+R_{10}+R_{21}\right]+R_{21}\left[s m_1 c_1 T_{10}+R_{10}T_0\right]}{s\left\{\left[m_1 c_1 s+R_{10}+R_{12}\right]\left[m_2 c_2 s+R_{20}+R_{21}\right]-R_{12}R_{21}\right\}} \tag{6.14}$$

If the calorimeter is symmetric and the two bodies have the same characteristics the above equations can be rewritten as

$$T_1(s)=\frac{\left[s m c T_{10}+R_{10}T_0\right]\left[m c s+R_{10}+R_{12}\right]+R_{12}\left[s m c T_{20}+R_{10}T_0\right]}{s\left\{\left[m c s+R_{10}+R_{12}\right]^2-R_{12}^2\right\}} \tag{6.15}$$

$$T_2(s)=\frac{\left[s m c T_{10}+R_{10}T_0\right]\left[m c s+R_{10}+R_{12}\right]+R_{12}\left[s m c T_{10}+R_{10}T_0\right]}{s\left\{\left[m c s+R_{10}+R_{12}\right]^2-R_{12}^2\right\}} \tag{6.16}$$

The denominator of (6.15)-(6.16) can be expanded in the following form

$$[mcs+R_{10}+R_{12}]^2-R_{12}^2=(mcs+R_{10})^2+2R_{12}(m_1c_1s+R_{10})+R_{12}^2-R_{12}^2 \tag{6.17}$$

and rewritten as follows

$$[mcs+R_{10}+R_{12}]^2-R_{12}^2=(mcs+R_{10})[mcs+R_{10}+2R_{12}] \tag{6.18}$$

Using (6.18) we have

$$T_1(s)=\frac{[smcT_{10}+R_{10}T_0][mcs+R_{10}+R_{12}]+R_{12}[smcT_{20}+R_{10}T_0]}{s(mcs+R_{10})[mcs+R_{10}+2R_{12}]} \tag{6.19}$$

$$T_2(s)=\frac{[smcT_{10}+R_{10}T_0][mcs+R_{10}+R_{12}]+R_{12}[smcT_{10}+R_{10}T_0]}{s(mcs+R_{10})[mcs+R_{10}+2R_{12}]} \tag{6.20}$$

or $$T_1(s)=\frac{\left[sT_{10}+\frac{R_{10}T_0}{mc}\right]\left[s+\frac{R_{10}+R_{12}}{mc}\right]+R_{12}\left[sT_{20}+\frac{R_{10}T_0}{mc}\right]}{s\left(s+\frac{R_{10}}{mc}\right)\left[s+\frac{R_{10}+2R_{12}}{mc}\right]} \tag{6.21}$$

$$T_2(s)=\frac{\left[sT_{10}+\frac{R_{10}T_0}{mc}\right]\left[s+\frac{R_{10}+R_{12}}{mc}\right]+R_{12}\left[sT_{10}+\frac{R_{10}T_0}{mc}\right]}{s\left(s+\frac{R_{10}}{mc}\right)\left[s+\frac{R_{10}+2R_{12}}{mc}\right]} \tag{6.22}$$

From the equations (6.21)-(6.22) it appears that the thermal system formed by the two bodies is characterized by two time constants given by

$$\alpha=\frac{R_{10}}{mc} \tag{6.23}$$

$$\beta=\frac{R_{10}+2R_{12}}{mc} \tag{6.24}$$

The Laplace transforms $T_1(s)$ and $T_2(s)$ can then be rewritten in a form useful to derive their time domain counterpart. We have

$$T_1(s) = \frac{T_{1\infty}}{s} + \frac{T_{1\alpha}}{s+\alpha} + \frac{T_{1\beta}}{s+\beta} \tag{6.25}$$

$$T_2(s) = \frac{T_{2\infty}}{s} + \frac{T_{2\alpha}}{s+\alpha} + \frac{T_{2\beta}}{s+\beta} \tag{6.26}$$

The coefficients $T_{j\infty}$, $T_{j\alpha}$, and $T_{j\beta}$, with j=1,2, can be determined using the well-known formulas

$$T_{j\infty} = \underset{s \to 0}{Lim}\, sT_j(s) \tag{6.27}$$

$$T_{j\alpha} = \underset{s \to -\alpha}{Lim}\, (s+\alpha)T_j(s) \tag{6.28}$$

$$T_{j\beta} = \underset{s \to -\beta}{Lim}\, (s+\beta)T_j(s) \tag{6.29}$$

We obtain

$$T_{1\infty} = T_0 \tag{6.30}$$

$$T_{1\alpha} = \frac{1}{2}(T_{10} + T_{20} - 2T_0) \tag{6.31}$$

$$T_{1\beta} = \frac{1}{2}(T_{10} - T_{20}) \tag{6.32}$$

$$T_{2\infty} = T_0 \tag{6.33}$$

$$T_{2\alpha} = \frac{1}{2}(T_{10} + T_{20} - 2T_0) \tag{6.34}$$

$$T_{2\beta} = \frac{1}{2}(T_{20} - T_{10}) \tag{6.35}$$

Using the above equations it is straightforward to express $T_1(t)$ and $T_2(t)$ as follows

$$T_1(t) = T_0 + \frac{1}{2}(T_{10} + T_{20} - 2T_0)e^{-\frac{R_{10}}{mc}} + \frac{1}{2}(T_{10} - T_{20})e^{-\frac{R_{10}+2R_{12}}{mc}} \tag{6.36}$$

$$T_2(t) = T_0 + \frac{1}{2}(T_{10} + T_{20} - 2T_0)e^{-\frac{R_{10}}{mc}} - \frac{1}{2}(T_{10} - T_{20})e^{-\frac{R_{10}+2R_{12}}{mc}} \tag{6.37}$$

Consequently, the voltage appearing at the port of the thermocouple, which is proportional to the difference between $T_1(t)$ and $T_2(t)$, writes

$$v(t) = (T_{20} - T_{10})e^{-\frac{(R_{10}+2R_{12})t}{mc}} \tag{6.38}$$

Finally, integrating the voltage $v(t)$ we obtain a term proportional to the heat difference between the two bodies

$$v(t) = \int_0^\infty (T_{20} - T_{10})e^{-\frac{(R_{10}+2R_{12})t}{mc}} dt = \frac{mc(T_{20} - T_{10})}{R_{10} + 2R_{12}} \tag{6.39}$$

where R_{10} is the thermal resistances between the well to envelope maintained at constant temperature T_0,and R_{12} is the thermal resistances between the two wells of the calorimeter.

It should be noted that (6.39) applies only when the two bodies have the same characteristics (mass and specific heat).

6.3.2 Numerical Analysis for "Twin-Well" Calorimeter

MATLAB was used to numerically solve the heat flow between the wells of the Twin-Well calorimeter; a partial differential equation was used for the heat flow in the twin-well calorimeter. Since the Twin-Well is a complex but symmetrical system containing two identical well for loads, to simplify matters a one-dimensional section of the calorimeter system is chosen as shown in the Fig.32.

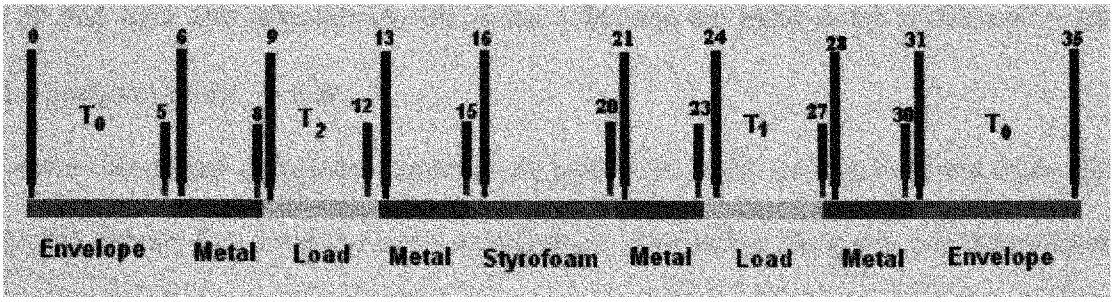

Fig.32.One-Dimensional Structure of Twin-Well Calorimeter used for Simulation.

In a one -dimensional medium between two points x_1 and x_2 with in a solid is, the conduction of heat is given by the equation

$$q_x = -k\left(\frac{T(x_2)-T(x_1)}{x_2-x_1}\right) \tag{6.40}$$

Where $T(x)$ is the local temperature and q_x is the thermal flux and has units W/m^2 .The quantity k is the material thermal conductivity with units $J/m\text{-}K$ [21]. The flux is proportional to the temperature difference and inversely proportional to the distance between the locations.

As the thermal flux or the heat flow is proportional to the thermal conductivity at a position and temperature at an instance. The one-dimensional heat flow inside the calorimeter can be treated in terms of temperature and conductivity.

The partial differential equation in terms of temperature is

$$\frac{\partial T}{\partial t} = k(x)\frac{\partial^2 T}{\partial x^2} \tag{6.41}$$

where $T(x, t)$ is the temperature at time t a distance x along one-dimensional section of the calorimeter.

The solution space is divided into uniform sections of width Δx as shown in the Fig.32 and time into intervals Δt. the index i denotes the mesh point position $x_i = i\Delta x$ and n designates time, $t = n\Delta t$.

To solve this partial differential equation we need both initial conditions of the form $T(x, 0) = f(x)$, where $f(x)$ gives the initial temperature distribution along the one dimensional line of the calorimeter as shown in the figure as the value of x varies from 0 to 35. At $t = 0$, and *boundary conditions* at the envelope of the system are $x_i = T_0$ for $5 \geq x_i \geq 1$ and $35 \geq x_i \geq 31$ and remains the same for all the time t.

The partial differential equation in terms of finite difference approximations to the derivatives, we get

$$\frac{T_i^{n+1} - T_i^n}{\Delta t} = k\frac{T_{i+1}^n - 2T_i^n + T_{i-1}^n}{\Delta x^2} \tag{6.42}$$

Thus if for a particular n, we know the values of T_i^n for all i, we can solve the equation above to find T_i^{n+1} for each i:

$$T_i^{n+1} = T_i^n + \frac{k\Delta t}{\Delta x^2}\left(T_{i+1}^n - 2T_i^n + T_{i-1}^n\right) = s\left(T_{i+1}^n + T_{i-1}^n\right) + (1-2s)T_i^n \tag{6.43}$$

where $s = k(x)\Delta t/(\Delta x)^2$ [21]. In other words, this equation tells us how to find the temperature distribution at time step $n+1$ given the temperature distribution at time step n.

The above equation can be interpreted, as the temperature at a given location at the next time step is a weighted average of its temperature and the temperatures of its neighbors at the current time step. In other words, in time Δt, a given section of length Δx transfers to each of its neighbors a portion s of its heat energy and keeps the remaining portion $1-2s$ of its heat energy.

The following M-file, which is named twin.m, iterates the procedure described above.

```
t = linspace(0,1200,6200);
x = linspace(0,35,35);
k(1,1:5)=0.2;
k(1,6:8)=1;
k(1,9:12)=.7;
k(1,13:15)=1;
k(1,16:20)=0.2;
k(1,21:23)=1;
k(1,24:27)=.7;
k(1,28:30)=1;
k(1,31:35)=0.2;
J = length(x);
N = length(t);
dx = mean(diff(x));
dt = mean(diff(t));
s = k*dt/dx^2;
T = zeros(N,J);
T(:,1:5) = 23;
T(1,6:8)=23;
T(1,9:12)=40;
T(1,13:15)=23;
T(1,16:20)=23;
T(1,21:23)=23;
T(1,24:27)=30;
T(1,28:30)=23;
T(:,31:35)=23;
for p= 2:N
   for n = 6:30
        T(p,n) = s(1,n)*(T(p-1,n+1) + T(p-1,n-1)) + (1 - 2*s(1,n))*T(p-1,n);
end
end
figure(1);
surf(T)
```

```
v1=T(:,7);
v2=T(:,29);
figure(2);
contour(T);
M=(v1-v2)/3;
figure(3);
plot(t*60,M);
```

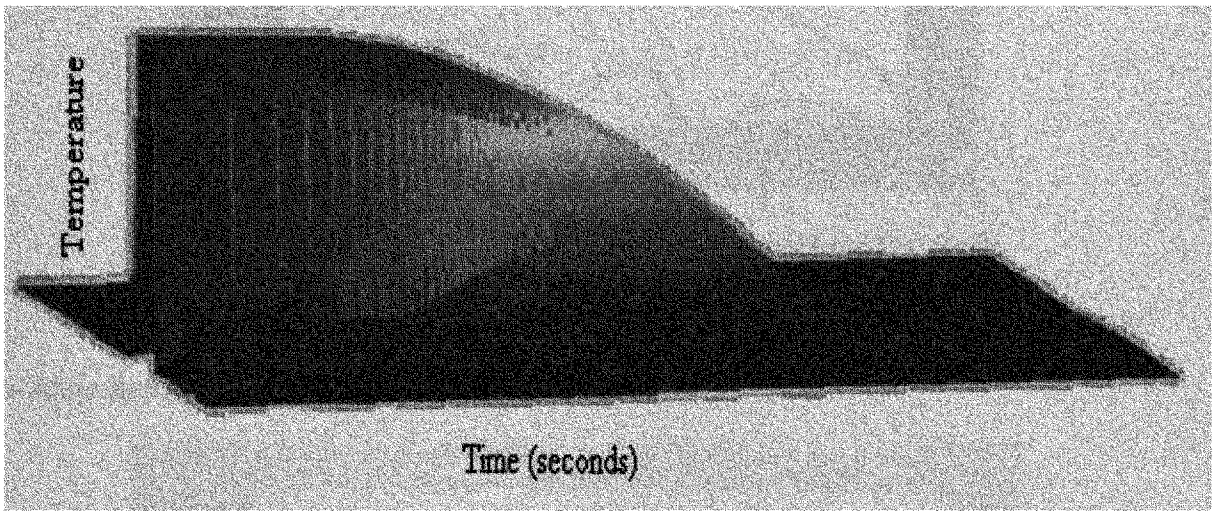

Fig.33. One-Dimensional Heat flow between the two wells of Twin -Well Calorimeter and its Envelope.

Fig.33 shows the one-dimensional heat flow, which is proportional to temperature between the two wells, maintained at T_1 and T_2 and the envelope temperature maintained at T_0 .As the time increases the temperature all the points on the one-dimensional space of Twin-Well tend to reach the envelope temperature. Fig.34 shows the flow of the heat between the two wells of the Twin-Well calorimeter as temperature counters. The counters show the flow of heat from the well at higher temperature to the well at lower temperature.

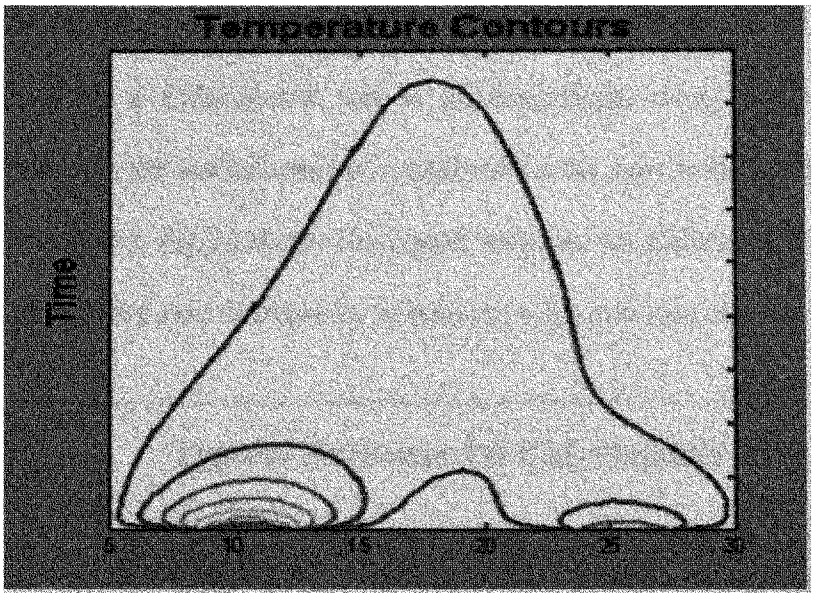

Fig.34. Temperature Contours for heat flow between the two wells.

The simulated response for the heat exchange between the wells in terms of voltage during a calorimetric test is shown in Fig.35.

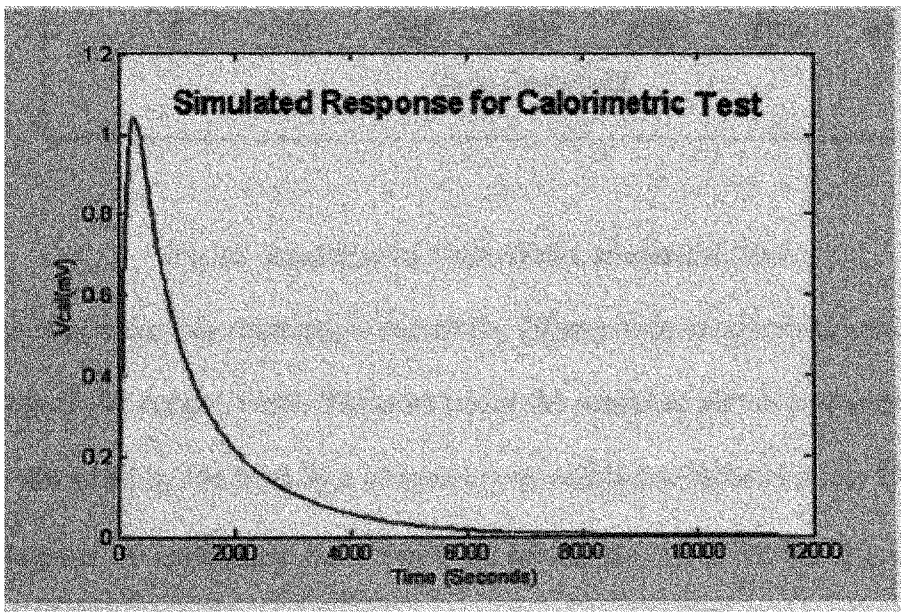

Fig.35.Simulated Response for a Calorimetric Test.

6.4 Calculation for Whole-Body SAR using Calorimetric Technique

Response for a Calorimetric test is an exponential decay when the voltage difference between is the thermocouples connected to the two wells of the Twin-Well calorimeter is measured. Fig.36 shows the typical response for Calorimetric test, which is similar to that of the response obtained by simulation in the previous section.

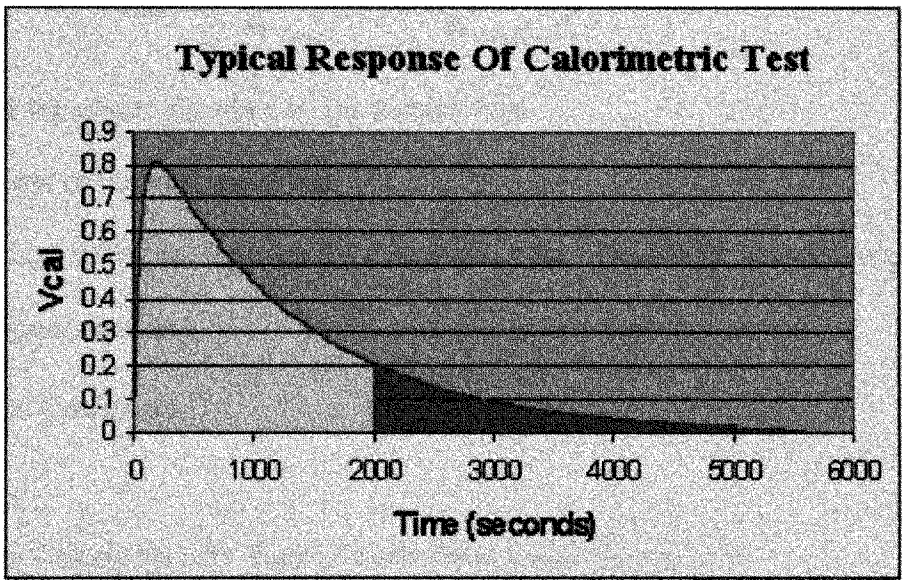

Fig.36. Response of Twin-Well Calorimetric Test.

The reason for this response is due to the difference in conductivity coefficients of loads to that of the copper wells. The area under the response plot is proportional to the RF energy absorbed by the load by a conversion or calibration factor $\gamma \cong 10$. The factor $\gamma \cong 10$ is obtained by calibrating the Twin-Well calorimeter with ice water and acetone. After a number of exposures and analyzing the heat transfer between the loads it is observed that the voltage difference between the wells follows an exponential decay around 1800 seconds. In order to increase the number of experimental measurements in a

day the area under the exponential decay is extrapolated, after stopping the test around 2000 seconds. Fig.36 shows the area under response curve is divided into two parts .The area shaded red is extrapolated using a time constant of 2492 seconds.

The Whole-Body SAR in a dummy of mass m used in the calorimeter can be:

$$SAR_{Load} = \frac{P_{Load}}{m_{Load}} = \frac{\gamma \cdot \int_0^{\infty} V_{cal}(\tau) d\tau}{m_{Load} \cdot \Delta t} \qquad (6.44)$$

where P_{Load} is the power absorbed by the dummy load,

m_{Load} is the mass of the load under test,

V_{cal} is the voltage difference between the two wells of the "Twin-Well" calorimeter,

Δt is the exposure duration,

γ is Calibration Coefficient.

6.5 Efficiency Calculation for Ferris Wheel from Calorimetric Tests

For efficiency calculation, we assume that all load positions at the wheel absorb the same amount of energy as the load position, so in order to get the total energy absorbed by all loads in wheel, we multiply energy absorbed by load times 40. The efficiency discussed here for a the load at a position is a relative term to the ideal load which absorbs fortieth of net power into the system, so sometimes this relative efficiency could be more than 100%.

On the other hand, the net power impinging the antenna is the difference between the forward and reflected power into the FW. The Lab View Data Acquisition program is used to collect the forward and reflected power data from their respective power meters.

The ratio in percentage of the power absorbed in the dummy bottle to that of the net power gives the efficiency of the Ferris Wheel. The relative efficiency of the Ferris Wheel at a position was estimated as follows:

$$e = (N_{Load} \cdot SAR_{WB} \cdot m_{Load}) / P_{Net} \tag{6.45}$$

where e is the relative efficiency of the Ferris Wheel at a particular position of Interest,

P_{Load} is the power absorbed by the loads in the FW,

P_{Net} is the total net power impinging on the loads in the FW

N_{Load} is the number of loads and is equal to forty,

SAR_{WB} is the Whole-Body SAR obtained from Calorimetric process,

m_{Load} is the mass of the load.

The average efficiency of the Ferris Wheel exposure system is found as

$$e_{FW} = (e_{Top} + e_{Bottom} + e_{Left} + e_{Right})/4 \tag{6.46}$$

where e_{FW} is the average efficiency of the system

and e_{Top}, e_{Bottom}, e_{Left} and e_{Right} are the average relative efficiency obtained at the positions of interest TOP, BOTTOM, LEFT, RIGHT positions respectively.

6.6 Calorimetric Test Procedure for loads

As already discussed, the types of loads used for the exposure experiments as loads are used in Calorimetric tests. They are dummy bottles filled with 37 g simulated tissue for the initial characterization. For the complete dosimetric characterization of Ferris Wheel mice cadavers of three weights 24 g, 32 g and 36 g are used.

6.6.1 Dummy Loads

1. Forty-two symmetrical bottles are filled with 37 grams of weight by volume of simulated tissue with +/- 0.1 g tolerance. The bottles are selected in such way that they easy fit into the Twin-Well calorimeter. Tie up three bottles with strings in a way that allows us to hold the bottles with the help of long strings during the exposure periods.
2. Place the three bottles in similar conditions and make sure both settle to room temperature.
3. Load the thirty nine bottles into the Ferris Wheel
4. Of the remaining three bottles, two are named A and B used as exposure loads alternatively at the position of interest and the third bottle named C is always used as sham.
5. Calibrate the Network Analyzer for the cable loss and tune the antenna for the load condition at and frequency of 915 MHz.
6. Ensure that the Lab View program is set up correctly. (i.e., General Purpose Interface Board (GPIB) Address 1 is set to Digital Voltmeter (DVM) reading the Twin-Well output, GPIB Address 2 and 3 for the power meters of Forward and Reflected powers respectively). Make sure that the gain is set to 30 dB for Instrument I (Twin-Well output) and 0 dB for power meters. Data should be collected from GPIB ports for every 2 seconds for at least 30 minutes or so.
7. Make sure that the power meters are calibrated with the offset value according to values on the bi-directional coupler (Forward and Reverse respectively) and the correction value according to the frequency of operation.

8. Make sure that reflected power meter reading is around 10% of the forward one.
9. Start data collection with the Lab View program.
10. Take A/B bottle place the sham one in a safe place at room temperature. Place the one to be exposed into plastic rocket and put all together into the selected carousel in the Ferris Wheel (i.e., Top, Left, Right or Bottom position)
11. Turn on the power amplifier and let it stabilize a few minutes. Determine the amount of exposure time (usually 30 seconds). Using a stopwatch toggle the switch to enable the RF exposure. At 30 seconds on the stopwatch toggle back the switch to disable the RF power.
12. Take the exposed bottle from the carousel and the sham with the help of the strings (make sure not to touch the bottles), and place them into the Twin-Well calorimeter at the same time.
13. Mark the well that contain the exposed and sham mice respectively and use always the same convention for different exposures.
14. Analyze Data.
15. Use the left over bottle for the next exposure after 45 minutes, which is sufficient time for the loads in the FW to reach room temperature.

6.6.2 Mouse Cadavers

1. Thaw forty-three mice of similar weight with +/- 0.5 g tolerance. Tie up two pairs of similar mice in a way that allows us to hold the mice with the help of a long string and also see that they will fit easily into the twin-well.
2. Place mice in similar conditions and make sure both settle to room temperature.

3. Ensure that the Lab View program is set up correctly. (i.e, GPIB Address 1 is set to DVM reading the Twin-Well output, GPIB Address 2 and 3 for the Power meters of Forward and Reflected powers respectively). Make sure that the gain is set to 30 dB for Instrument I (Twin-Well output) and 0 dB for power meters. Data should be collected from GPIB ports for every 2 seconds for at least 1800 seconds.
4. Make sure that the power meters are calibrated with the offset value according to values on the bi-directional coupler (Forward and Reverse respectively) and the correction value according to the frequency of operation.
5. After mice have been settled at room temperature, load thirty-nine mice into the Ferris Wheel with same orientation (i.e, all belly's of the mice downwards). The remaining two pairs are used as sham and exposed mice.
6. Calibrate the Network Analyzer for the cable loss and tune the antenna for that load condition at and frequency of 915 MHz.
7. Make sure that reflected power meter reading is around 10% of the forward one.
8. Start data collection with the Lab View program.
9. Take one pair of mice (mark the sham and exposed one); place the sham one in a safe place at room temperature. Place the one to be exposed into plastic rocket and put all together into the selected carousel in the Ferris Wheel (i.e., Top, Left, Right or Bottom position)
10. Turn on the power amplifier and let it stabilize a few minutes. Determine the amount of exposure time (usually 30 seconds). Using a stopwatch toggle the

switch to enable the RF exposure. At 30 seconds on the stopwatch toggle back the switch to disable the RF power.

11. Take the exposed mice from the carousel and the sham with the help of the strings (make sure not to touch the mice or the part of the rocket that touches the mice), and place them into the Twin-Well calorimeter at the same time.
12. Mark the well that contain the exposed and sham mice respectively and use always the same convention for different exposures.
13. Analyze Data.
14. Use the next pair of mice for the next exposure after 45 minutes, which is sufficient time for the loads in the FW to reach room temperature.

6.7 Data Analysis Procedure for Calorimetric Tests

1. Convert raw data file in .dat format into an excel spreadsheet (.xls). There should be four columns of data logged into the excel sheet, for the time T in seconds, the mV DC reading of calorimeter, Forward and Reverse power respectively.
2. Create a new column to calculate the net power, which is the difference of the forward and reflected power columns.
3. Integrate the area of the curve created by the data in the net power column to get the net energy supplied to the system.
4. From the column of the mV DC out put of differential calorimeter, integrate the area under this curve to get the total area under the curve of heat transfer between the wells.

5. Take the total area and divide by ten (Conversion Factor) to get a value (in Joules) of the heat dissipated in the load.
6. Take the above value and divide by the weight of that particular load to get the SAR value.
7. Compute the Efficiency of the FW.
8. To get the Normalized SAR, divide SAR with Net power per load (i.e. divide by 40).
9. Compute the 95% confidence interval level for the set of exposures.

CHAPTER VII

CALORIMETRIC RESULTS

Calorimetric experiments determine the SAR and efficiency to characterize the Ferris Wheel. Dummy loads were used for the initial characterization of the Ferris Wheel in order to get good repeatability. In order to simulate the life cycle of mice, the measurements were performed on 24 g, 32 g, 36 g mice. The Ferris Wheel is loaded with forty mice of similar weight with a deviation of +/- 0.5 g. Since we were using the dead mice and to compare with the live scenario, the mice elevated on a Styrofoam slab in order to place the collective center of mass in the center of the restrainer. As discussed in Chapter V a small offset of the collective mice center may introduce a large asymmetry, as the positioning of the mice in the restrainers is very critical.

Large numbers of exposures are done at each of four different positions of interest in the Ferris Wheel to attain repeatability. The positions of interest are the Left (9 :00 in clock) Top (12:00 in clock), Right (3:00 in clock) and Bottom (6:00 in clock) and the results of each position are as follows:

7.1 Dummy Bottles (Simulated Tissue)

7.1.1 Measurement of Normalized SAR

The below table shows the mean values of the Normalized SAR values obtained for different positions of interest and the mean Normalized SAR value for different for the whole set of loads.

Table 5. Calorimetric Results for Dummy Bottles as loads in terms of Normalized SAR

DATA FROM CALORIMETRIC TESTS FOR DUMMY LOADS			
TOP	BOTTOM	LEFT	RIGHT
0.45	0.62	0.52	0.56
Average Normalized SAR [W/kg/W]		0.54	

Lab View data acquisition program used for the collection of heat transfer between the loads in terms of voltage difference between the wells of Twin-Well calorimeter. The program collects the data at an instance and waits for 2 seconds to in collect for next data value. During the data collection for the exposure tests this software looses the heat content in a second for each minute because of the delay in collecting the data. So the error in heat can be acoounted by introducing a correction factor of 1.06667 for the loss in time.

Table 6. Normalized SAR after Correction Factor for Lab View Data Acquisition

CORRECTION FACTOR OF 1.06667 FOR LABVIEW INTEGRATION STEP			
TOP	BOTTOM	LEFT	RIGHT
0.46	0.63	0.53	0.57
Average Normalized SAR [W/kg/W]			0.55

There is some heat loss, which occurs during the time interval from the end of the exposure and the placement of loads into the Twin-Well calorimeter. As the above exposure tests are done in a very careful and repeatable process, the average time delay

for placing the loads into the Twin-Well is 5 seconds. In order to determine the percentage of heat loss in these 5 seconds, another set of measurements were carried out using the dummies with an intentional extending delay to 10 seconds and 15 seconds. Fig.37 shows the determination of the correction factor for the 5-second delay but for with the dummy bottles with 30 grams. The Normalized SAR might have higher values to the

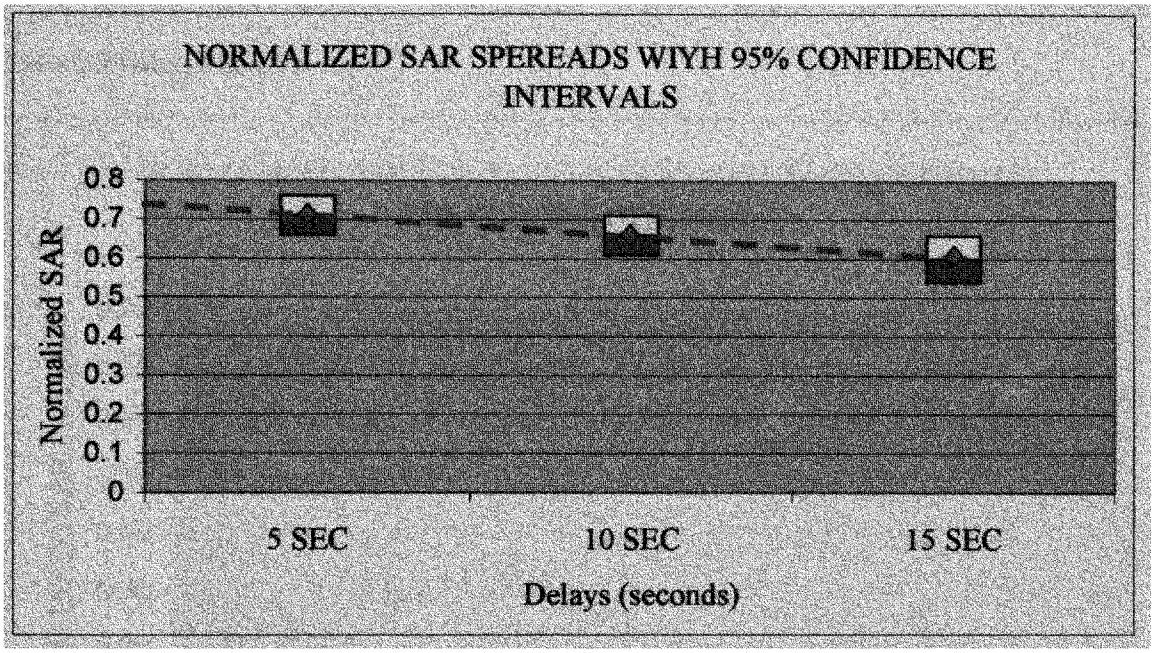

Fig.37. Extrapolation for the heat loss in 5-second delay.

Table 7. Correction factor for 5-second delay for Dummy Loads

Ratio of Normalized SAR for 5-second to 10- second Delay	1.08
Ratio of Normalized SAR for 10-second to 15- second Delay	1.12
Averaged Correction Factor	1.1

Table 8. Normalized SAR after Correction Factor for 5 second Delay

CORRECTION OF 1.1 FOR 5 SEC DELAY			
TOP	BOTTOM	LEFT	RIGHT
0.50	0.69	0.58	0.63
AVERAGE EFFCIENCY [%]			0.60

Also introducing the correction factor for transferring the loads form the wheel we have following Table 3.

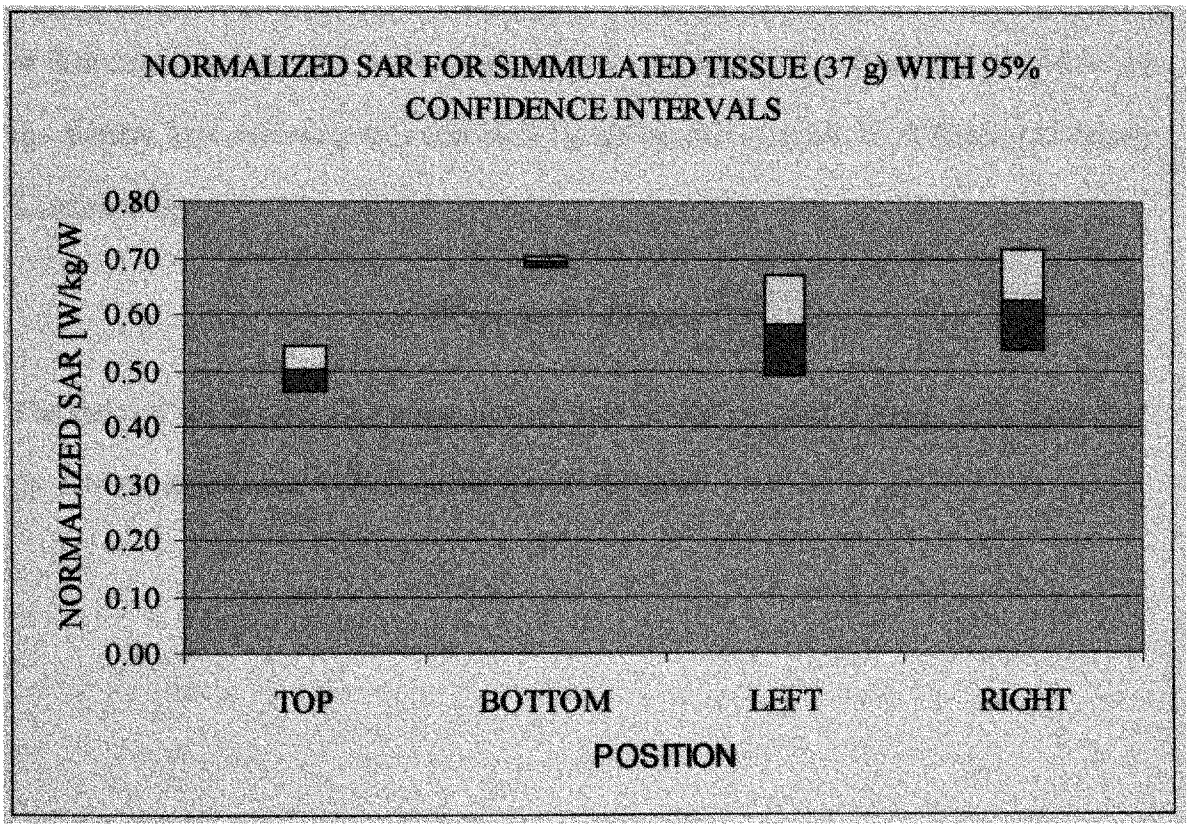

Fig.38. Normalized SAR (W/kg/W) Vs Position for the Dummy Loads.

The figure above shows the Normalized Whole-Body SAR averages to the net power at four different positions with their corresponding deviations for several

experiments using Calorimetric tests. Number of experiments ware repeated at that particular position until the standard error fall below 10% for that set of data.

The deviation of the average SAR is higher at the right and left positions is the positioning of the bottles is not always at the same in all exposures, but at top and bottom position the bottle seems to be resting at the same position with more consistency. In the Fig.29 it can be seen that change in displacement of 2.5 mm of the load from center has a large impact on the amount of energy absorbed by the body.

As discussed in Chapter IV the dummy load which is equivalent to mice in terms of dielectric properties but not in terms of average density. The Whole Body SAR in the the dummy load assuming as a real mice by taking into account the difference in density is obtained by

$$SAR_{WB-Mice} = SAR_{Dummy} \frac{\rho_{Dummy}}{\rho_{Mice}} \tag{7.1}$$

The ratio of the densities between dummy load to that of mice is about 1.25. Therefore, the average normalized SAR obtained is 0.75 W/kg/W.

7.1.2 Efficiency Measurements for the Exposure System

The following tables show the average efficiency at the respective positions and the

Table 9. Efficiency data from Calorimetric tests at different positions of interest on FW using Dummy Loads

EFFCIENCY DATA FROM CALORIMETRIC TESTS FOR DUMMY LOADS			
TOP	BOTTOM	LEFT	RIGHT
66.96	92.30	76.82	82.76
AVERAGE EFFCIENCY [%]			79.71

averaged efficiency of the wheel and equal to 79.71 %. This efficiency is based on the Calorimetric experimental results. The efficiency results from calorimetric tests also will have same correction factors as which are applicable for the Normalized SAR. Tables 9 and 10 show the efficiency results after the corrections factors are accounted for.

Table 10. Correction Factor for Lab View Data Acquisition Program

CORRECTION FACTOR OF 1.06667 FOR LABVIEW INTEGRATION STEP			
TOP	BOTTOM	LEFT	RIGHT
68.08	93.84	78.10	84.14
AVERAGE EFFCIENCY [%]			81.03

Table 11. Final Efficiency of FW using Dummy Loads including Correction Factor for 5-seconds delay

CORRECTION FACTOR OF 1.1 FOR 5 SECONDS DELAY			
TOP	BOTTOM	LEFT	RIGHT
78.88	103.22	85.91	92.55
AVERAGE EFFCIENCY [%]			89.14

So the final efficiency system is 89.14 %.

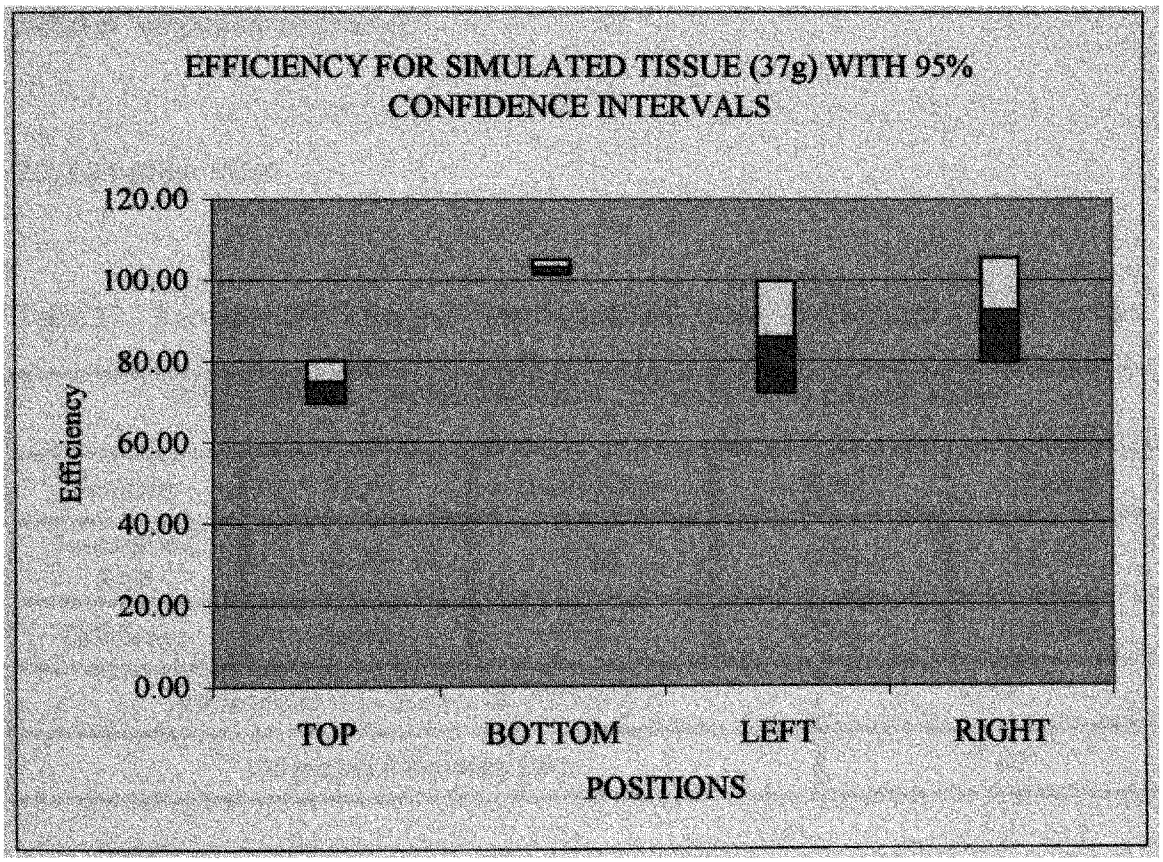

Fig.39. Efficiency Vs Position for the dummy loads.

7.2 Mice Cadavers

A number of Calorimetric tests on mice at different weights have been performed to refine the experimental techniques on mice and to achieve a good repeatability .The correction applied for the dummy bottles as loads will also apply for mice of the three different weights. But the correction factor for the 5 seconds delay in transferring the loads from the Ferris Wheel to Twin-Well calorimeter is not used because of this small delay in the case of mice cadavers is not so significant as the heat loss during the transfer of mice is very less when compared to the dummy loads. The results for the three different weights are as follows:

7.2.1 24-gram Mice

Table 12. Averaged Efficiency and Normalized SAR values for 24-grams mice as Loads

DATA FROM CALORIMETRIC TESTS FOR 24 GRAM MICE				
Position	TOP	BOTTOM	LEFT	RIGHT
Normalized SAR	0.71	0.85	0.79	0.75
Efficiency	66.52	77.77	72.8	69.38
Averaged Normalized SAR (W/kg/W):				0.78
Averaged Efficiency (%):				71.62

Table 13. Correction Factor for Lab View Data Acquisition Program

CORRECTION FACTOR OF 1.06667 FOR LABVIEW INTEGRATION STEP				
Position	TOP	BOTTOM	LEFT	RIGHT
Normalized SAR	0.72	0.86	0.80	0.76
Efficiency	67.63	79.07	74.01	70.54
Averaged Normalized SAR (W/kg/W):				72.81
Averaged Efficiency (%):				0.79

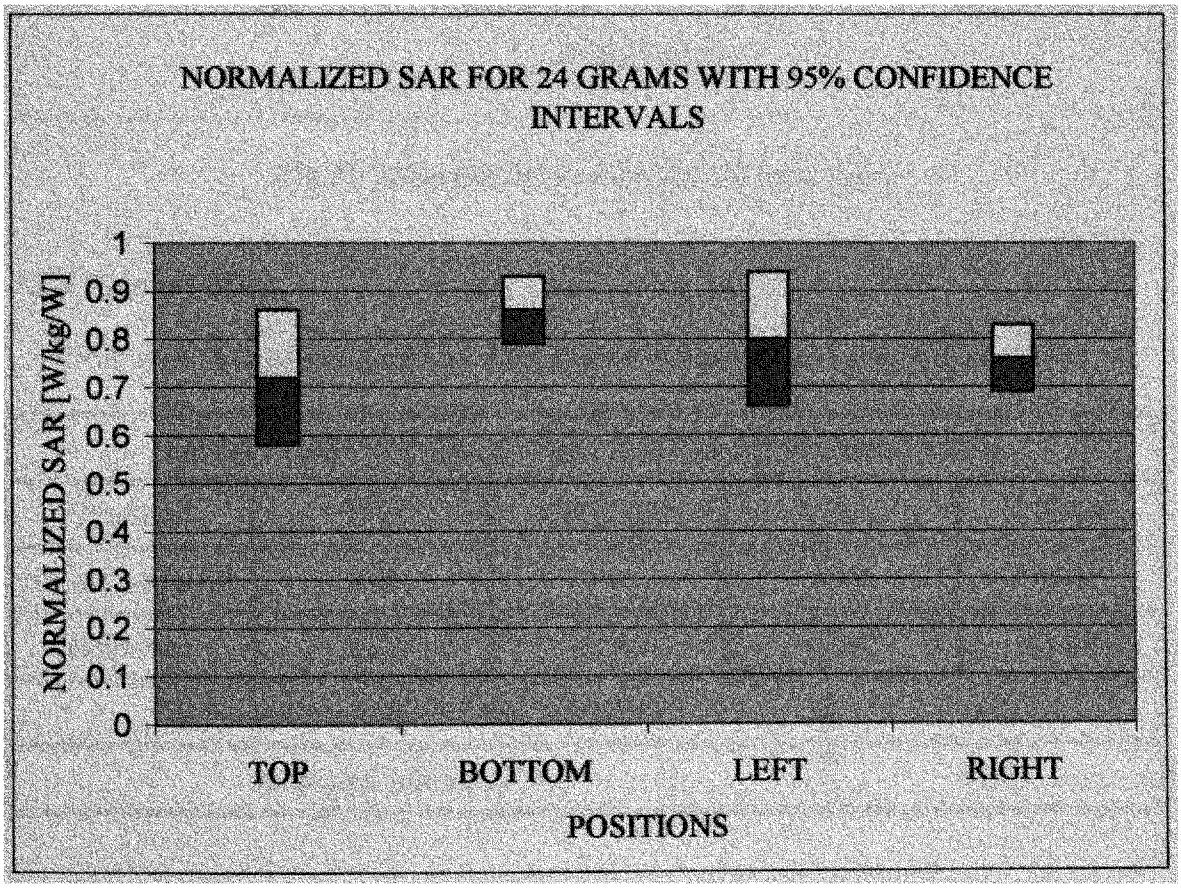

Fig.40. Normalized SAR (W/kg/W) Vs Position for the 24 g mice.

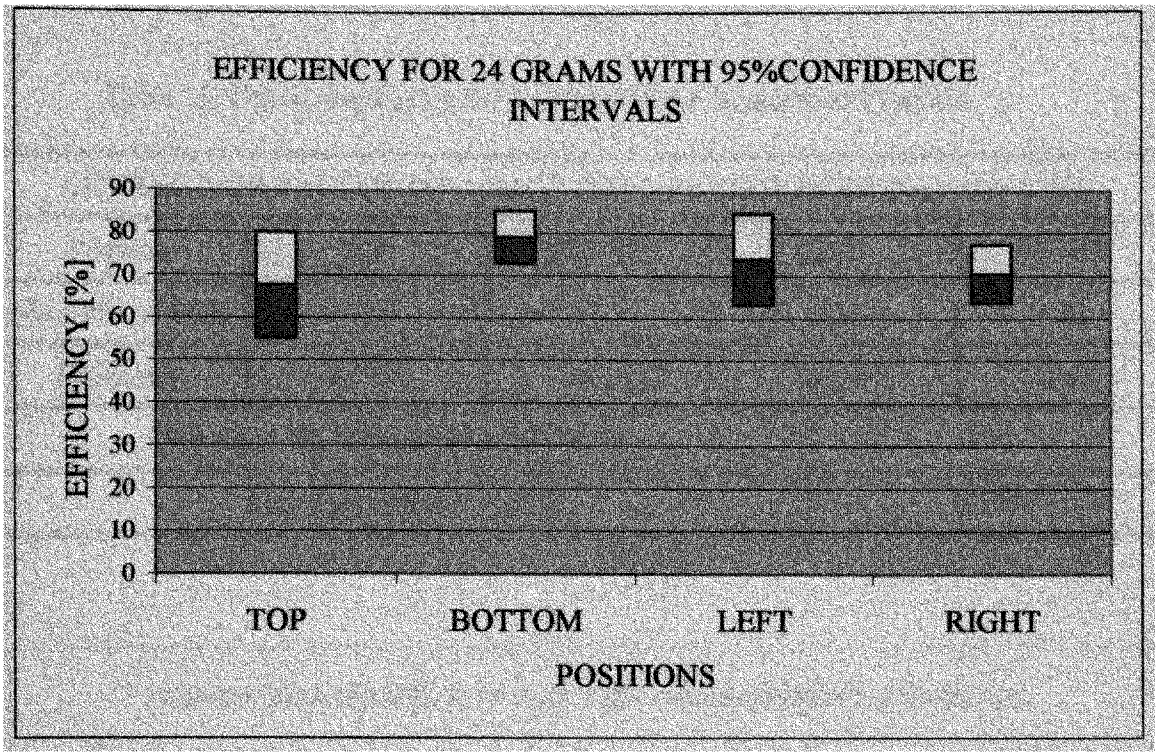

Fig.41. Efficiency Vs Position for the 24-g mice.

7.2.2 32-gram Mice

Table 14. Averaged Efficiency of the Ferries Wheel using 32 grams mice as load

DATA FROM CALORIMETRIC TESTS FOR 36 GRAM MICE				
Position	TOP	BOTTOM	LEFT	RIGHT
Normalized SAR	0.68	0.72	0.74	0.71
Efficiency	84.2	92.66	94.92	92.41
Averaged Normalized SAR (W/kg/W):				0.71
Averaged Efficiency (%):				91.05

Table 15. Correction Factor for Lab View Data Acquisition Program

CORRECTION FACTOR OF 1.06667 FOR LABVIEW INTEGRATION STEP				
Position	TOP	BOTTOM	LEFT	RIGHT
Normalized SAR	0.69	0.73	0.75	0.72
Efficiency	85.60	94.20	96.50	93.95
Averaged Normalized SAR (W/kg/W):				0.72
Averaged Efficiency (%):				92.56

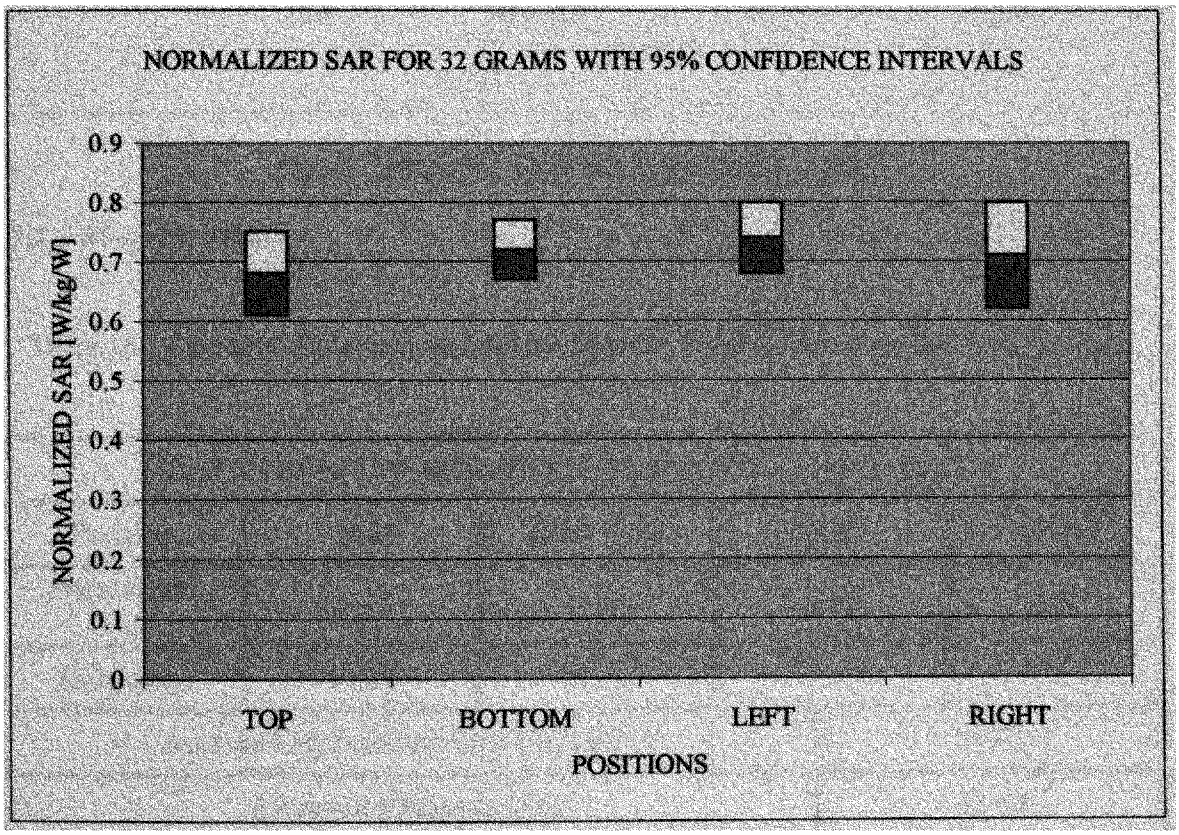

Fig.42. Normalized SAR (W/kg/W) Vs Position for the 32-g mice

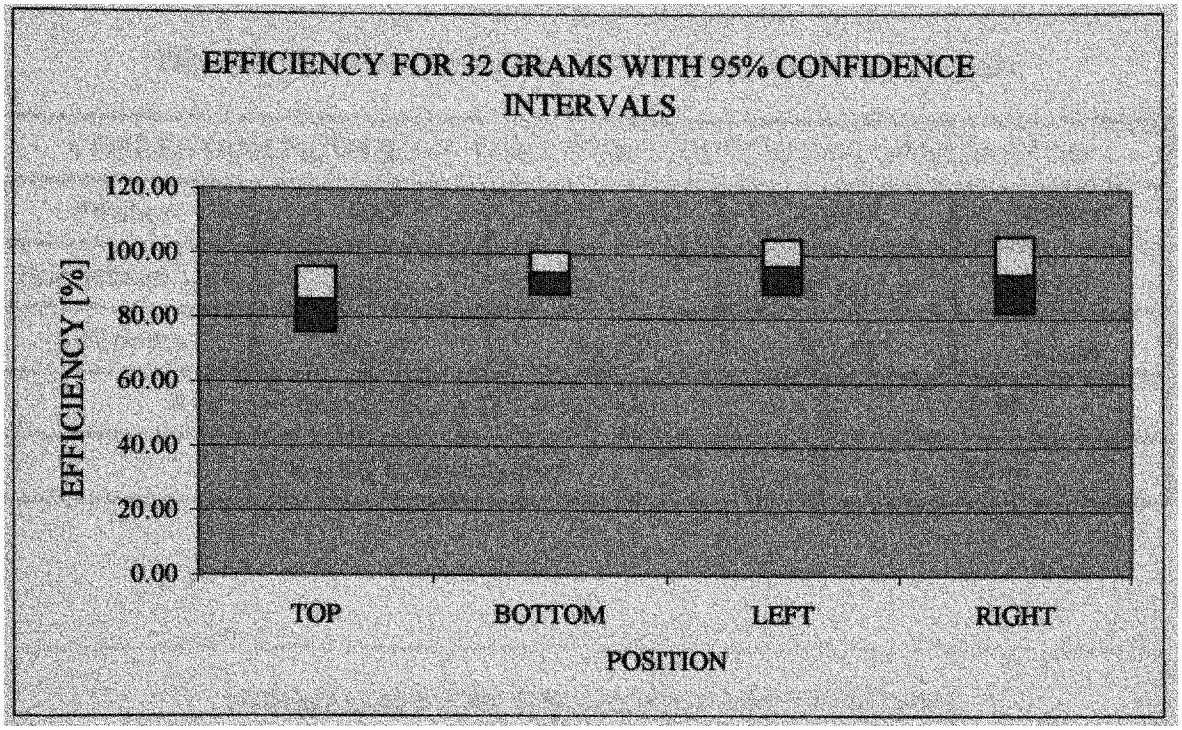

Fig.43. Efficiency Vs Position for the 32-g mice.

7.2.3 36-gram Mice

Table 16. Averaged Efficiency and Normalized SAR values for 36-grams mice as loads

DATA FROM CALORIMETRIC TESTS FOR 36 GRAM MICE				
Position	TOP	BOTTOM	LEFT	RIGHT
Normalized SAR	0.63	0.57	0.54	0.55
Efficiency	89.87	81.41	75.92	79.12
Averaged Normalized SAR (W/kg/W):				0.57
Averaged Efficiency (%):				81.58

Table 17. Correction Factor for Lab View Data Acquisition Program

CORRECTION FACTOR OF 1.06667 FOR LABVIEW INTEGRATION STEP				
Position	TOP	BOTTOM	LEFT	RIGHT
Normalized SAR	0.64	0.58	0.55	0.56
Efficiency	91.37	82.77	77.19	80.44
Averaged Normalized SAR (W/kg/W):				0.58
Averaged Efficiency (%):				82.94

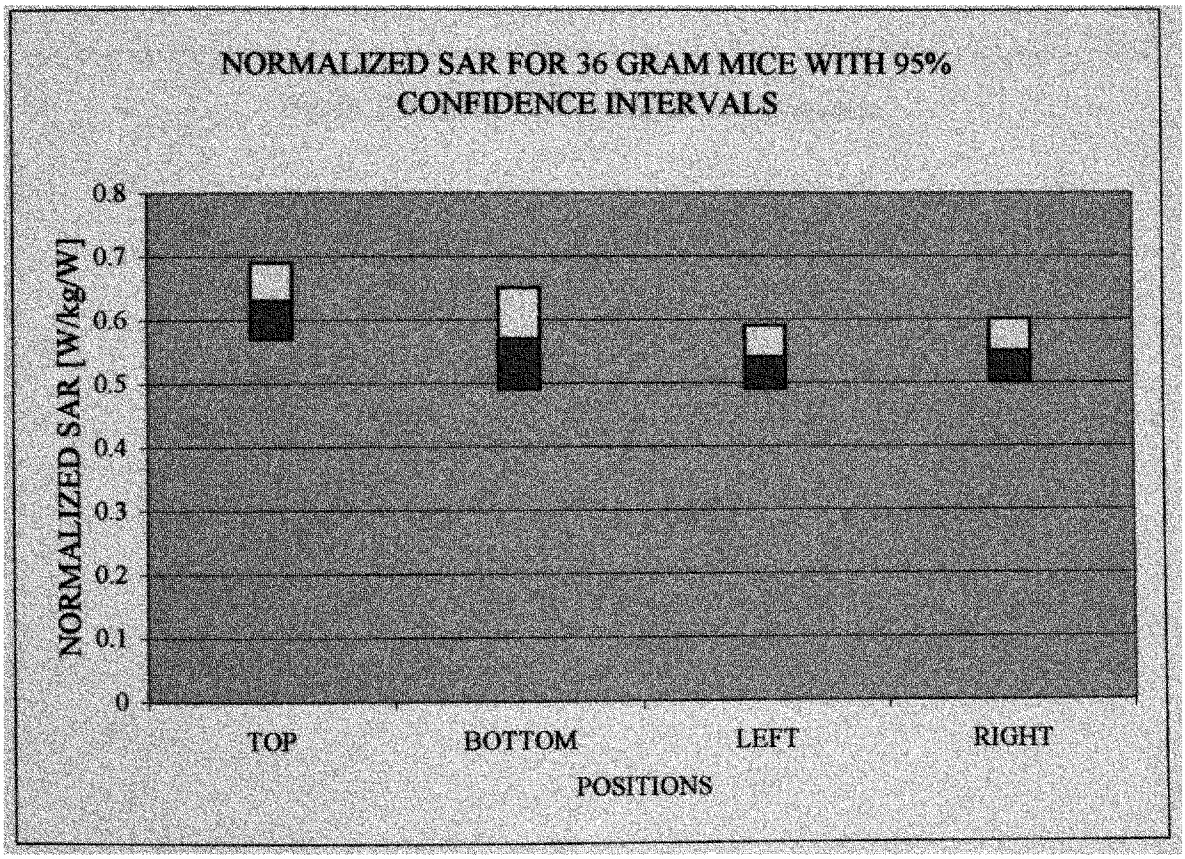

Fig.44. Normalized SAR (W/kg/W) Vs Position for the 36-g mice.

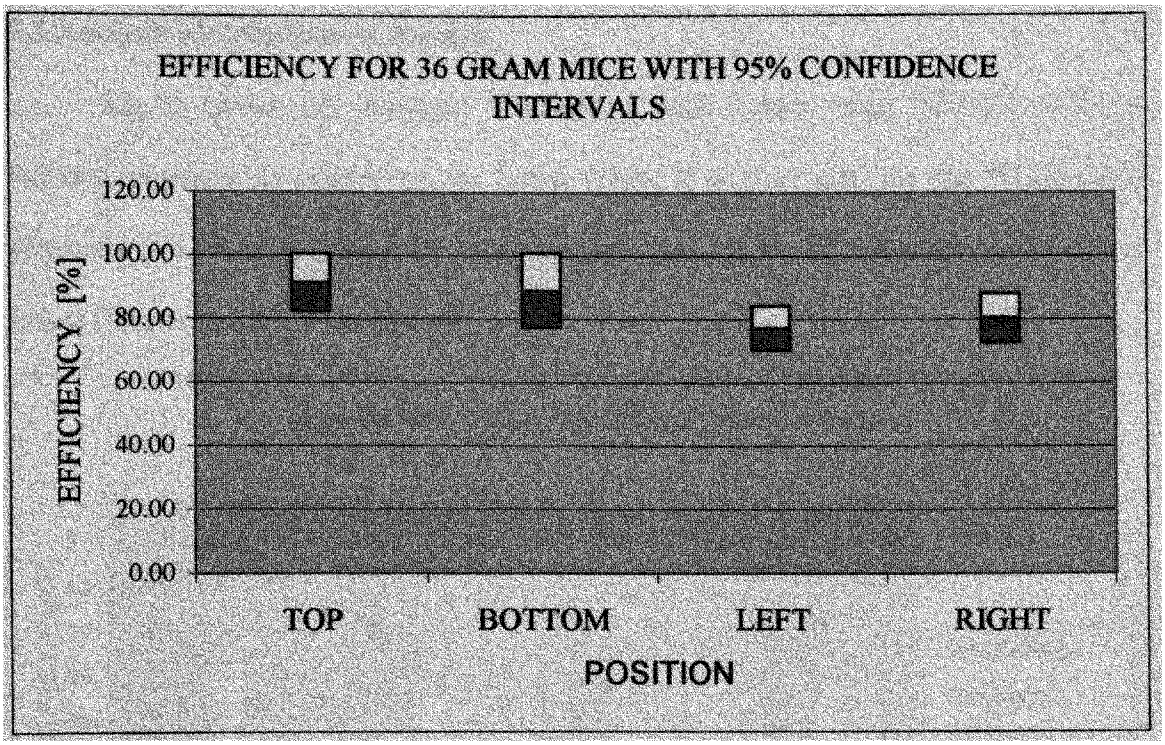

Fig.45. Efficiency Vs Position for the 36-g mice.

7.3 Analysis of Calorimetric Results

Fig.46 shows the averaged Normalized SAR values using different loads at different positions of interest on the Ferris Wheel It can be seen that the Whole-Body Normalized SAR is in 24-g mice is higher than that of the 32, 36 grams and Dummy Loads (Marked as ST in the figures).

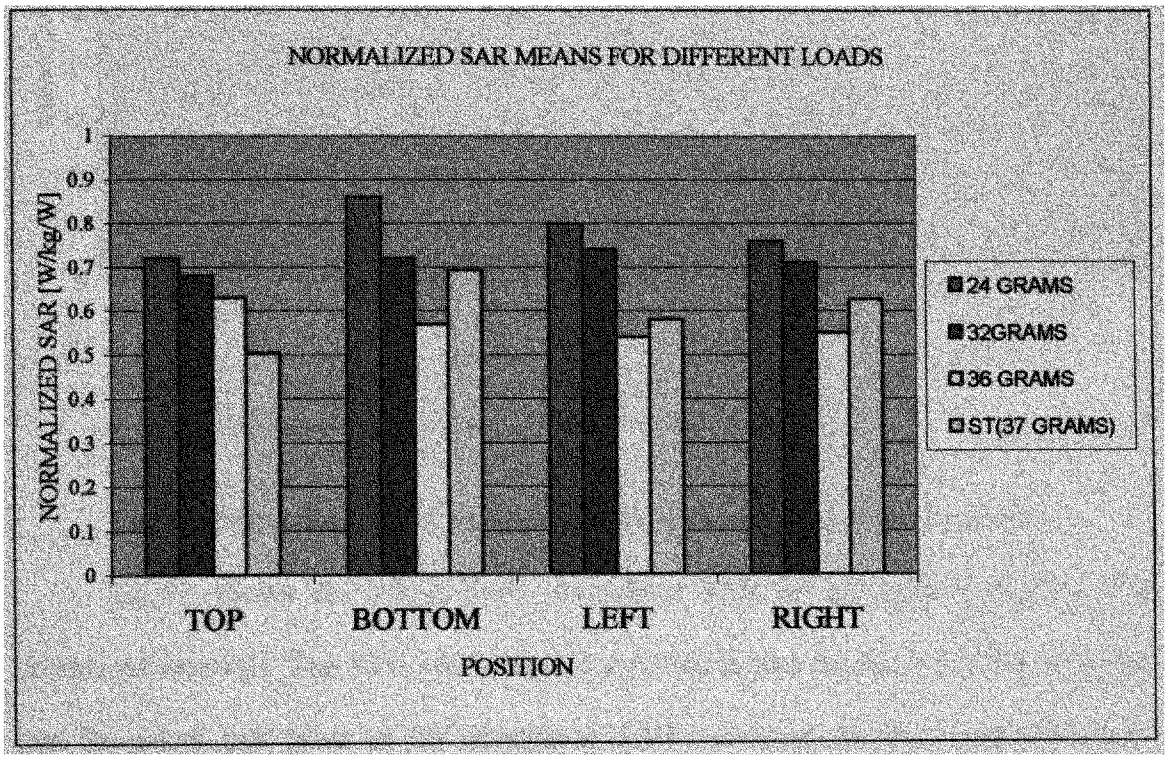

Fig.46. Whole- Body SAR values for Different weights versus Positions.

It can be also seen that the Normalized SAR values for three different mice weights and dummy loads at four positions on the Ferris Wheel lie between the 0. 50 - 0.85 W/kg/W.

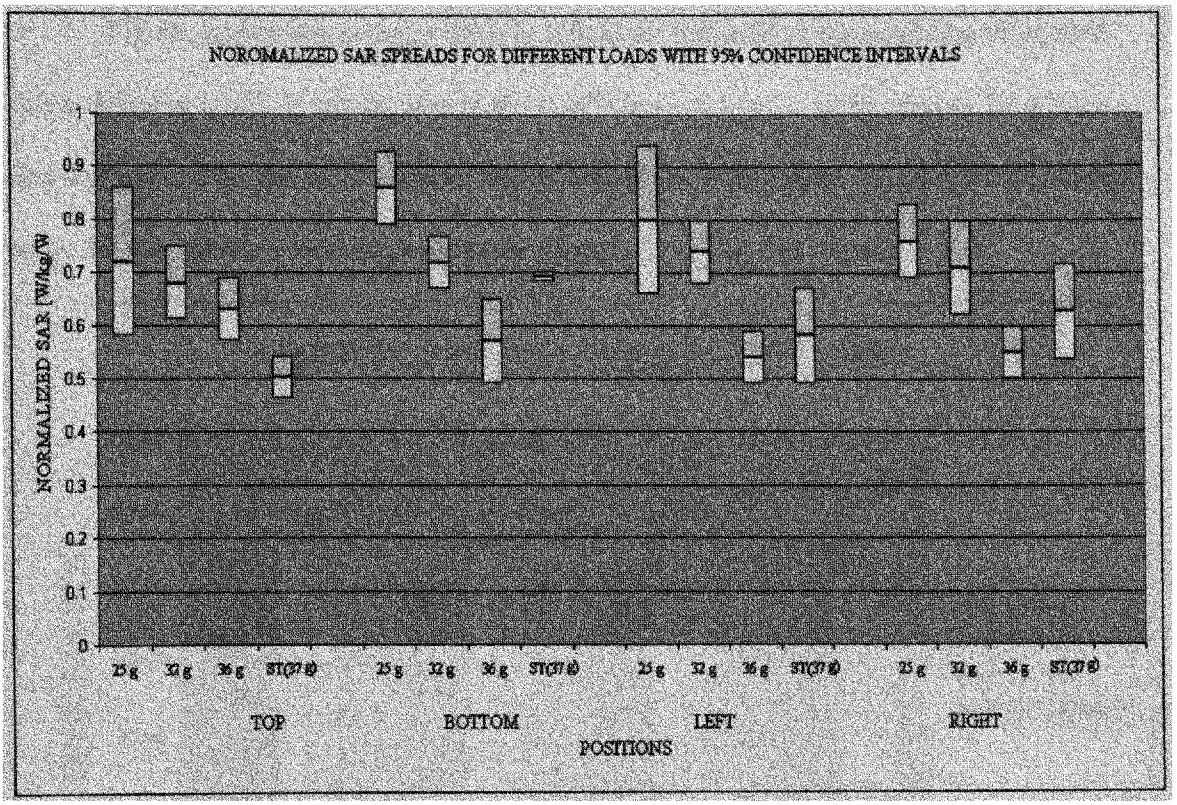

Fig.47. Whole-Body SAR values for Different Loads with their Deviations.

Fig.47. shows the Whole-Body normalized SAR for all loads with their 95% confidence intervals. The 95% confidence interval states that we have a 95% confidence that the actual true mean of the normalized SAR measurements lies in between these intervals. It's also seen that at position of interest the deviations from the mean are higher for the 24 g rather than the 32 and 36 g. The reason for the higher deviations in 24-g mice is due to the higher uncertainty in placing it not exactly at the center of the carousel as these mice very compared to 32, 36g. So chances of positioning the mice on the steep side of the curve shown in Fig.6 are higher in case of 24-g mice. This will lead to higher deviations in the case of 24 than the 32 and 36 g.

Fig.48. shows the average relative efficiency obtained at the positions of interest using different loads. It can be seen that the efficiency is lowest in the case of 24-g mice and highest in the case of 32-g mice. The average power efficiency of the system is found to be 84.4%, which is very high when compared to the earlier systems.

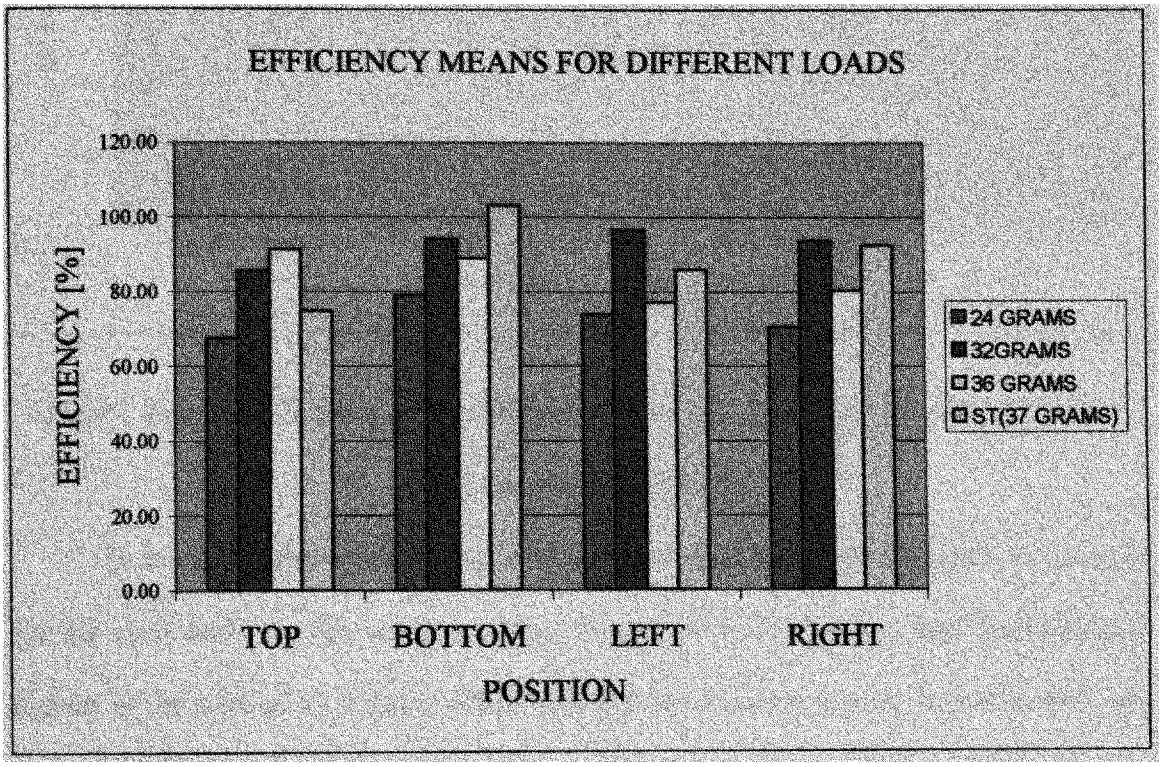

Fig.48. Relative Efficiency of the FW at Positions of Interest using Different Loads.

It is also seen that the highest deviations of the relative efficiency between the Top and Bottom positions for any type of load is 0.69 dB and the Left and the Right positions is 0.32 dB, which shows that the system is very symmetrical about the positions of interest.

Fig.49 shows the relative efficiency spreads at the positions of interest for different loads with their 95% confidence intervals.

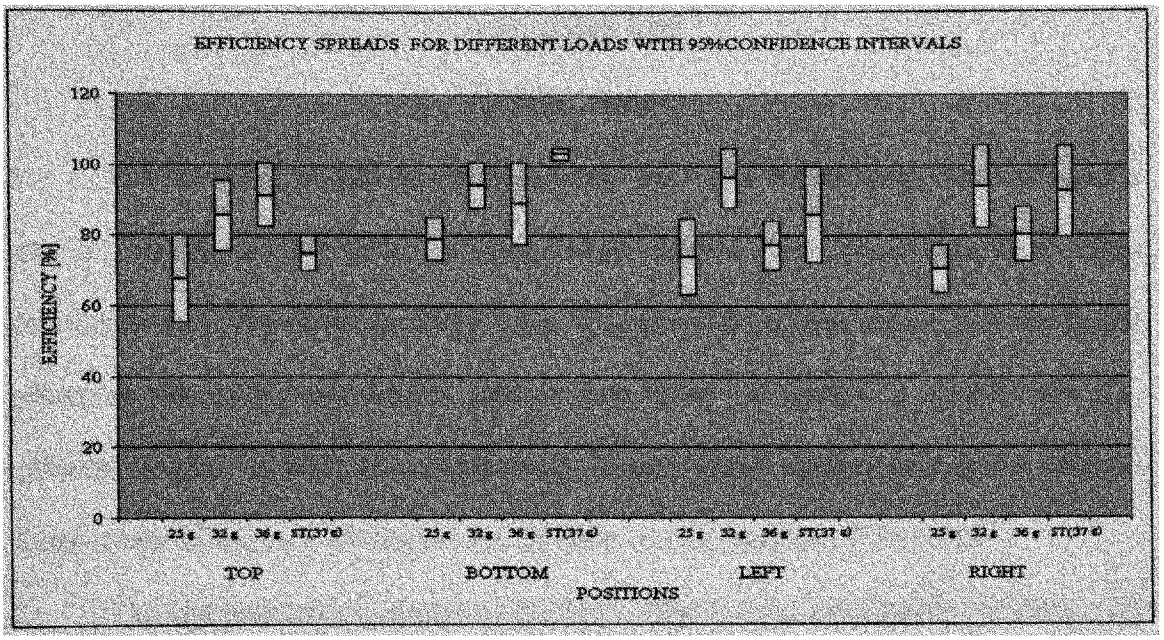

Fig.49. Relative Efficiency at the Positions of Interest for Different Loads with their 95% Confidence Intervals.

In the Australian study it is seen that mouse weighs around 32-grams for most of the life cycle and very few weeks at 25-g. As seen from the Ferris wheel is operating at highest in the case of 32-g mice, which says that the systems used in Australia study are working at their highest efficiencies for most of the time in the two year period.

CHAPTER VIII

CONCLUSIONS

The measured E-field distributions inside the Ferris Wheel along the ρ-axis and z-axis i.e., (inside the restrainer) by using E-field measurement probes have an excellent correlation with that of the simulated ones. The simulations have shown that the system preserves the E-field distribution pattern even when the system is loaded with four different weights of loads in a symmetrical fashion. Small displacement in the effective Barry-center of the load will induce an asymmetry in distribution of the fields.

The characterization results of the Ferris Wheel using calorimetric technique with dummy loads and mice cadavers Chapter 5 shows that the obtained Normalized SAR values are very consistent in all positions of interest and has a range from 0.5 to 0.9 W/kg/W. The average efficiency obtained from these experiments using different loads (dummy and mice cadavers) is 84.4%, which shows that the system is efficient in transferring the energy into its loads. The highest deviation in efficiency between top and bottom positions is 0.69 dB. The left to right difference is about 0.32 dB for any type of load, which shows that the system in symmetrical distributing power into the loads.

The tunable antenna of the FW exposure has good tuning capability over the wide range of loading conditions during characterization of the FW using calorimetric technique. The system was used for a huge number of exposure experiments and it has shown good reliability and consistency.

The Ferris Wheel Exposure system provides an efficient means for conducting long-term animal studies of Whole-Body RF exposure.

REFERENCES

[1] Michael H. Rapacholi, Anthony Basten, Val Gedski, Denise Noonan, John Finnie and Alan W. Harris "Lymphomas in Eμ-*PIM 1* Transgenic Mice Exposed to Pulsed 900 MHz Electromagnetic Fields," Radiation Research, Vol.147, pp.631-640, 1997.

[2] Tammy D. Utteridge, Val Gebski, John W. Finnie, Barrie Vernon-Roberts and Tim R. Kuchel "Long-Term Exposure of Eμ- Pim1 Transgenic Mice to 898.4 MHz Microwaves does not Increase Lymphoma Incidence," Radiation Research, Vol.158, pp.357-364, 2002.

[3] Q. Balzano, C.K. Chou, A. Faraone, Renato Cicchetti an d Roger Y. Tay "An Efficient RF Exposure System with Precise Whole-Body Average SAR Determination for vivo Animal Studies at 900 MHZ," *IEEE Trans. On Microwave Theory and Techniques*, vol.48, no.11, pp-2040-2049, Nov 2000.

[4] A.W.Guy, "Miniature anechoic chamber for chronic exposure of small animals to plane-wave microwave fields," *J. Microwave Power*, vol. 14,no. 4, pp. 327–338, 1979.

[5] C.K.Chou and A.W.Guy, "Systems for exposing mice to 2,450-MHz electromagnetic fields," *Bioelectromagnectics*, vol. 3, no. 4, pp. 401–412,1982.

[6] V.W. Hansen, A. K. Bitz, and J. R. Streckert, "RF exposure of biological systems in radial wave guides," *IEEE Trans. Electromagnetic Compatibility*, vol. 41, pp. 487–493, Nov.1999.

[7] P.Russo and A.Faraone " Numerical Analysis of the " Ferris Wheel" Mice exposure system using an efficient cylindrical FDTD Scheme".

[8] C.K.Chou, H. Bassen, J.Osepchuk, Q. Balzano, R.Petersen, M.Meltz, R. Cleveland J.C. Lin, and L.Heynick "Radio frequency electromagnetic exposure: Tutorial review on experimental dosimetry," *Bioelectromagnectics*, vol.17, pp.195-208, 1996.

[9] *IEEE Standard for Safety Levels with Respect to Human Exposure to Radio Frequency Electromagnetic Fields, 3 kHz to 300 GHz*, IEEE Standard C95.1, ICNIRP, 1991.

[10] "Evaluating compliance with FCC guidelines for human exposure to radio frequency electromagnetic fields," Federal Communications Com-mission, Washington, D.C, OET Bull. 65, Aug. 1997.

[11] "Radio frequency electromagnetic fields; properties, quantities and units, biophysical interaction, and measurements," National Council on Radiation Protection and Measurements, Bethesda, MD, NCRP Rep. 67, 1981.

[12] Durney CH, Massooudi H, and Iskander MF (1986): " Radio frequency Radiation Dosimetry Hand book, 4th Edition (Report TR-85-73)."Brooks Air-force Base, TX: USAF School of Aerospace Medicine.

[13] Durney CH, Johnson CC, Barber PW, Massooudi H, and Iskander MF, Lords JL, Ryser DK, Allen SJ, Mitchell JC (1978): " Radio frequency Radiation Dosimetry Hand book, Second Edition (Report TR-78-22)."Brooks Air-force Base, TX: USAF School of Aerospace Medicine.

[14] Gandhi Op, Hunt EL and D'Andrea JA (1977): Deposition of electromagnetic energy in animals and in models of man with and without grounding and reflector effects. Radio Sci 12(6s): 39-47.

[15] Charles Polk and Elliot Postow, *CRC Handbook of Biological Effects of electromagnetic fields.* Boca Raton, Florida: CRC Press, Inc.

[16] Luengas Wilson, "Determination of Localized SAR by Thermography and Thermometric processes using Ferris Wheel as an Exposure System" Master's Thesis in Preparation, Florida International University, Electrical and Computer Engineering, 2002.

[17] K.S.Yee, "Numerical Solution of Initial Boundary Value Problems Involving Maxwell's Equations in Isotropic Media," *IEEE Transactions on Antennas and Propagation*, Vol.14, No.4, pp.302-307, 1966.

[18] H. Bassen, M. Swicord, and J. Abita, "A Miniature Broad-Band Electric Field Probe," *Annals New York Academy of Sciences*, vol. 247, pp.481-493, 1975.

[19] A.Faraone," Preliminary report on the Ferris Wheel Exposure System dosimetry". Motorola internal Report, July 2002.

[20] Renato Cicchetti. "Mathematical Model for Twin-Well Calorimeter". Motorola Internal report, September 2002.

[21] Stanley Humpheies, Jr., *Field Solutions on Computers* Boca Raton, Florida: CRC Press, Inc.